

Study and design of a DC/DC converter for series connected wind farms

– Examensarbete av Javier Aguado Esteban–

February, 2005



Institutionen för Energi och Miljö
Elektrotekniklinjen 180 p
CHALMERS TEKNISKA HÖGSKOLA
Göteborg, Sverige, 2005
Examinator: Torbjörn Thiringer
Handledare: Stefan Lundberg

Abstract

In this Master Thesis, the design of a DC/DC converter for a series connected DC wind park was investigated. The features of this kind of wind park were presented, and possible topologies of the converter were studied. Finally its advantages and drawbacks for the specific application were discussed.

It was found that the most appropriate model was the full bridge converter, which there was theoretically analyzed. One investigated aspect was how the converter performance was affected by the transformer parameters. Then, an economical criteria was defined to choose the most suitable one: the energy cost.

At last the selected design was simulated in Pspice® in order to check that it satisfies the application requirements, and the simulated waveforms were compared with those found from the theoretical study.

Acknowledgement

To Almudena. To know she was there encourage me to reach the end. Thanks for waiting for me.

Thanks also to my parents. Without their love and support this project would never be done.

Contents

ABSTRACT.....	iii
ACKNOWLEDGEMENT.....	v
1 INTRODUCTION	1
1.1 PROBLEM BACKGROUND.....	1
1.2 OVERVIEW OF PREVIOUS WORK	1
1.3 PURPOSE OF THE REPORT	2
1.4 LAYOUT OF THE REPORT	2
2 PRINCIPLES OF WIND TURBINES.....	3
2.1 GENERAL DESCRIPTION OF WIND TURBINES AND OPERATING PRINCIPLES	3
2.2 VARIABLE SPEED DC WIND TURBINES	4
3 LAYOUT OF A SERIES-CONNECTED DC WIND FARM	7
3.1 GENERAL WIND PARK CONCEPTS	7
3.2 LAYOUT OF A SERIES CONNECTED WIND FARM WITH DC VOLTAGE OUTPUT.....	8
3.3 CONTROL OF THE SYSTEM.....	11
4 TOPOLOGIES OF DC/DC CONVERTERS	13
4.1 THE FULL BRIDGE ISOLATED BOOST CONVERTER (FBIB).....	13
4.2 THE FULL BRIDGE CONVERTER (FB)	17
5 DEFINITION OF THE TRANSFORMER.....	21
5.1 ELECTRICAL MODEL OF THE TRANSFORMER	21
5.2 DESCRIPTION OF THE TRANSFORMER AND THE DESIGN VARIABLES	22
5.3 DEFINITION OF THE TRANSFORMER PARAMETERS	25
5.3.1 <i>Dimensions</i>	28
5.3.2 <i>Inductances</i>	32
5.3.3 <i>Losses</i>	34

6	ANALYSIS OF THE DIFFERENT TOPOLOGIES FOR THE STUDIED WIND TURBINE APPLICATION.....	37
6.1	SPECIFICATIONS OF THE WIND TURBINE	37
6.2	TASK OF THE DC/DC CONVERTER	38
6.3	STUDY OF THE DC/DC CONVERTER TOPOLOGIES PROPOSED	39
6.3.1	<i>Full bridge isolated boost (FBIB) topology</i>	40
6.3.2	<i>Full bridge (FB) topology</i>	44
6.4	MODELS COMPARISON AND SELECTION OF THE MOST SUITABLE TOPOLOGY	47
7	ANALYSIS OF THE REAL CONVERTER	49
7.1	ANALYSES OF THE CIRCUIT	49
7.1.1	<i>Step 0</i>	50
7.1.2	<i>Step 1</i>	52
7.1.3	<i>Step 2</i>	54
7.1.4	<i>Step 3</i>	55
7.1.5	<i>Step 4</i>	56
7.2	VOLTAGE AND CURRENT WAVEFORMS OF THE FULL BRIDGE	56
7.3	ANALYSIS OF THE FULL BRIDGE DEPENDING ON THE TRANSFORMER PARAMETERS	60
7.3.1	<i>Definition of the transformer parameters and equations</i>	60
7.3.2	<i>Influence of the winding ratio on the output voltage</i>	63
7.3.3	<i>Influence of the transformer inductances on the output voltage</i>	63
7.3.4	<i>Influence of the switching frequency on the output voltage</i>	64
7.3.5	<i>Analysis of the main inductance as function of the frequency and the winding ratio</i>	65
8	DESIGN OF THE CONVERTER	67
8.1	DEFINITION OF THE DESIGN PROCESS	67
8.1.1	<i>Converter database</i>	67
8.1.2	<i>Converter optimization</i>	70
8.2	DEFINITION OF THE CORE MATERIALS.....	73
8.3	DEFINITION OF THE TRANSFORMER CONDUCTORS	75
8.4	DIMENSIONING OF THE TRANSFORMER. THE WORST OPERATION POINT	79
8.5	DEFINITION OF THE SEMICONDUCTORS	80
8.5.1	<i>IGBTs dimensioning</i>	80
8.5.2	<i>Diodes dimensioning</i>	84
8.6	ANALYSIS OF THE CONVERTER DESIGNS	86
8.6.1	<i>Frequency analysis</i>	87
8.6.2	<i>Flux analysis</i>	89
8.6.3	<i>Thickness analysis</i>	90
8.6.4	<i>Current density analysis</i>	92
8.7	OPTIMIZATION RESULTS	93
8.8	ANALYSIS OF THE CONVERTER DESIGN PERFORMANCE WITH THE EVOLUTION OF THE SEMICONDUCTORS	100

9	SIMULATION OF THE CONVERTER	103
9.1	CHECK-UP OF THE CONVERTER PERFORMANCE.....	103
9.2	COMPARISON OF THE CONVERTER WAVEFORMS	106
10	CONCLUSIONS.....	113
	REFERENCES	117
A	TRANSFORMER ANALYSIS.....	119
A.1	CURRENT DENSITY ANALYSIS	120
A.2	FLUX ANALYSIS	125
A.3	FREQUENCY ANALYSIS	128
A.4	THICKNESS ANALYSIS.....	128
A.5	LAYERS ON THE PRIMARY ANALYSIS	132
A.6	LAYERS ON THE SECONDARY ANALYSIS	134
B	MATLAB® CODES	137
B.1	MATLAB® CODE FOR THE ANALYSIS OF THE CONVERTER DEPENDING ON THE TRANSFORMER PARAMETERS	137
B.2	MATLAB® CODE FOR CONVERTER DATABASE	138
B.3	MATLAB® CODE FOR THE CONVERTER OPTIMIZATION	143
B.4	MATLAB® CODE FOR THE ANALYSIS OF THE TRANSFORMER	146

Chapter 1

Introduction

1.1 Problem background

Wind energy has become an important power source for instance in Europe, and wind farms are getting larger. Sometimes there are large windy regions far from a suitable grid connection point. The distances are so long that DC transmission could be better than the traditional AC transmission. If this will be the case, DC wind farms are getting interesting as power plants. In fact, some researches have shown the potential to provide low-priced energy of series connected DC wind parks.

This layout of wind farms requires a DC/DC converter located in each wind turbine to control the output voltage provided to system. This converter must manage the power differences between the turbines due to the uneven performance of the wind. The converter also must adjust the output voltage of the turbine to a level suitable for transmission.

The design of this converter present several issues, such as the choice of the most suitable topology, the dimensioning and shape of the transformer, or the selection of the semiconductor devices.

1.2 Overview of previous work

Studies of general wind parks can be found in [1, 2]. For detailed information about series connected DC wind farms and its control system [3] can be consulted.

About power electronic principles, applications and, in particular DC converters, a lot of information is presented in [5, 6, 7]. Furthermore, detailed data about an interesting converter topology, the full bridge isolated boost converter, can be found in [4].

The cost data for the converter components that were obtained from different manufacturers and presented, lack reference to manufacturers due to confidentially reasons. Based on these cost data, it was possible to obtain energy production cost values in [2].

In [8] useful information of schemes is given.

1.3 Purpose of the report

The purpose of this thesis is to investigate the performance of the DC wind turbine system, to develop and present a design of a DC/DC converter which can manage the requirements of the application. In addition, it was considered important to follow a complete design process, from the theoretical studies to the optimizations assisted by the computer. Finally, a goal was to present simulations from the selected design and compare these with the theoretical results from the study.

1.4 Layout of the report

In Chapter 2 the general principles of wind turbines are presented. Later on, the DC wind turbines are described.

In Chapter 3 some general concepts of wind parks are discussed. The layout of a series connected DC wind farm is presented and its characteristics illustrated. Finally, a short description of the control system of the DC wind farms is introduced.

In Chapter 4 the different topologies of suitable converters will be studied. First, the full bridge isolated boost converter is presented, followed by a presentation of the full bridge converter.

In Chapter 5 the transformer is defined, as well as the variables that affects its characteristics.

In Chapter 6 the selection of the most suitable DC/DC converter is complete. First, the specifications of the wind turbine are indicated. Next, the task of the converter is investigated and the two potential topologies are analyzed. At last, the two models are compared and the most appropriate is chosen.

In Chapter 7, the full bridge converter is theoretically studied, and the differential equations that describe its performance are derived. Furthermore, the converter waveforms from these equations are plotted. Finally, the influence of the transformer parameters on the converter design is studied.

In Chapter 8 the design for the specific application is accomplished. For that, the converter components are defined, and the design process is described and executed.

In Chapter 9 the design obtained is simulated in Pspice® to check that it satisfies the specifications. In addition, the waveforms obtained in the simulation are compared with those obtained in the theoretical analysis.

In Chapter 10, the conclusions are presented.

In Appendix A, the transformer performance is studied based on its variables.

In Appendix B the Matlab® codes used the thesis are presented.

Chapter 2

Principles of wind turbines

In this chapter, a short review of wind turbines will be presented. To start with, the general wind turbine and its operating principles will be described. Then, the variable speed DC wind turbines will be studied due to the fact that this is the kind of turbines that is of interest for this work.

2.1 General description of wind turbines and operating principles

A wind turbine is a device used to convert energy from the wind into electrical energy. The turbine consists of a tower, a nacelle, a rotor and a power train.

The rotor transforms some of the available wind energy into mechanical energy. The mechanical energy is transferred through the power train to the generator where it is converted in electricity. The power train consists of a shaft which connects the rotor to the gearbox which adapts the rotor speed to a rotational speed suitable for the generator.

Wind turbines reach their power rating at a specific wind speed. If the wind speed is lower, the available and thus, the produced power, is reduced. If the wind speed decreases below a minimum, the turbine will stop.

In case that the wind speed increases over the nominal value, the wind turbine rotor must limit the power transferred to the shaft. If the wind speed reaches exceptionally high values, the wind turbine will be disconnected, stopping the power production. In Figure 2.1 the output power of a wind turbine as a function of the wind speed is shown.

As mentioned before, the power transferred to the shaft must be limited. This can be done by controlling the efficiency of the conversion of the wind energy to mechanical energy. The efficiency of the conversion depends on several factors such as blade profile, pitch angle or tip speed ratio. The pitch angle (β) is the angle of the blades towards the rotational plane.

At the beginning, the stall control was the dominating concept. This method is based on that the blades are designed in such a way that the air flow becomes disturbed and in this way the efficiency will be reduced. This system is considered unfeasible for MW size turbines due to a very large brake in the primary shaft that is necessary.

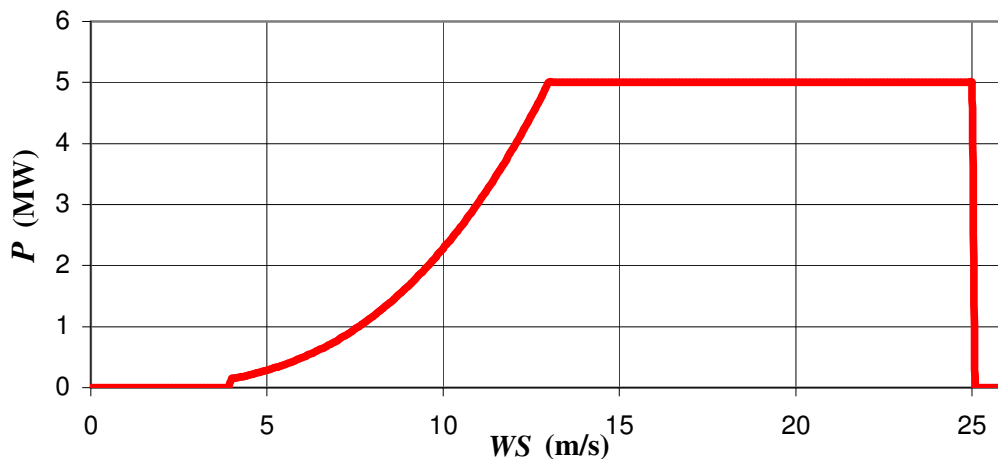


Figure 2.1: Wind turbine output power depending on the wind speed.

Two more advanced system of control are active stall control and pitch control, which are based on a mechanism able to vary the pitch angle. So, if the wind speed is low, the blades will be almost perpendicular to the wind, in order to obtain the maximum energy from it. However, if the wind speed is very high, the blades will stand almost in parallel with the hub direction to decrease the efficiency of the energy conversion of the rotor. In addition, a smaller brake can be installed because before breaking the turbine, the pitch angle can be regulated to reduce the driving torque and thus the rotor speed.

2.2 Variable speed DC wind turbines

The layout of this kind of wind turbine is presented in Figure 2.2. As can be seen, the generator is represented as an AC generator followed by a diode rectifier. The device that connects this rectifier to the general system is the DC/DC converter that is studied in this work.

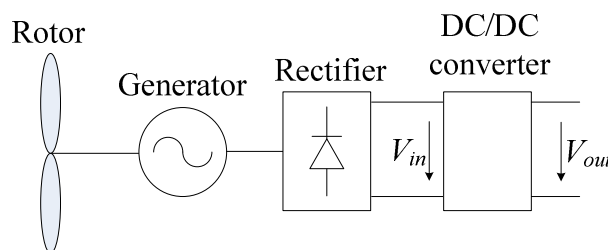


Figure 2.2: Scheme of a variable speed DC wind turbine.

From our point of view it is interesting to know how the rectified output voltage of the turbine behaves, because this signal will be the input voltage for our DC/DC converter. Accordingly, this voltage will be called V_{in} . This can be clarified in Figure 2.2.

In order to study this voltage, the generator of this kind of turbine is assumed to be a low speed permanently magnetized generator. This means that a model for a synchronous generator must be derived. For this model, the rotational speed of the generator is controlled so that the turbine is operating at its maximum efficiency; this control gives higher rotating speed if the wind speed increases. Nevertheless, as mention before, the upper rotating speed of the turbine is limited. To control the stator voltage, its amplitude is kept equal to the amplitude of the internal emf, due to the fact that this method utilizes the generator and converter best. For further details of this control [1] can be consulted. As a result, the output voltage of the generator, that is the input voltage to the converter (V_i), will performance as shown in Figure 2.3.

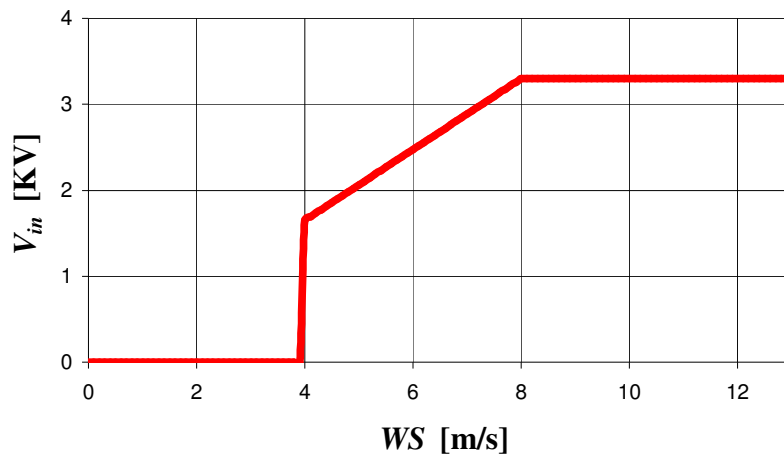


Figure 2.3: Converter input voltage (generator output voltage) depending on the wind speed.

Chapter 3

Layout of a series-connected DC wind farm

In this chapter, some general concepts of a wind park are presented. Later the series connected DC wind farm is described due to that this is the layout that is of interest for this work. Finally a short description of the control system of the DC wind farms is discussed.

3.1 General wind park concepts

A wind park consists of a group of wind turbines, a local wind turbine grid, a collecting point, a transmission system and a wind park interface to the PCC (point of common connection), as is seen in Figure 3.1.

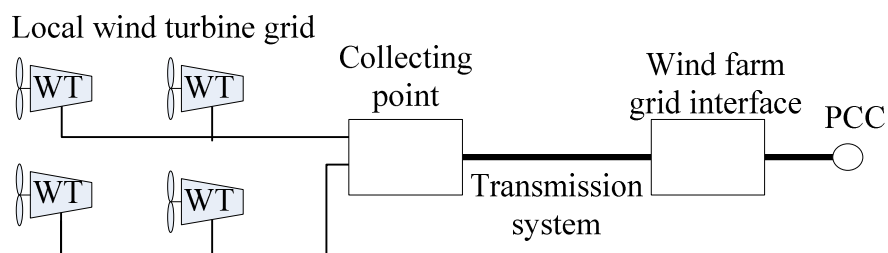


Figure 3.1: General wind park layout.

As mentioned in the previous chapter, the wind turbine converts part of the wind energy into electricity. The local wind turbine grid connects all the wind turbines to the collecting point, which is linked to the wind farm grid interface by the transmission system. There, the voltage, frequency, and the reactive power are adapted to be transmitted to the general system through the PCC.

Obviously, the rated power of the wind park will depend on the output power of the wind turbines and the number of turbines. Nowadays, several kinds of wind energy systems are available.

A wind park requires a large area, because the distance between the wind turbines in the wind direction must be long enough so that the wind recovers after passing through a previous turbine, due to when the air passes through the rotor of the wind turbine it gets very turbulent, and the wind speed decreases. Usually, this distance is above 5-7 rotor diameters. If the wind is mainly coming from one direction, the wind turbines can be placed closer in the direction perpendicular to the prevailing winds. This can be seen in

some wind parks placed in the south of Spain where the wind always comes from Africa, but in the Nordic countries, the wind direction can vary widely so the turbines must be placed with an equal distance in all directions.

3.2 Layout of a series connected wind farm with DC voltage output

The layout of a series-connected wind park is shaped by legs that contain n wind turbines connected in serial in order to provide the desired voltage level for transmission. In this chapter when we are talking about wind turbines, we consider the complete system: wind turbine, rectifier and DC/DC converter as shown in Figure 2.2. The legs are connected in parallel to increase the power level of the farm. A wind park formed by two legs with three turbines in each one is presented in Figure 3.2.

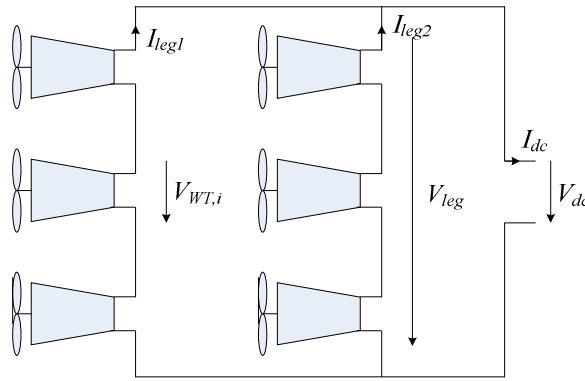


Figure 3.2: Layout of a series connected wind farm with DC voltage output.

In [2] the equations describing the system can be found as

$$I_{leg} = \frac{\sum_0^n P_{WT,i}}{V_{dc}} \quad (3.1)$$

$$V_{WT,i} = \frac{P_{WT,i}}{I_{leg}} \quad (3.2)$$

$$V_{dc} = \sum_0^n V_{WT,i} \quad (3.3)$$

Where:

- $V_{WT,i}$ Voltage of a specific wind turbine
- $P_{WT,i}$ Output power of a specific wind turbine
- V_{leg} Voltage of a leg
- I_{leg} Current of a leg
- V_{DC} Voltage of the wind farm
- I_{DC} Current of the wind farm

It can be noticed that if the number of turbines in a leg is high, the leg current is quite independent of the output power from one single turbine. So does Equation (3.2) can be expressed as

$$V_{WT,i} = P_{WT,i} \frac{\frac{\sum_0^n V_{WT,i}}{n}}{\frac{\sum_0^n P_{WT,i}}{n}} \quad (3.4)$$

Where:

$$\frac{\sum_0^n V_{WT,i}}{n} \quad \text{Average voltage of the turbines on the leg}$$

$$\frac{\sum_0^n P_{WT,i}}{n} \quad \text{Average power of the turbines on the leg}$$

Despite the fact that one single turbine output power will vary with the wind speed, the average power of the leg can be assumed to be fairly constant for a specific working situation if there is a large number of turbines in it. The voltage average, in a normal operating point, will be a value close to the wind turbine rated output voltage. So, it can be found that the output voltage of a single turbine (turbine, rectifier and DC/DC converter) will be

$$V_{WT,i} = kP_{WT,i} \quad (3.5)$$

Where k is the rated output voltage of one single wind turbine divided by the power average of the turbines in the leg.

So, when the leg is working in a specific point of operation, the average power of the turbines will be approximately constant, as well as the average voltage. In addition, the voltage over the leg will be fixed, controlled by the main local wind park transmission system. Now, if the wind speed of one wind turbine begins to decrease, the output power will decrease too. And, if we assume that the other turbines have not changed their power production, the average values of voltage and power will not be substantially changed. So, that means that the output voltage of the turbine will also begin to decrease, and this lack of voltage must be supplied by the other turbines in the leg, increasing their output power and, consequently, their output voltage.

This can easily be understood by an example:

Assume a leg that consists of 10 wind turbines. Each turbine is producing 2MW with 15kV of output voltage. The voltage over the leg is fixed at 150kV.

In this situation the average output voltage is 15kV and the average output power is 2MW. k will be

$$k = \frac{15}{2} = 7.5 \text{ MW / KV} . \quad (3.6)$$

Now, the output power of one turbine decreases to 1.5MW. To obtain the output voltage (3.5) will be used, assuming that the average values have not changed and, consequently k is constant.

$$V_{WT,i} = 7 \cdot 1.5 = 10.5 \text{ KV} . \quad (3.7)$$

So, the other nine wind turbines must increase their output voltage to supply the 4.5KV required to keep the voltage over the leg constant.

At last, the assumption of that k is kept constant must be checked. The new power average will be 1.95 MW and the new voltage average 14.55 KV. That leads to that the new k value will be 7.46 MW/KV. As can be seen the variation of the values is less than the 6% so the assumption can be accepted.

To conclude, it is necessary to be able to operate the wind turbines towards a little higher output voltage than the nominal V_{dc}/n .

Additionally, according to equation (3.5), the output voltage of a wind turbine will be proportional to the output power. And, as shown in Figure 2.1, it depends on the wind speed, so does; the output voltage will depend too. This relation can be seen in Figure 3.3.

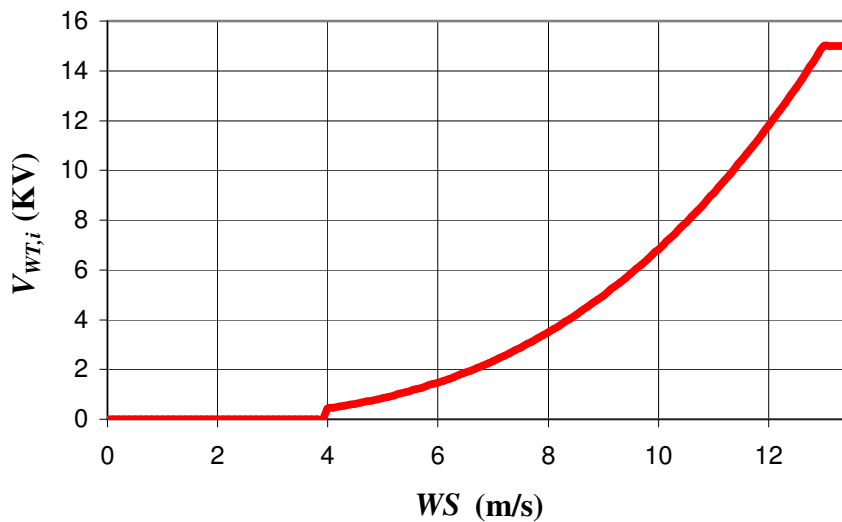


Figure 3.3: Wind turbine output voltage depending on the wind speed.

Note: In the next chapters, $V_{WT,i}$ will be named V_{out} , due to this will be the output voltage in the converter.

3.3 Control of the system

Due to uneven power production in a wind farm, there is a serious risk of having very high voltages over some specific turbines if they are connected in serial (if the production of several turbines in a leg decreases, the others must compensate it increasing their output voltage). It makes the controlling of a series-connected farm more difficult than the control of parallel-connected ones.

In order to operate the system the following controllers are needed:

- Main wind turbine controller
- Voltage controller
- Current controller

The scheme of these controllers can be seen in Figure 3.3.

The main wind turbine controller tries to obtain the maximum power from the wind when its speed is lower than the rated, and limits the power given if it exceeds the rated value. The way to do this is to control the current from the rectifier (i_{in}), since it is approximately proportional to the breaking torque of the generator. To control this current the controller generates a current reference to the current controller. The main controller also generates a pitch angle reference to the blades.

If the voltage over one turbine becomes too high, a special voltage controller overrides the main wind turbine controller. The control law for the voltage controller is obtained from the energy balance for the converter and acts when the output voltage reaches the over- or under-voltage limit by changing the switch for the input current reference to the current controller and generating a new one. This feature can be seen in Figure 3.3.

The current controller obtains its reference from the main controller or from the voltage controller and generates a voltage reference to the modulator. There the control signal to the converter is generated providing a suitable duty cycle of the converter and thus, controlling the relation between V_{out} and V_{in} by modifying the input current (i_{in}). More information about this control system can be found in [3].

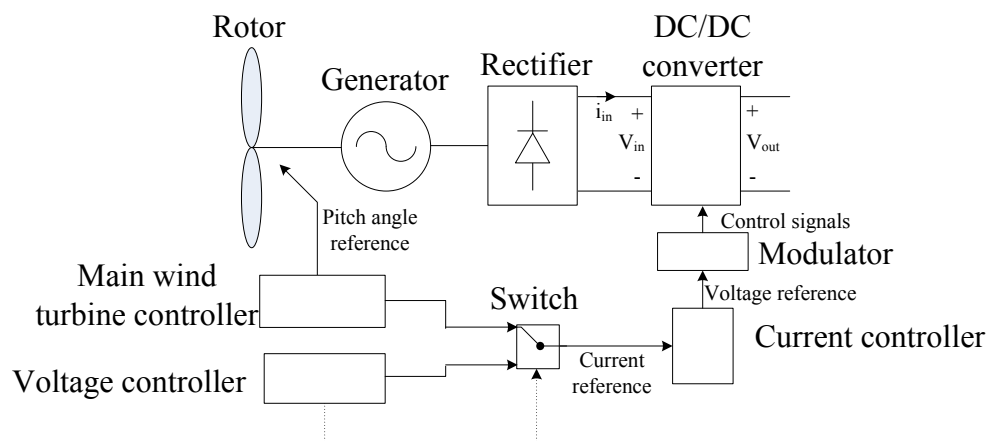


Figure 3.3: Control system of a wind turbine in a series-connected DC wind farm.

Chapter 4

Topologies of DC/DC converters

Here, the most suitable DC/DC converters for the studied wind turbine application will be described. This study will include a brief description of the operating mode, the most important plots, its advantages and drawbacks. It should be mentioned that in the analysis it is assumed that all the components are ideal and that the circuits are working in CCM (continuous current mode).

4.1 The full bridge isolated boost converter (FBIB)

The full bridge isolated boost converter is composed of a bridge of switches on the low voltage side, where the boost inductor are located, the transformer and a full-wave rectifier with a filter on the high voltage side, as shown in Figure 4.1.

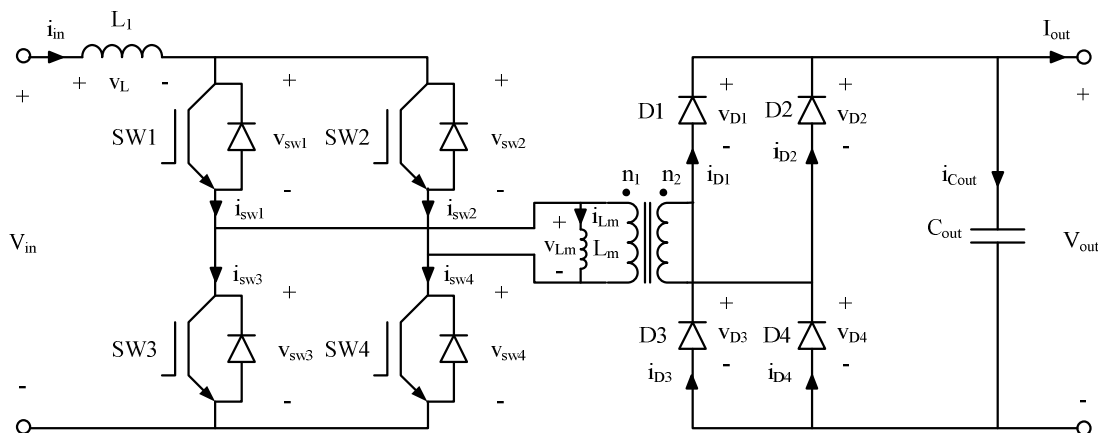


Figure 4.1: Full isolated boost converter circuit.

The operating principle of the circuit is based on shifting the energy between the inductor L_1 and the capacitor C_{out} . To do that, the circuit follows several steps.

First of all the inductor must be charged. For that, the four switches are turned on. In this manner, the transformer is short-circuited and over the coil a positive voltage drop that equals V_{in} appears. Due to the applied voltage, the current on the inductor increases linearly (i_{in}).

Next, SW2 and SW3 are switched off, removing the short-circuit over the primary of the transformer. This leads to that the current begins to flow through the primary side of the transformer and this leads to that current also appears on the high voltage side,

opening D1 and D4 and delivering energy to the output capacitor. Now, the voltage over the transformer is determined by a voltage equal to V_{out} that is transferred to the primary as $(n1/n2)V_{out}$ making a negative voltage drop to appear over the inductor, decreasing the input current.

Then, the four switches are turned on again, in order to reload the inductor as done in the first step.

After that, SW1 and SW4 are turned off generating a negative flux in the transformer. Now, a negative current will appear in the secondary, opening D2 and D4 and, of course, reloading the capacitor. As before, a negative voltage appears over the inductor reducing the input current again. All this events can be seen in Figure 4.2.

In order to find the currents, a volt-second balance calculation must be refined.

$$\frac{V_{in}t_{on}}{L} = \frac{(n1/n2)V_{out} - V_{in}}{L}t_{off} . \quad (4.1)$$

With the knowledge of

$$2t_{on} + 2t_{off} = T . \quad (4.2)$$

$$\frac{t_{on}}{T} = D . \quad (4.3)$$

The relationship between the voltages will be

$$V_{out} = \frac{n2}{n1} \frac{1}{1-2D} V_{in} . \quad (4.4)$$

And, assuming the power of the converter constant, the currents equation can be written as

$$I_{out} = \frac{n1}{n2} (1-2D) I_{in} . \quad (4.5)$$

As can be seen in (4.4), the maximum duty cycle is mathematically limited at $D=1/2$ since the equation would be equal infinite. The minimum output voltage will be limited by the winding ratio of the transformer. The minimum value equals $(n2/n1)V_{in}$.

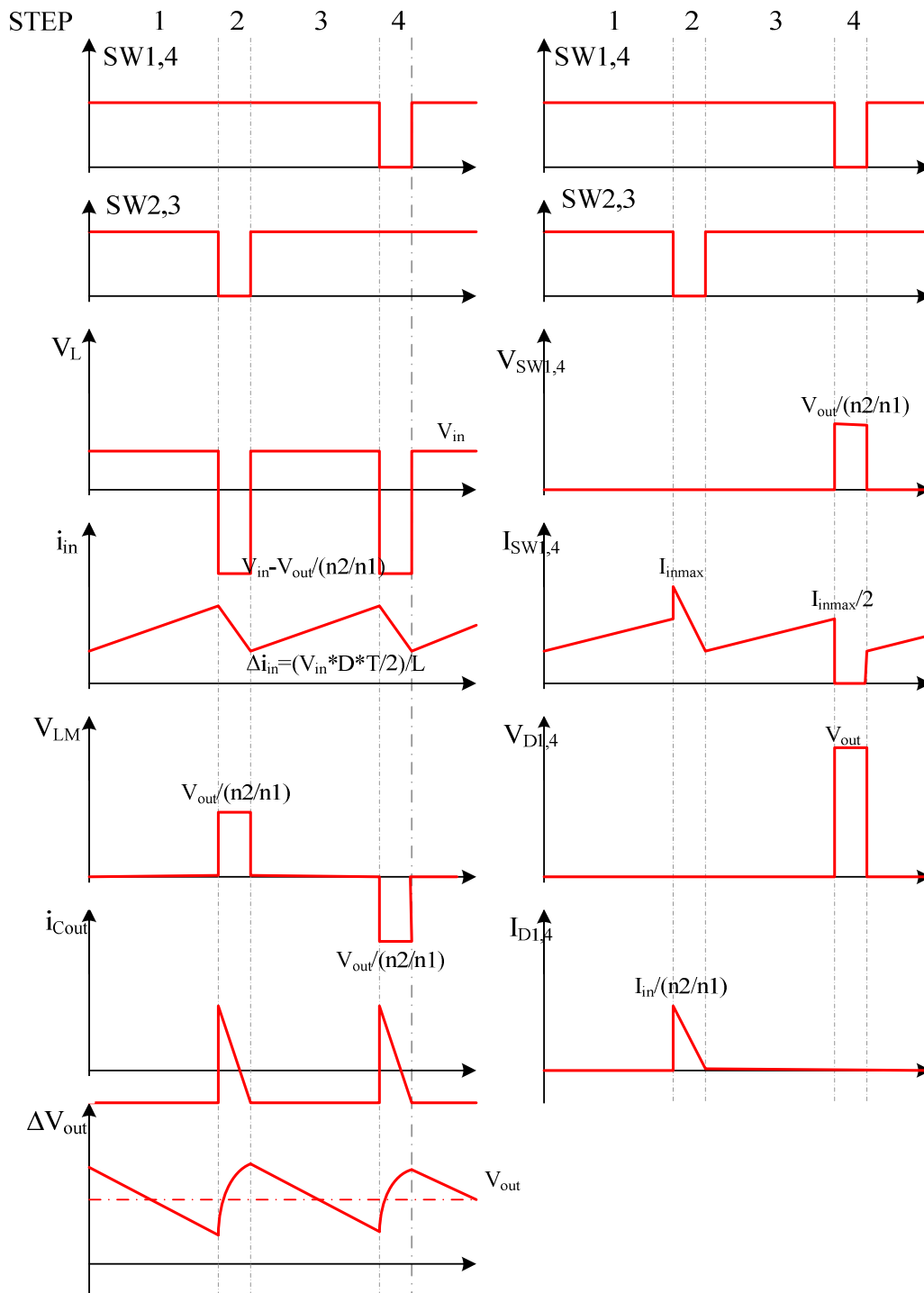


Figure 4.2: Idealized voltage and current waveforms of the full bridge isolated boost converter.

It should also be noticed that, if the output voltage is very low, it will not be possible to discharge the inductor and the input current will increase until the upper limit of the coil is reached, producing a failure in the converter. This situation can be seen in Figure 4.3.

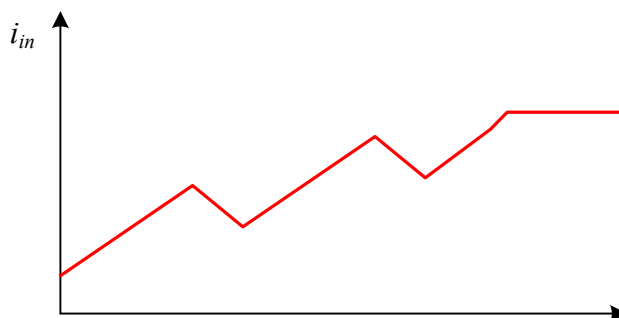


Figure 4.3: Effect of a too low output voltage on the input current in a FBIB converter.

If there is no volt-second balance on the primary of the transformer the magnetizing will increase and after a time it will be saturated. This situation can be eliminated by a current controller.

Studying the voltages over the diodes, it can be noticed that the maximum value will be V_{out} . This voltage will drop during step 4, when two of the diodes are conducting, for instance D2 and D3 and the two opposites are opened, as can be seen in Figure 4.4. It is not a serious problem because there exit diodes on the market that can manage the voltage levels we are operating at.

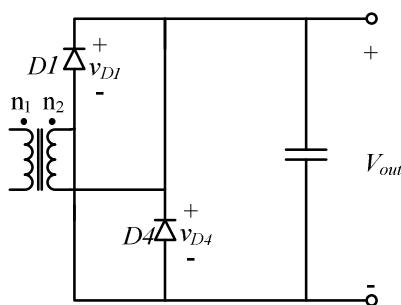


Figure 4.4: Equivalent circuit of high voltage side of the FBIB converter during step 4.

If the voltage over the switches is studied, its maximum value will be $V_{out}/(n_2/n_1)$. This will happen when two switches are disconnected (for example during step 4 for SW1 and SW4). In this situation, the low voltage side of the circuit can be plotted as in Figure 4.5, where the voltage drop over the switches can be noted. So, if the winding ratio of the transformer is low, quite high voltages will appear over them.

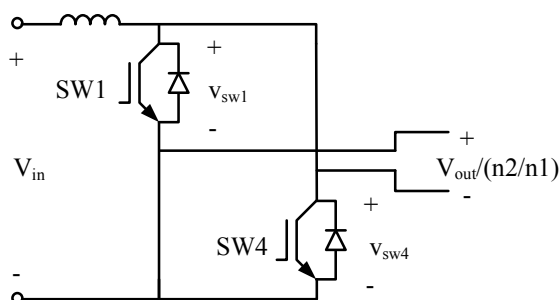


Figure 4.5: Equivalent circuit of low voltage side of the FBIB converter during step 4.

As a result, the advantages and drawbacks of this topology can be summarized as:

- ↑ Cheap design of the inductor due to that it is placed on the low voltage side.
- ↑ Low input current ripple because of the position of the inductor.
- ↑ Good utilization of the transformer with positive and negative flux.
- ↑ Cheap design of the output filter owing to the double frequency switching.
- ↓ High minimum output voltage.
- ↓ Risk of saturating the transformer.
- ↓ Quite high voltages over the switches on the low voltage side.

4.2 The full bridge converter (FB)

The full bridge converter shows a very similar topology to the FBIB, only the position of the inductor is changed, which is now placed on the high voltage side as shown in Figure 4.6.

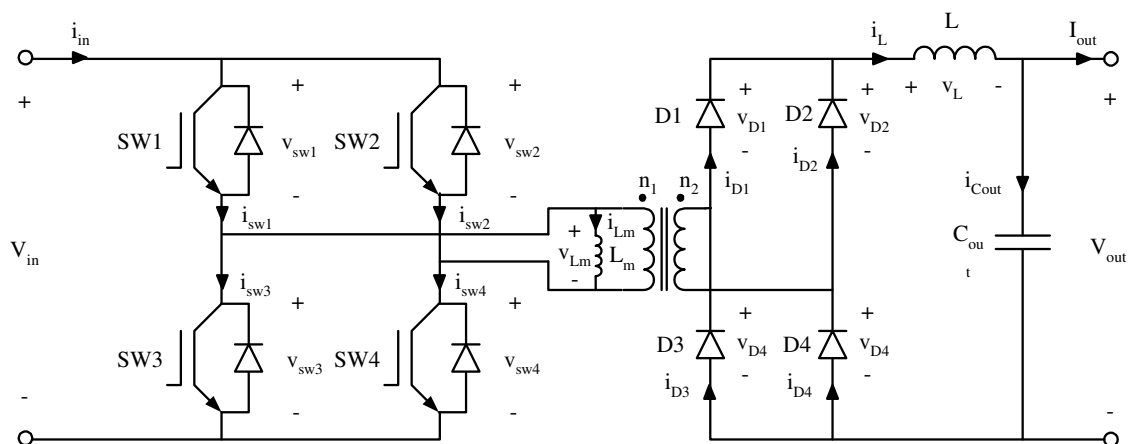


Figure 4.6: Full bridge converter circuit

The operating principle is based on transmitting the energy through the transformer to the inductor and, from that, to the output capacitor. In order to do that, several steps are performed.

In the first step, SW1 and SW4 are switched on. Due to that, a positive voltage appears over the transformer and an increasing current flow through it into the high voltage side, opening D1 and D4 and loading the inductor, which use part of the current to load the output capacitor.

Then, SW1 and SW4 are turned off. Now, the four diodes in the rectifier are opened by the inductor current and the secondary of the transformer is short-circuited. This short-circuit pass to the primary, holding the magnetizing current constant. By observing the high voltage side, it is noticed that in the inductor appears a negative voltage drop, decreasing the current through it.

Next, SW2 and SW3 are turned on, feeding out a negative voltage on the primary side of the transformer, which generates a negative current in the secondary side. That leads to the opening of D2 and D3 (keeping the others close), and then a positive voltage over the inductor is achieved again.

Finally, SW2 and SW3 are turned off again as in the second step. All the steps are shown in Figure 4.7.

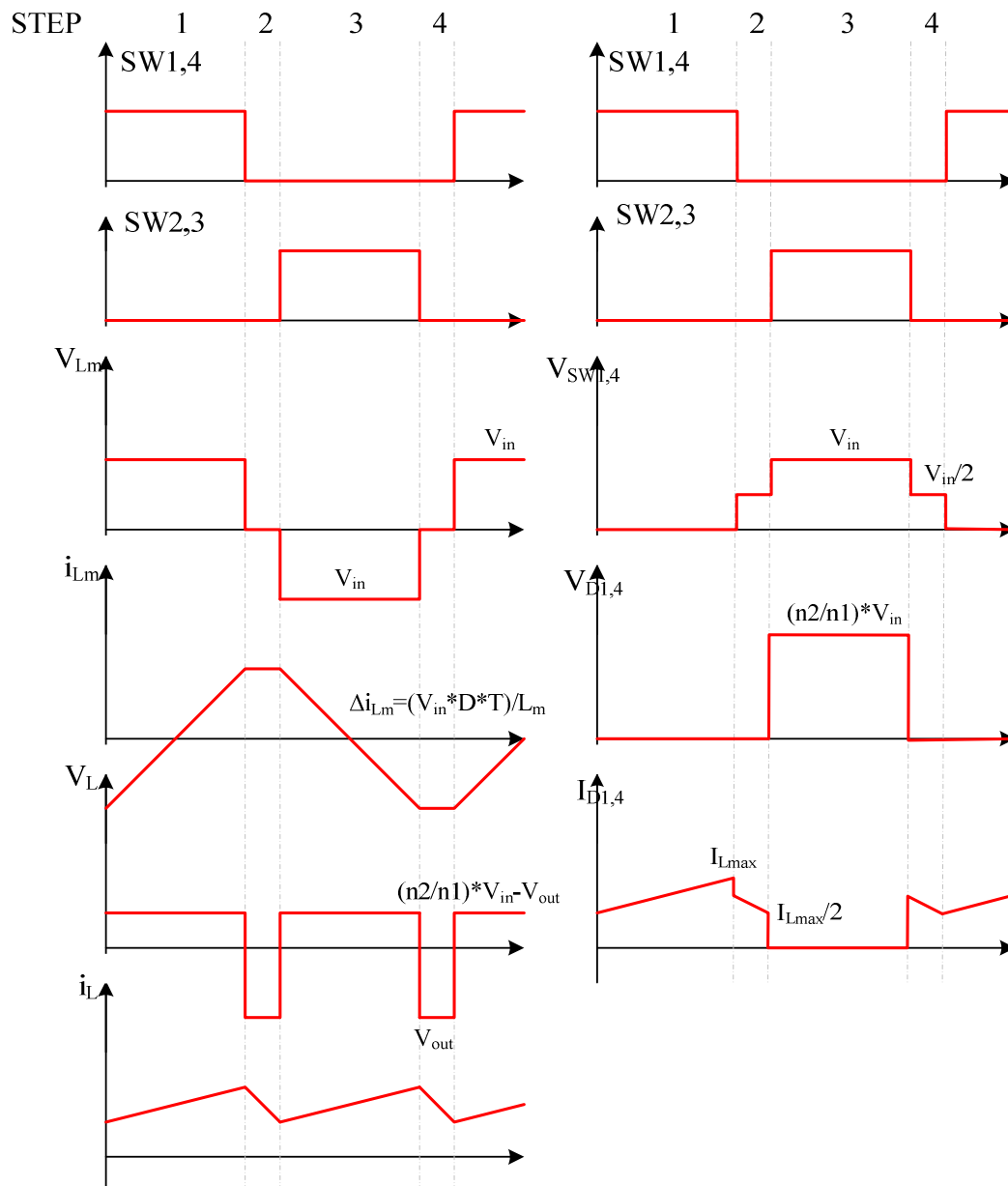


Figure 4.7: Idealized voltage and current waveforms of the full bridge converter.

It should be emphasized that the input current i_{in} will be the sum of i_{Lm} and $(n1/n2)i_L$. This current will depend on the values of the inductances.

In order to obtain the relationship between V_{in} and V_{out} , it is appropriate to use the volt-second balance of the inductor:

$$\frac{((n2/n1)V_{in} - V_{out})t_{on}}{L} = \frac{V_{out}t_{off}}{L} \quad (4.7)$$

That can be expressed as

$$V_{out} = 2 \frac{n2}{n1} D V_{in} \quad (4.8)$$

And the currents relationship assuming constant power

$$I_{out} = \frac{1}{2} \frac{n1}{n2} \frac{1}{D} I_{in} \quad (4.9)$$

It should also be noted that

$$2t_{on} + 2t_{off} = T \quad (4.10)$$

The maximum duty cycle is limited to a value that equals $\frac{1}{2}$.

Analyzing equation (4.8) it can be observed that the maximum output voltage will be the winding ratio of the transformer, and the minimum will be almost zero. However, if (4.9) is studied, it can be noticed that the input current will be the winding ratio times the output current, and if the voltage takes a very low value (with output power constant), the input current will be strongly increased.

Due to the anti parallel diodes of the switches, the leakage current of the transformer will have a path to return to the source, reducing the risk of saturating the transformer. Here it must be mentioned that the input current ripple will be quite high because the inductor now is located on the high voltage site.

When studying the semiconductor devices it can be seen that the maximum voltage over the switches will be V_{in} . This will happen when two switches are disconnected. For example, for SW1 and SW4 it will happen in step 3. In this situation, the low voltage side of the converter can be plotted as in Figure 4.8. However, the current that is passing through them will be quite high if the output voltage is low.

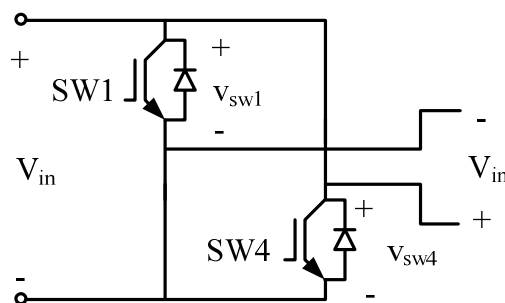


Figure 4.8: Equivalent circuit of the low voltage side of the FB converter during step 3.

The maximum voltage drop over the diodes will be $(n_2/n_1)V_{in}$. This will happen when only two of the diodes of the high voltage rectifier are conducting. Thus, for D1 and D4 this will happen in step 3. The equivalent circuit for the high voltage side of the transformer can be seen in Figure 4.9. This is a smaller problem than having this level of voltage over the controlled semiconductors, because it is easier to connect diodes in series than IGBTs. Despite of the fact that connecting semiconductors in series always is problematical.

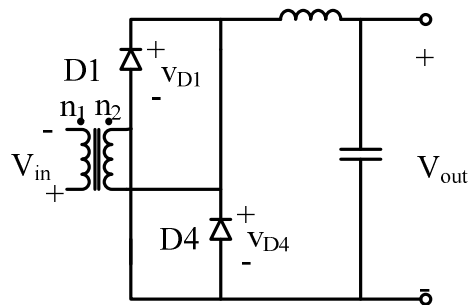


Figure 4.9: Equivalent circuit of the high voltage side of the FB converter during step 3

Finally, most important advantages and drawbacks of this topology are:

- ↑ The minimum output voltage can be as smaller than desired, allowing to a wide voltage range.
- ↑ Small voltage drop over the switches.
- ↑ Low risk of saturating the transformer.
- ↑ Good utilization of the transformer with positive and negative flux.
- ↑ Cheap design of the output filter due to the double frequency switching.
- ↓ Very high input current with low values of output voltage and large current ripple due to the position of the inductor.
- ↓ High current over the switches.
- ↓ Difficult design of the inductor because it is placed in the high voltage side.

Chapter 5

Definition of the transformer

Once the converter topologies have been studied, the converter transformer will be presented in this chapter. In order to do that, the electrical model of the transformer will first be presented, followed by the description of the real device that will be used in this work. Then, the important design variables will be commented and the chapter will finish with the definition of the transformer parameters and its equations.

5.1 Electrical model of the transformer

To model a transformer, several schemes can be used, depending on the grade of accuracy required. For this study the model chosen will consist of a leakage inductance in the primary that will represent the flux losses, a magnetizing inductance that will model the core material, and the resistances of the windings. With that, the electrical scheme of the transformer will be as presented in Figure 5.1.

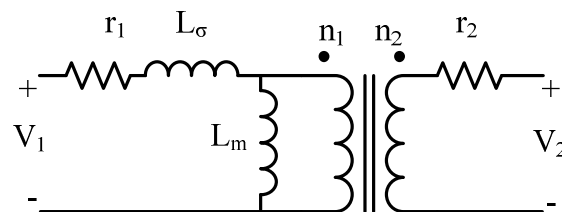


Figure 5.1: Electrical scheme of the transformer.

In addition, it must be considered that the transformer performance will tend to the ideal one if:

- $L_\sigma \rightarrow 0$
- $L_M \rightarrow \infty$
- $r_1, r_2 \rightarrow 0$

5.2 Description of the transformer and the design variables

Once the electrical model has been defined, the transformer will be defined as a real device in this section. For that, the first step must be to define the transformer shape. Following the advices of the Department of Power Electronics of Chalmers University of Technology, the chosen shape will present quite innovating features.

The transformer will be composed by two windings that will be disposed as a circumference and several U-cores that will cover them as can be seen in Figure 5.2. This means that, while in a standard transformer the windings are which rounds the core, in this case is the core which surrounds the wires.

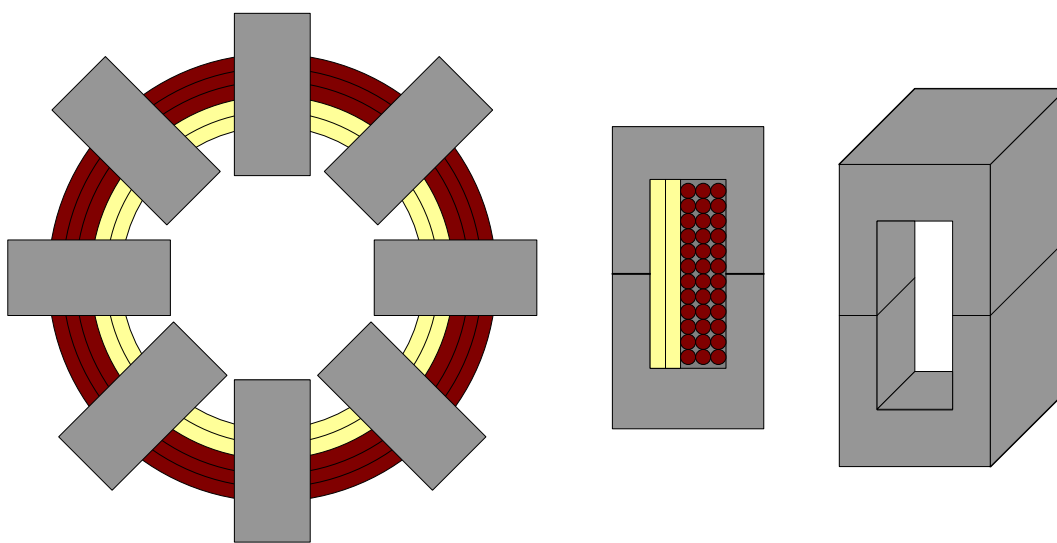


Figure 5.2: Transformer shape, core vertical section and a single U-core.

The primary winding will be manufactured using copper foils, and the secondary with cable.

The selection of cable is based on the requirement of a strong isolation due to the fact that the wind turbines will be disposed in serial, leading the cable to hold up not only the voltage level on one converter, but the voltage on the whole leg.

It must be emphasized that the special shape of the transformer is a consequence of the cable winding. Usually, an E-core is used, and the windings are rounded inside it. Nevertheless, as the cable cannot be turned as a conventional wire, the secondary winding will require very large turns. This means that most of the core would be wasted. A possible solution would be to separate the E-core in two U-cores, rolling the windings between them. Furthermore, if more U-cores are added in order to improve the flux path, it will lead to the shape described.

After the transformer has been presented, the variables we are able to modify in order to design the transformer and thus, the converter will be defined. These variables will be referred to as construction and operating variables.

In fact, to design the transformer for the converter, there will be two different kinds of variables.

The first group will be the construction variables, which are the core thickness and the layers on the windings. It can be noticed that all of them belong to the building features of the transformer.

The second group defines the operating point of the converter and will be composed by the current density, the core peak flux and the switching frequency.

Now, each variable of the first group is defined and commented:

- Core thickness: This variable represents the magnitude of thickness of the transformer core. This dimension will define the cross-section core area in the inner part of the core, which will depend on this thickness and in the cable diameter. Moreover, in order to simplify the core characteristics, the core will be designed in such a way that the cross-section will be constant, so the core thickness will define the core area of the transformer. The core thickness will also have a strong influence on the core volume.
- Layers on the primary: As was mentioned earlier, the primary winding will be manufactured with copper foils. The area of these foils will be determined by the current density, and their thickness limited by the skin effect as will be seen later. However, despite the area and that one of the dimensions are fixed, the height of the foils can be modified by dividing them in several parts that will be called layers. It must be noticed that it does not mean that we are increasing the number of turns in the primary, due to the layers of a specific turn are connected in parallel, and the different turns are connected in serial.

Therefore, if the height of the foils is the variable that determines the transformer height, increasing the number of layers (increasing also the width of the winding window) it can be decreased. This feature can be cleared in Figure 5.3, where a one-turn transformer is showed with one or various layers on the primary. It shall be noted that, in order to simplify the figure, the secondary winding has been omitted.

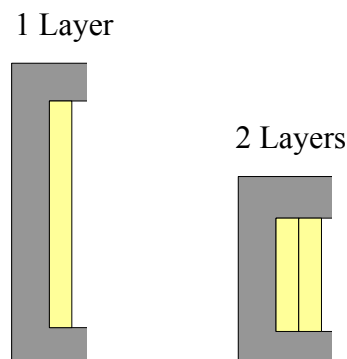


Figure 5.3: Effect of the layers on the primary on the transformer dimensions.

- Layers on the secondary: This variable determines the number of columns in which is disposed the secondary winding. Compared with the primary winding, here it is easier to divide the wires in several layers because, as each turn is small compared with the winding window, it is not necessary to divide the turns and connect them in parallel.

Obviously, the effects of this variable will be similar to that of the layers on the primary. So, it will be important for the transformer dimensions if the turns on the secondary are those that determine the winding height, and thus the transformer height. A scheme of how the secondary winding can be arranged in several layers is shown in Figure 5.4.

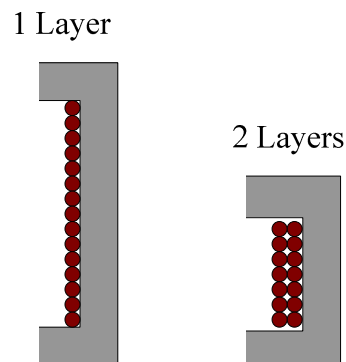


Figure 5.4: Layout of the secondary winding depending on the number of layers and its effect on the transformer dimensions.

The group of variables that define the operating point of the converter will be composed by:

- Current density: While the currents on the transformer will be fixed by the converter specifications, the current density will affect the size of the conductors areas. Controlling this variable directly, and knowing that the acceptable levels will be between 2 or 3 A/mm², it is not necessary to deal with a thermal analysis of the transformer. It must be noticed that, to simplify the design process, the same current density will be used for both windings.

As has been mentioned, the current density will affect directly the conductors areas, and thus the cable dimensions. As the turns radius depends on the cable diameter, the current density will affect it, and consequently the dimensions of the transformer. This variable will also influence the size of the winding area and thus the height of the transformer.

- Core peak flux density: This will be the flux density allowed in the transformer core. This variable will have a strong influence on the number of wires of the transformer, and will also affect the core losses as will be explained later.
- Switching frequency: This variable will have a substantial influence on the transformer performance, due to that it will be one of the factors that determines the number of turns, as well as the fact that it affects the skin effect and the core losses, as will be explained in the next section.

5.3 Definition of the transformer parameters

In order to be able to evaluate and design the transformer, it is necessary to calculate the constants that are derived from its features, and the important parameters must be studied.

The first issue that will be considered is the fact that the transformer shape will present some difficulties for the transformer design due to that we would obtain the same results with multiple solutions, depending on the number of cores used and their lengths. Thus, in order to analyze and design the transformer it will be simplified assuming that there will appear only one core that will present a toroidal shape and that will cover the complete winding. This new shape is presented in Figure 5.4. The transformer dimensions are summarized in Table 5.1.

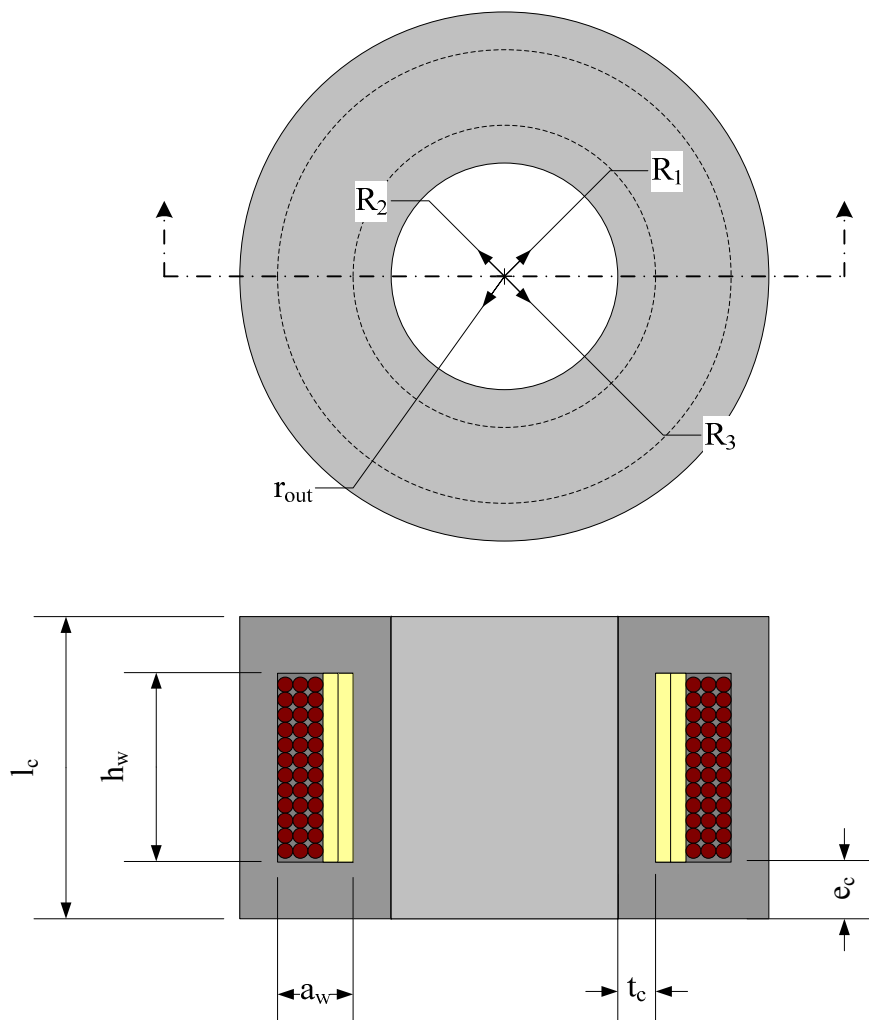


Figure 5.4: Simplified transformer shape and dimensions.

Table 5.1. Dimensions of the transformer.

Symbol	Dimension
R_1	Inner radius of the winding window
R_2	Inner radius of the core
R_3	Outer radius of the winding window
r_{out}	Outer radius of the core
a_w	Thickness of the winding window
h_w	Height of the winding window
l_c	Core height
t_c	Core thickness
e_c	Thickness of the core covers

In fact, this shape is exactly what we aimed of by disposing the U-cores as was described, and the only differences that will present compared with the real construction will be some leakage effects on the faces of the cores that will be neglected in this study.

Figure 5.4 also presents the dimensions of the transformer. It is important to mention the dimension t_c because, as was mentioned before, the transformer dimensions will depend on it.

Studying the windings, as was mentioned the primary one will be developed using copper foils. These foils will present a thickness low enough to allow neglect of the skin effect. In order to guarantee this, this dimension should be determined by

$$e \leq \delta = \sqrt{\frac{2\rho}{w\mu}}. \quad (5.1)$$

where:

- δ is the skin depth [m]
- ρ is the copper resistivity in [$\Omega \cdot m$]
- w is the switching frequency in [rad/s]
- μ is the copper magnetic permeability

It must be comment that to find more information about the skin effect [6] can be consulted.

To obtain the fill factor knowledge of the dimensions of the isolation is needed. It will be considered that the isolation thickness is about 1.5mm. With that the total foil area, in mm^2 , will be

$$T_{area} = (e + 3)(h_w + 3). \quad (5.2)$$

Where h_w is the height of the winding window.

The copper area will depend on the current density allowed. A reasonable value for that will be 2 A/mm^2 . It is also necessary to define the quantity of the current that will flow through the conductor. For the DC wind turbines investigated here, a realistic value would be about 1.5 kA. With that, the copper area mm^2 will be

$$A_{Cu1} = h_w e = \frac{I}{J} = \frac{1500}{2} = 750 \text{mm}^2. \quad (5.3)$$

Using (5.1) the thickness e can be obtained. The frequency used to obtain it will be 1000 Hz due to it is a reasonable value for the converter. For this frequency the maximum thickness is $e = 3.7 \text{mm}$.

With the thickness, h_w can be calculated from (5.3) obtaining a value of around 200mm.

At last, the fill factor can be obtained as

$$K_{Cu1} = \frac{A_{Cu1}}{T_{area}} = \frac{750}{(3.73+3)(200+3)} = 0.55. \quad (5.4)$$

It must be noticed that the fill factor will depend on the current, the current density and the frequency, but in order to simplify the design it will be considered to be constant.

As was explained, the secondary winding will be manufactured with cable due to the requirement of a high voltage isolation. For dimensioning this isolation, it will be supposed that the voltage on the leg will be about 170kV, and assuming that the cable isolation can hold up about 10kV/mm, the isolation thickness will be 17mm, that will be called r_{Is} .

In order to avoid the skin effect, the cable will be composed by several wires forming a Litz structure.

With that, the fill factor for the cable can be obtained. The copper area will be calculated for a current value around 330A, which will be a reasonable quantity for this kind of device. As before, the current density will be fixed at 2A/mm^2 . That leads to a copper area of

$$A_{Cu2} = \frac{I}{J} = \frac{330}{2} = 165 \text{mm}^2. \quad (5.5)$$

Due to the Litz structure, the conductor area will be larger than the copper area. The usual factor used in Litz wires is 0.75. This leads to a conductor area of

$$A_{Con} = \frac{A_{Cu2}}{0.75} = 220 \text{mm}^2. \quad (5.6)$$

From (5.6) the conductor radius can directly be obtained, arriving at a value of r_{Con} of 8.36mm.

The total area can be expressed as

$$T_{area} = \pi(r_{Con} + r_{Is})^2 = \pi(8.36 + 17)^2 = 2020mm^2 . \quad (5.7)$$

Using (5.5) and (5.6) the relation between the copper area and the cable area can be obtained, which will be called copper factor.

$$K_C = \frac{A_{Cu2}}{T_{area}} = \frac{165}{2020} = 8.2 \cdot 10^{-2} . \quad (5.8)$$

In addition, it must be considered that the cable has a round shape. This geometrical effect is studied in the literature. From [6] this round wire factor is between 0.5-0.7. So the cable fill factor can be calculated as

$$K_{Cu2} = K_{round} K_C . \quad (5.9)$$

Using (5.9) the cable fill factor will be between 0.04 – 0.057. In order to use a simple value, the fill factor that will be used for this study will be 0.05.

Once the transformer constants have been calculated, now the most important parameters must be defined. Basically, there will be three important groups: dimensions, inductances and losses. These groups will be studied in detail

5.3.1 Dimensions

In this group all the geometrical characteristics are included, as well as their relations. These parameters are very important because they will determine the materials and building costs of the transformer, and can limit the properties of it in order to obtain a reasonable compact design.

In order to begin to describe the transformer geometry, it is important to remember here that the cable size will affect the transformer dimensions, due to that the circumference of the windings will depend on the cable diameter. It is shown in the literature and in several practical experiences that the minimum radius of curvature for turning a wire is 10 times its diameter. Thus, the windings circumference will be determined by this parameter. Moreover, the inner radius of the winding window (R_1) will be designed to fit with this requirement, leading to

$$R_1 = 10D_{cable} . \quad (5.10)$$

Where the cable diameter is two times the sum of the conductor radius plus the isolation radius.

$$D_{cable} = 2(r_{Con} + r_{Is}) . \quad (5.11)$$

As the conductor radius is derived directly from the copper radius, which in turn is derived from the copper area, this parameter will depend inversely on the current density allowed in the cable.

The second dimension that is derived directly from a construction variable is the core thickness.

By using R_1 and t_c , the inner radius R_2 can be calculated as

$$R_2 = R_1 - t_c . \quad (5.12)$$

And, knowing that the cross-sectional core area is a crown, the equation that provides it can be found as

$$a_c = \pi(R_1^2 - R_2^2) . \quad (5.13)$$

Next, the number of turns on the primary can be obtained. It must be notice that this will be one of the most important design parameters, due to that it will have a strong influence on the transformer dimensions, as well as on the losses and inductances.

To determine this volume, the following equation can be used

$$\hat{V}_1 = N_1 a_c \left| \frac{dB}{dt} \right|_{\max} . \quad (5.14)$$

Further information about (5.14) can be found in [6].

To obtain the maximum of the derivate of the flux density, the voltage on the primary of the theoretical converter can be studied, since it will be related to the core flux as

$$V_1 = N_1 \frac{d\phi}{dt} . \quad (5.15)$$

In addition, if it is assumed that the flux in the core is uniform, the flux density can be expressed as

$$V_1 = N_1 a_c \frac{dB}{dt} . \quad (5.16)$$

From here, the full bridge will be analyzed. The same arguments could also be used to analyze the FBIB

If the magnetizing voltage waveform of Figure 4.7 is studied, and realizing that the derivate of the flux will depend on the area under the voltage signal, the number of turns will be found as

$$N_1 = \frac{V_1 t_{on}}{2 a_c B} . \quad (5.17)$$

This expression can be developed by knowing that $t_{on} = DT$ and using (4.8) to

$$N_1 = \frac{V_{out}}{4a_c \hat{B} f \frac{n_2}{n_1}}. \quad (5.18)$$

Once the number of turns on the primary has been determinate, the turns on the secondary can easily be obtained by

$$N_2 = \frac{n_2}{n_1} N_1. \quad (5.19)$$

With the number of turns, the winding area can be calculated using

$$A_w = N_1 \frac{A_{Cu1}}{K_{Cu1}} + N_2 \frac{A_{Cu1}}{K_{Cu1}}. \quad (5.20)$$

Where A_{Cu1} and A_{Cu2} are the copper areas that were described before and K_{Cu1} , K_{Cu2} the filling factors for the windings.

The winding width a_w can be obtained using

$$a_w = ns_1 e N_1 + ns_2 D_{cable}. \quad (5.21)$$

Where ns_1 and ns_2 are the number of layers in the primary and in the secondary respectively, and e the foil thickness determined by the skin effect.

The next parameter that can be calculated is h_w . This will be the highest of three different values that fits different requirements.

First, h_w must be higher enough to shelter the primary foils. The equation which satisfies that is

$$h_{w1} = \frac{A_{Cu1}}{ns_1 e}. \quad (5.22)$$

The second value comes from the necessity of fitting the windings in the winding area.

$$h_{w2} = \frac{A_w}{a_w}. \quad (5.23)$$

The last value guarantees that the height of the secondary winding will fits with the height of the winding window.

$$h_{w3} = \frac{N_2 D_{cable}}{ns_2}. \quad (5.24)$$

Due to that these values depend on multiple variables it is difficult to guess which one will determine the final value of h_w . Nevertheless it can be observed that, if the number of turns increases, h_{w2} and h_{w3} will increase while h_{w1} will not be affected. In addition, it can be noticed that in the three cases if the number of layers on the windings increases, the winding height will be reduced and thus the total height.

With these winding dimensions, the outer core dimensions can be obtained. First, R_3 can be calculated from

$$R_3 = R_1 + a_w. \quad (5.25)$$

The outer core radius will be defined in such a way that the core area along the entire flux path is kept constant. To guarantee it, the outer circular crown must satisfy

$$a_c = \pi(r_{out}^2 - R_3^2). \quad (5.26)$$

Where the outer radius can be isolated as

$$r_{out} = \sqrt{\frac{a_c}{\pi} + R_3^2}. \quad (5.27)$$

Using the constant core area condition, e_c can be derived from

$$e_c = \frac{a_c}{2\pi r_1}. \quad (5.28)$$

Where r_1 is the radius of the middle of the winding area and can be described as

$$r_1 = R_1 + \frac{a_w}{2}. \quad (5.29)$$

It must be noticed that Equation (5.28) is a simplification due to that this transverse core area will increase with the radius if the thickness (e_c) is kept constant. This means that from R_1 to r_1 the core area will be smaller than the value obtained in (5.13), but it will be compensated because from r_1 to R_3 the core area will be larger.

With that, the total height of the transformer can be determined using the expression

$$l_c = h_w + 2e_c. \quad (5.30)$$

Finally, two more parameters can be calculated related with the dimensions. The first one is the average flux path that will be useful to analyze the transformer inductances. This flux path can be expressed as

$$l_{path} = 2(a_w + h_w) + t_c + 2e_c + (r_{out} - R_3). \quad (5.31)$$

The last dimension parameter is the core volume that will be necessary to determine in order to be able to obtain the core losses and cost. The core volume is found as

$$V_c = \pi \left((r_{out}^2 - R_2^2) l_c - (R_3^2 - R_1^2) h_w \right). \quad (5.32)$$

5.3.2 Inductances

The second group of design parameters will be the values of the inductances that are used to model the transformer, the leakage and the magnetizing one.

The leakage inductance arises from the fact that the magnetic flux that does not completely link the primary and secondary windings, or does not link all the turns in the winding that generates flux. The value that will be calculated here comes from the flux lost in the winding window, as can be seen in Figure 5.5.

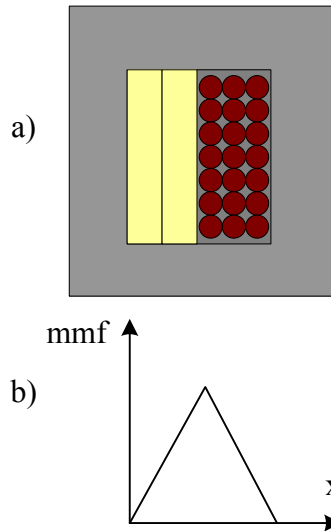


Figure 5.5: a) Winding window of the transformer. b) Mmf distribution versus position.

The technique to determine the leakage inductances is explained in detail in [6] and is based on the equation

$$\frac{1}{2} L_{\sigma} I_1^2 = \frac{1}{2} \int_{V_w} \mu_0 H^2 dV. \quad (5.33)$$

Where V_w is the winding volume. This volume can be estimated as the winding area times the turn length (the length of the windings circumference). So, the volume differential can be calculated as

$$dV = l_w h_w dx. \quad (5.34)$$

The H field, as is shown in Figure 5.5, can be expressed as

$$\begin{cases} H = \frac{2N_1 I_1 x}{h_w a_w} \longrightarrow 0 < x < \frac{a_w}{2} \\ H = \frac{2N_2 I_2}{h_w a_w} \left(1 - \frac{x}{a_w}\right) \longrightarrow \frac{a_w}{2} < x < a_w \end{cases} \quad (5.35)$$

It must be noticed that, in (5.35) it is assumed that each winding fills one half of the winding area.

With that, and using that $N_1 I_1 = N_2 I_2$, the leakage inductance can be calculated from

$$L_\sigma = \frac{2}{I_1^2} \int_0^{a_w/2} \mu_0 \left(\frac{2N_1 I_1 x}{h_w a_w} \right)^2 l_w h_w dx. \quad (5.36)$$

The result is that the leakage inductance can be expressed as

$$L_\sigma = \frac{\mu_0 N_1^2 l_w a_w}{3 h_w}. \quad (5.37)$$

From (7.53) some conclusions can be inferred:

- If $N_l \uparrow$ the leakage inductance grows squared.
- If $a_w \uparrow$ the inductance increases.
- If $h_w \uparrow$ the inductance decreases.

So, a good transformer from the leakage inductance point of view would be one which presents a low number of turns, a tall core and a thin winding window.

The second important inductance will be the magnetizing inductance, which models the magnetization of the core material, and relates the core flux with the magnetizing current.

The equation used in this study to define the magnetizing inductance has been directly obtained from [7].

$$L_M = \frac{\mu_0 \mu_r N_1^2 a_c}{l_{path}}. \quad (5.38)$$

Where μ_r is the relative permeability of the core material.

(5.38) shows that the magnetizing inductance will grow if the number of turns and the core area are increased, that means that a wide core will be required. In addition, the inductance will be decreased if the flux path is long, that leads to a reduction of the height of the transformer (that depends on h_w) and the thickness of the winding window, as (5.30) defines.

Therefore, a good transformer for the magnetizing inductance will be one which presents a high number of turns, a wide core and a short and thin winding window.

It is interesting to compare the characteristics that would present the transformer to be fine from the inductances points of view. It is seen that a high number of turns will increase the value of the magnetizing inductance, which approach the design of an ideal transformer. Nevertheless, increasing N_I leads to an increment in the leakage inductance, which will deteriorate the performance of the transformer. To conclude, an intermediate solution must be reached. The same argument can be hold regarding to the winding length.

5.3.3 Losses

At last, the transformer losses will be one of the most important design parameters, due to that it will always be of interest to reduce the losses as much as possible. Nevertheless, to obtain the minimum losses, the transformer would request very expensive materials to be used or very big sizes, so, as before, it is usual to aim for an intermediate solution.

The transformer losses can be divided in two parts; the windings losses and the core losses.

The windings losses are estimated modelling the windings as resistances, and calculating the power dissipated on them.

To obtain the value of the resistance the equation that should be used is

$$R = \frac{\rho l}{A} . \quad (5.39)$$

Where:

- ρ Copper resistivity.
- l Wire length.
- A Wire area.

And the equation that determines the power dissipation in a resistance can be expressed as

$$P_R = RI^2 . \quad (5.40)$$

Where I is the current through the resistance.

For that case, the wire length for the primary winding will be the length of one turn times the number of turns, and the wire area will be directly the copper area

$$l = lwN_1. \quad (5.41)$$

$$A = A_{Cu1}. \quad (5.42)$$

With that, the power dissipated in the primary winding will be

$$P_{W1} = \frac{\rho l_w N_1}{A_{Cu1}} I_1^2. \quad (5.43)$$

That can be expressed in terms of the density current as

$$P_{W1} = \rho l_w N_1 A_{Cu1} J_1^2. \quad (5.44)$$

Using the same argument, the losses in the secondary winding will be

$$P_{W2} = \rho l_w N_2 A_{Cu2} J_2^2. \quad (5.45)$$

The core losses can be estimated using the data tables of the material manufacturer, which provides the density losses as a function of the core flux and the frequency. The typical performance of this equation is

$$p_{core} = K f^a B^d. \quad (5.46)$$

Where K , a and d are constants of the material.

With that, the losses of the core can be obtained by multiplying (5.46) times the core volume.

$$P_{core} = K f^a B^d V_c. \quad (5.47)$$

Thus, the total transformer losses will be the sum of the two windings losses plus the core losses. The final result is found as

$$P_{transformer} = K f^a B^d V_c + \rho l_w N_1 A_{Cu1} J_1^2 + \rho l_w N_2 A_{Cu2} J_2^2 \quad (5.48)$$

At last, it must be commented that in Appendix A, a thorough analysis of the transformer parameters depending on the variables described can be found.

Chapter 6

Analysis of the different topologies for the studied wind turbine application

In this chapter, the selection of the most suitable DC/DC converter for the studied application will be done.

First of all, the specifications of the wind turbine will be presented. Next, the task of the DC/DC converter will be studied and later the two topologies presented in the previous chapter will be analyzed. At last, the two models will be compared and the most appropriate will be chosen.

6.1 Specifications of the wind turbine

As mentioned in chapter 2, in this work variable speed DC wind turbines will be used. These wind turbines, will have a power rating of 5 MW, reached at a wind speed of 13 m/s. The wind turbine will operate down to a wind speed of 4 m/s; below this value the turbine will stop. The upper wind speed limit will be 25 m/s. Above this the turbine will also stop. Figure 2.1 describes all this features.

To summarize:

$$\left\{ \begin{array}{ll} \text{if } WS < 4 \text{ m/s} & \rightarrow P = 0MW \\ \text{if } 4 < WS < 13\text{m/s} & \rightarrow P = kWS^3 \\ \text{if } 13 < WS < 25\text{m/s} & \rightarrow P = 5MW \\ \text{if } WS > 25\text{m/s} & \rightarrow P = 0MW. \end{array} \right. \quad (6.1)$$

Where:

P	Output power of the wind turbine [MW]
WS	Wind speed [m/s]
k	Constant equal 2.27 [KW/ (m/s)]

For this application, it is necessary to know how the rectified output voltage of the turbine behaves, because this will be the input voltage for the converter, as shown in Figure 2.2.

The selected turbine has a rating rectified output voltage of 3.3KV, reached at a wind speed of 8 m/s. The equation that summarizes it can be found as

$$\begin{cases} \text{if } WS < 4 \text{ m/s} & \rightarrow V_{in} = 0KV \\ \text{if } WS = 4 \text{ m/s} & \rightarrow V_{in} = 1.66KV \\ \text{if } 4 < WS < 8\text{m/s} & \rightarrow V_{in} = k'WS \\ \text{if } WS > 8\text{m/s} & \rightarrow V_{in} = 3.3KV. \end{cases} \quad (6.2)$$

Where:

$$\begin{array}{ll} V_{in} & \text{Converter input voltage [KV]} \\ WS & \text{Wind speed [m/s]} \\ k' & \text{Constant equal } 0.41 \text{ [KV/ (m/s)].} \end{array}$$

Here, it must be noticed that the minimum input voltage will be $\frac{1}{2}$ of the rated value. The plot of this voltage can be checked in Figure 2.3.

At last, knowledge of how the output voltage specifications of the complete wind turbine system (wind turbine, rectifier and DC/DC converter) is required, assuming that it will be operating in a series-connected DC wind farm.

For the studied system, the output voltage can be expressed as

$$\begin{cases} \text{if } WS < 4 \text{ m/s} & \rightarrow V_{out} = 0KW \\ \text{if } 4 < WS < 13\text{m/s} & \rightarrow V_{out} = k''WS^3 \\ \text{if } WS > 13\text{m/s} & \rightarrow V_{out} = 15KV. \end{cases} \quad (6.3)$$

Where:

$$k'' \quad \text{Constant equal } 6,8 \cdot 10^{-3} \text{ [KV/(m/s)]}$$

This was shown in Figure 3.3.

6.2 Task of the DC/DC converter

As is observed in Figure 2.2 the DC/DC converter will be located between the rectifier and the leg connection. So, it must provide the suitable output voltage to the leg independently of the voltage from the rectifier.

In an ideal case, the output voltage should be the rated value. But, as mentioned in Chapter 3, if the wind speed over one turbine decreases, its output voltage will be lower than the average one, and the other turbines must be able to increase their voltage in order to hold the leg voltage constant.

So, for the dimensioning of the converter, we must assume that the maximum output voltage must be somewhat higher than the rated one. In [2], an overrating of 1.35 is found to be appropriate and is the one used here. This means that each wind turbine converter should be able to supply

$$V_{out,max}=1.35V_{out,rated}. \quad (6.4)$$

In our case, knowing that the $V_{out,rated}$ is 15kV, the maximum voltage should be

$$V_{out,max}=20.25kV. \quad (6.5)$$

Lets us now continue by studying the minimum output voltage. Observe that there does not exist studies about which would be the optimum value. We will dimension the converter for two different values

$$V_{out,min1}=0.65 V_{out,rated}. \quad (6.6)$$

$$V_{out,min2}=0.3 V_{out,rated}. \quad (6.7)$$

For our study that means

$$V_{out,min1}=9.75kV. \quad (6.8)$$

$$V_{out,min2}=4.5kV. \quad (6.9)$$

The input voltage of the converter (V_{in}) will depend on the wind speed. As shown in (6.2) the voltage reaches its rated value at 8 m/s, decreasing linearly with the wind speed until 4 m/s where it takes about $\frac{1}{2}$ of the rated value. Below this wind speed the turbine stops.

For our converter, these values will be

$$V_{in,rated}=3.3kV. \quad (6.10)$$

$$V_{in,min}=1.65kV. \quad (6.11)$$

Finally, as mentioned before, the input power supplied by the turbine will also depend on the wind speed, reaching its rated value (5MW) at 13m/s. As the wind speed is reduced, the power drops approximately with the cube of the wind speed until it reaches 4m/s, where the turbine stops, as was shown in equation (6.1).

6.3 Study of the DC/DC converter topologies proposed

In this section the worst operating point for the converters in the studied application will be analyzed. Then, in order to compare both topologies, a first estimation of the most important parameters will be performed.

6.3.1 Full bridge isolated boost (FBIB) topology

As it was studied before, the FBIB will not present problems to fit the maximum output voltage. Nevertheless, the minimum value will be limited by the winding ratio of the transformer. Due to that, this parameter will depend on it. Also, the winding ratio will have an effect on the voltage drop over the switches.

The worst operating point for this topology will occur when the minimum output voltage is required and the input voltage is the maximum value. It must be noticed that the maximum input voltage in the wind turbine studied will coincide with the rated, as can be checked in (6.2).

This situation would happen when the wind turbine is working at its rated voltage and the leg request to the converter the minimum value. It will occur when the other turbines in a leg are providing more voltage than the rated.

The worst situation for the input current will happen when the turbine is producing the rated power.

With this, the converter model can be designed. In this basic model the only design parameter will be the winding ratio of the transformer, because the inductor and the capacitor design will depend on the switching frequency, as will be studied later.

To start with, the maximum boost of the converter must be considered because in theory it would be infinite. A value of 10 seems to be appropriate.

Then, the output voltage range must be defined. As was commented in the previous section, it will be designed using two different minimum output voltages. At last, the values will be

$$V_{out,max}=20.25kV. \quad (6.12)$$

$$V_{out,rated}=15kV. \quad (6.13)$$

$$V_{out,min1}=9.75kV. \quad (6.14)$$

$$V_{out,min2}=4.5kV. \quad (6.15)$$

Considering the worst situation described before, and using (4.4), the equation that expresses the input voltage necessary to satisfy the output voltage requirements is

$$V_{in,rated} = \frac{n1}{n2} V_{out,min}. \quad (6.16)$$

The equation describing the input current can be found as

$$I_{in} = \frac{P}{V_{in,rated}}. \quad (6.17)$$

In (6.17) it can be seen that, as mentioned before, the worst point of operation will be when P is at its maximum value, which is the rated one.

For the voltage drop over the switches the relationship will be

$$V_{SW,max} = \frac{n1}{n2} V_{out,max} . \quad (6.18)$$

Notice that the worst situation for the switches will occur when the converter is providing its maximum output voltage.

The voltage over the diodes, as was studied in the previous chapter, will be directly the output voltage; so, its worst case will be when it reaches the maximum value.

Another important parameter to study is the boosting of the converter in order to check that it is not exceeding the maximum value. The equation that governs this parameter is

$$Boost_{max} = \frac{V_{out,max}}{(n2/n1)V_{in,min}} . \quad (6.19)$$

If this expression is combined with (6.2), the following result is found

$$Boost_{max} = \frac{2V_{out,max}}{(n2/n1)V_{in,rated}} . \quad (6.20)$$

At last, the rated duty cycle will be investigated to check that it is in the correct range. It can be done using

$$D_{rated} = \frac{1}{2} \left(1 - \frac{(n2/n1)V_{in,rated}}{V_{out,rated}} \right) . \quad (6.21)$$

All these parameters can be estimated depending on the winding ratio of the transformer. Two studies will be done depending on the minimum input voltage chosen. These features can be seen in Figures 6.1 and 6.2

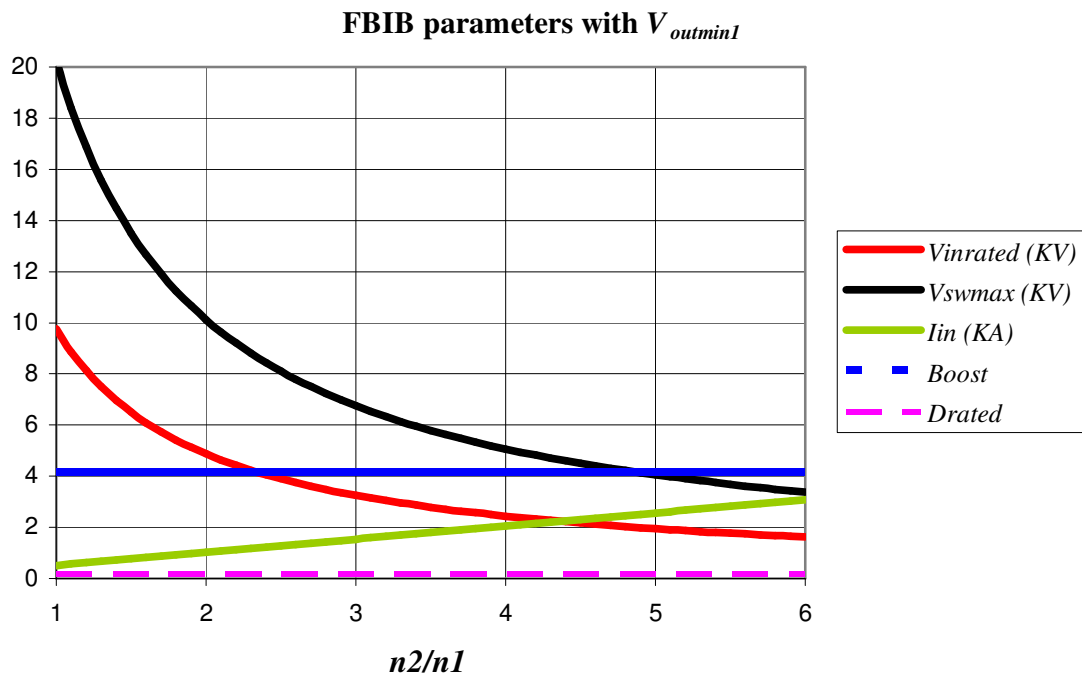


Figure 6.1: Parameters of FBIB model depending on the winding ratio of the transformer for $V_{out,min1}$.

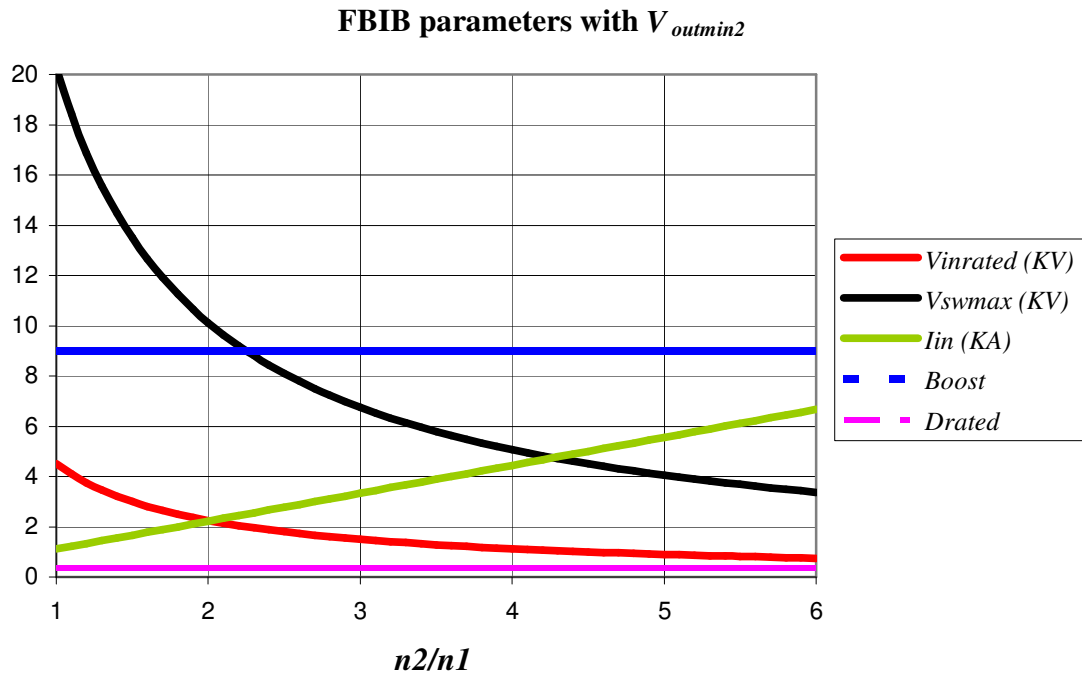


Figure 6.2: Parameters of FBIB model depending on the winding ratio of the transformer for $V_{out,min2}$.

If the less restrictive minimum output voltage was considered, Figure 6.1 shows that the better value for the winding ratio of the transformer (n_2/n_1) would be between 3 or 4. The values of the parameters for these winding ratios are presented in Table 6.1.

Table 6.1: FBIB parameters depending on the winding ratio for $V_{out,min1}$.

n_2/n_1	$V_{in,rated}$ (kV)	I_{in} (kA)	$V_{SW,max}$ (kV)	$Boost_{max}$	D_{rated}
3	3.25	1.54	6.75	4.15	0.175
3.5	2.78	1.79	5.78	4.15	0.175
4	2.44	2.05	5.06	4.15	0.175

The topology presents two important drawbacks. First; the circuit requires a small input voltage to supply the minimum output voltage, and the voltage over the switches is too large. This voltage is today (2005) inappropriate because it does not exist any IGBT on the market that can work at these voltage levels. Even, in spite of that in a near future IGBTs could afford this voltage, the problem of the small input voltage would remain. However, the input current, $Boost_{max}$ and D_{rated} will not be problem in this configuration.

Furthermore, if the more restrictive minimum output voltage is used to obtain the parameters, the input voltage will be lowered even more, as shows Figure 6.2. In that case, the value of the parameters can be seen in Table 6.2.

Table 6.2: FBIB parameters depending on the winding ratio for $V_{out,min2}$.

n_2/n_1	$V_{in,rated}$ (KV)	I_{in} (KA)	$V_{SW,max}$ (KV)	$Boost_{max}$	D_{rated}
3	1.5	3.33	6.75	9	0.35
3,5	1.23	8.89	5.78	9	0.35
4	1.12	4.44	5.06	9	0.35

To conclude, the most suitable model that could be designed with this topology (assuming that IGBTs could work in this voltage ranges) should have a winding ratio as low as possible in order to be as close as possible to the specification of the input voltage. This value will be $n_2/n_1=3$.

Table 6.3 summarizes the most important quantities for this configuration.

Table 6.3: Parameters of the most suitable FBIB model.

Topology:	FBIB
Winding ratio	3
Output voltage range	9.75 – 20.25 kV
Rated Input voltage	3.25 kV
Input current	1.54 kA
Maximum switches voltage	6.75 kV
Maximum diodes voltage	20.25kV
Maximum boost	4.15
Rated duty cycle	0.35

6.3.2 Full bridge (FB) topology

The FB topology will not present problems to reach any minimum output voltage. Nevertheless, the maximum output voltage will be limited by the winding ratio of the transformer.

In order to study the operating point of the converter, the equation that should be studied is

$$V_{out} = \frac{P}{P_{average}} V_{out, rated} \quad (6.22)$$

Where:

- V_{out} Output voltage of the converter
- P Output power of the converter
- $P_{average}$ Average power of the converters on the leg
- $V_{out, rated}$ Rated output voltage of the converter.

This equation is derived directly from (3.4) and can be used only for this specific application, as was earlier explained in Chapter 3.

If the power provided by one specific turbine is higher than the average, its output voltage will be higher than the rated value as can be noted in (6.22). As this overrating is limited to 1.35, a maximum output voltage of 20.25KV can be provided. Now, if the turbines in the leg (including this specific one) are operating at wind speed lower than the rated, the input voltage will be lower than the rated too. In the worst case, this input voltage could be the minimum value; that is, as showed in (6.2), $V_{in, rated}/2$.

Therefore, the worst situation for the converter will happen when the maximum output voltage is required and the minimum value is provided.

If we study the input current we will observe that this will depend directly on the power and inversely on the input voltage. As the power depends on the wind speed raised to the third power, and the input voltage has a linear increase, to find the worst operating point the equation that must be studied is

$$I_{in}(WS) = \frac{P(WS)}{V_{in}(WS)} \quad (6.23)$$

Where:

- $I_{in}(WS)$ Average input current
- $P(WS)$ Output power of the converter, described in (6.1)
- $V_{in}(WS)$ Input voltage of the converter, described in (6.2).

Figure 6.3 shows how the input voltage will depend on the wind speed. As can be seen, it will reach its maximum when the input voltage and the power reach their rated values

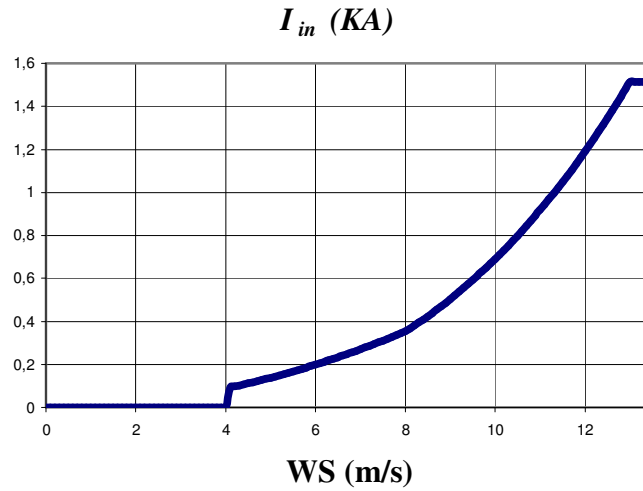


Figure 6.3: Average input current on the FB converter for the studied application depending on the wind speed.

The converter will be designed for the most restrictive operating point, which exists: Maximum output voltage, minimum input voltage and maximum power supplied. As before, the key design parameter will be the winding ratio. The specifications will be the output voltage range once more. These can be reviewed from (6.12) to (6.15).

To calculate the input voltage necessary to supply the demanded output voltage, equation (4.8) must be adapted to the worst situation as

$$V_{in, rated} = 2 \frac{n1}{n2} V_{out, max} . \quad (6.24)$$

The equation that provides the input current is, as in the FBIB

$$I_{in} = \frac{P}{V_{in, rated}} . \quad (6.25)$$

As mention before, the worst case will happen when the power reaches the rated value.

The voltage drop over the switches will be the input voltage, as was studied in Chapter 4. So, the worst situation will occur when the input voltage reaches the rated value.

The voltage drop over the diodes can be defined as

$$V_{diodes, max} = \frac{n2}{n1} V_{in, rated} . \quad (6.26)$$

If this expression is combined with (6.24) properly, it can be developed to

$$V_{diodes, max} = 2V_{out, max} . \quad (6.27)$$

Thus, the worst situation for the diodes on the high voltage side will be when the output voltage reaches the maximum value.

To calculate the rated duty cycle can be used

$$D = \frac{1}{2} \frac{n1}{n2} \frac{V_{out,rated}}{V_{in,rated}}. \quad (6.28)$$

Let's continue by studying the parameters depending on the winding ratio. Notice that only one analysis will be performed here, due to that the minimum output voltage does not affect to the parameters that are being studied. The results are presented in Figure 6.4.

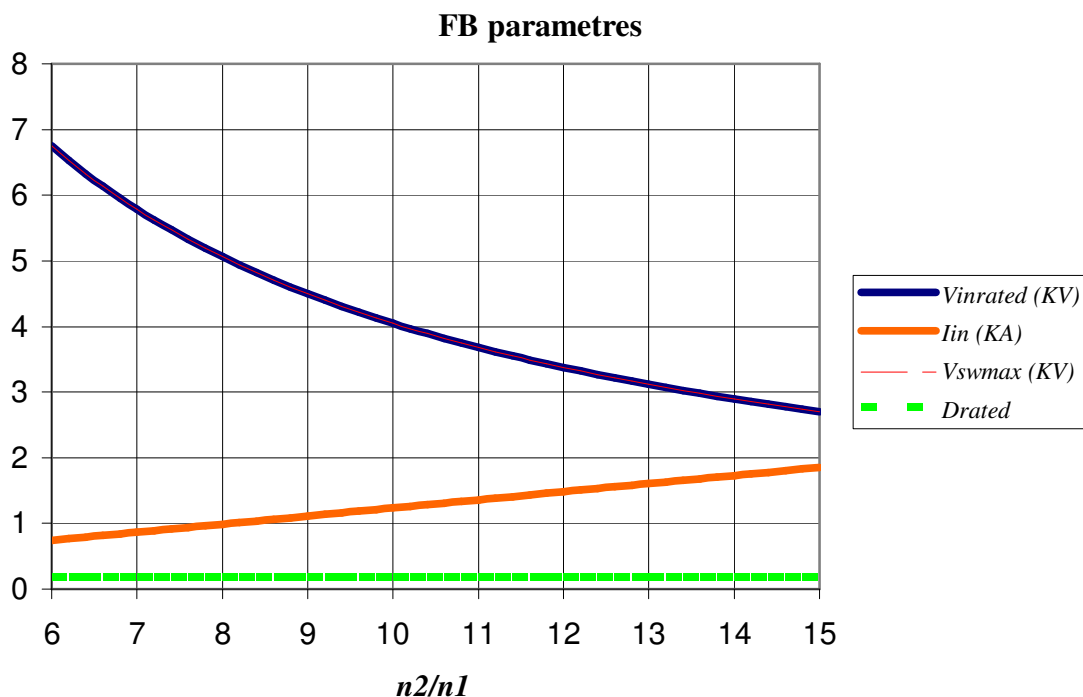


Figure 6.4: Parameters of FB model depending on the winding ratio of the transformer.

From Figure 6.4 it can be observed that, as the winding ratio increases, so does the input current. Consequently, this ratio must be as low as possible. Nevertheless, a lower winding ratio would require the input voltage to be increased, and it is the wind turbine that determines this voltage. So that, the best model would be one that features the lower winding ratio but can fulfil all the specifications.

As can be seen in the figure, a winding ratio around 12 will be necessary to satisfy the specifications if the input voltage is about 3.3KV (the wind turbine voltage). For that values the parameters studied are showed in Table 6.4.

Table 6.4: FB parameters depending on the winding ratio.

$n2/n1$	$V_{in, rated}$ (kV)	I_{in} (kA)	$V_{SW, max}$ (kV)	D_{rated}
12	3.37	1.48	3.37	0.185
12.2	3.32	1.50	3.32	0.185
12.4	3.27	1.53	3.27	0.185
12.6	3.21	1.56	3.21	0.185
12.8	3.16	1.58	3.16	0.185
13	3.11	1.60	3.11	0.185

As can be seen in Table 6.4, the first winding ratio which could fit the input voltage requirement is $n2/n1=12.4$. Nevertheless, to obtain this ratio a quite complicated winding would be needed. Due to that the device will work at a high frequency it would create problems; so, the most suitable winding ratio would be $n2/n1=13$.

Table 6.5 summarizes the most important values for this model.

Table 6.5: Parameters of the most suitable FB model.

Topology:	FB
Winding ratio	13
Output voltage range	~0 – 20.25 KV
Rated Input voltage	3.12 KV
Input current	1.6 KA
Maximum switches voltage	3.12 KV
Maximum diodes voltage	40.5 KV
Rated duty cycle	0.185

As can be seen, this model fulfils the output voltage specifications, and presents a reasonable voltage drop over the switches. Nevertheless, it causes a quite large voltage drop over the diodes, and generates a considerable input current.

6.4 Models comparison and selection of the most suitable topology

In order to facilitate the comparison between the two models, Tables 6.3 and 6.5 will be linked.

Table 6.6: Parameters of the two models studied.

Topology:	FBIB	FB
Winding ratio	3	13
Output voltage range	9.75 – 20.25 kV	~0 – 20.25 kV
Rated Input voltage	3.25 kV	3.12 kV
Input current	1.54 kA	1.6 kA
Maximum switches voltage	6.75 kV	3.12 kV
Maximum diodes voltage	20.25kV	40.5 kV
Maximum boost	4.15	-----
Rated duty cycle	0.35	0.185

The first parameter that we will discuss is the output voltage range. As can be seen in Table 6.6, the FBIB provides a limited minimum output voltage whereas the FB can reach almost zero. Studying the input voltage, it can be seen that both fit with the turbine specifications. Nevertheless, as the input voltage provided by the wind turbine gets higher than the one estimated in the model (3.3 kV), the minimum output voltage in the FBIB will increase, decreasing the output voltage range even more. However, in the FB the effect will be completely opposite, because it will increase the maximum output voltage, improving the voltage range.

Referring to the input currents, the FB model will present an almost 4% bigger value than the FBIB. Moreover these two values will be around 1.5 kA.

If we analyze the voltage drops over the switches, quite big differences can be observed between the two models. While the FBIB requires the IGBTs to hold up nearly 7 kV, the FB model only requires a voltage drop similar than the input voltage that will be 3.3 kV.

Studying the voltage drop over the diodes, the FB model has a voltage drop of 40.5 KV, just the double of the FBIB that only requires 20.25 kV (the maximum output voltage).

Consequently the FB topology will be the most suitable, because it is the only that can be built with the semiconductors that already exists in the market. In addition, this model presents a larger output voltage range than the FBIB.

As drawbacks, the FB model requires more input current (4% more) and stronger diodes due to the voltage drop over them (two times the FBIB voltage level). This problem could be solved by installing more powerful diodes or connecting various in series.

Chapter 7

Analysis of the real converter

Once the FB model has been chosen as the most suitable topology to the studied wind turbine application, it must be analyzed more in detail in order to realize how the different parameters will affect the performance of the converter.

In order to do that a theoretical analysis of the converter will be accomplished, which will consider the effect of the leakage and magnetizing inductances of the transformer, but that will consider the semiconductor devices (diodes and switches) as ideal. The studied model is shown in Figure 7.1. Then, with the differential equations obtained, the theoretical waveforms of the real converter will be plotted. At last, using a computer program, the performance of the converter will be analyzed depending on the transformer parameters.

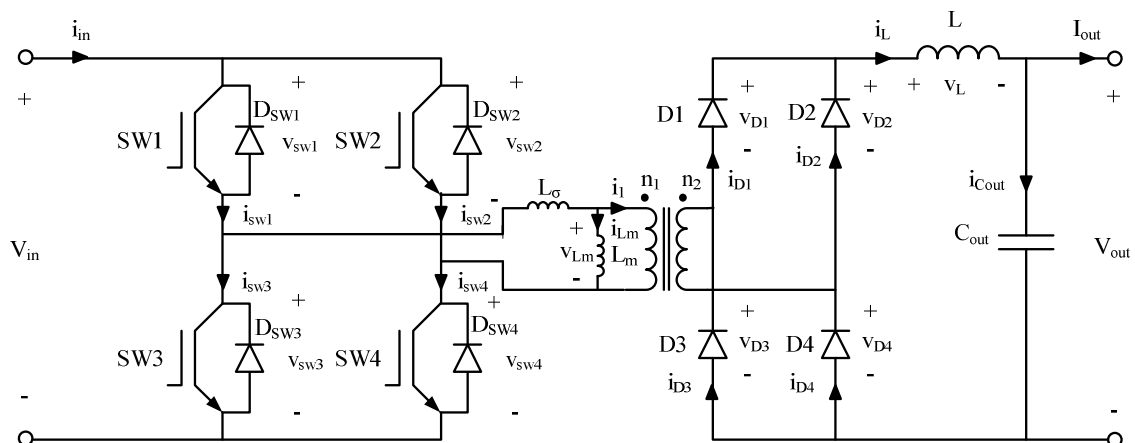


Figure 7.1: Real full bridge converter circuit.

7.1 Analyses of the circuit

Due to the non-linear performance of the semiconductor components, the working cycle of the converter will be divided into several steps in order to obtain the equations that describe the device.

7.1.1 Step 0

In this first step SW1 and SW4 has just been connected. Nevertheless, to describe the performance of the circuit, the previous situation must also be considered.

To describe this previous situation it must be assumed that the four switches were disconnected and the magnetizing current that was flowing in the secondary of the transformer (the current in the primary side divided by the winding ratio) was very low compared to the output current. Due to that, the four diodes on the high voltage side were conducting and the secondary of the transformer short-circuited. With these assumptions, the equivalent circuit of the previous situation can be plotted as in Figure 7.2.

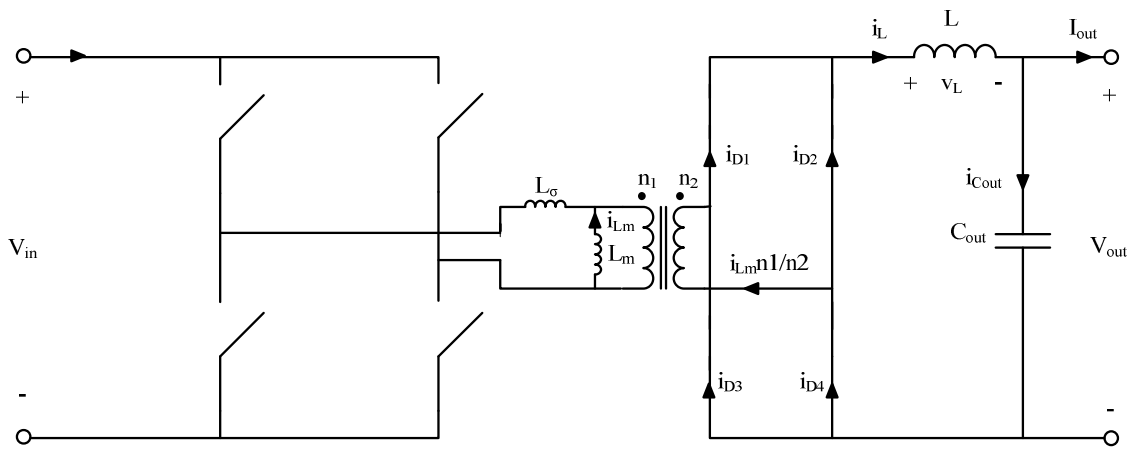


Figure 7.2: Equivalent circuit of the FB converter before step 0.

Thus, with these initial conditions the switches are turned on. Due to the short-circuit, the voltage over the magnetizing inductance will be zero, and the input voltage will end up over the leakage inductance and the result is increasing input current. Furthermore, as the voltage over the magnetizing inductance is zero, the magnetizing current will be constant. This means that the whole of the increasing input current will flow through the transformer, increasing the current in the diodes $D1$ and $D4$ and decreasing it in $D2$ and $D3$.

In this moment, the circuit can be represented as shown in Figure 7.3.

The information that can be obtained directly from the scheme is

$$i_{in}(t=0) = 0 \quad (7.1)$$

$$i_{Lm} = K \quad (7.2)$$

$$V_{in} = V_{\sigma} \quad (7.3)$$

$$V_{Lm} = 0 \quad (7.4)$$

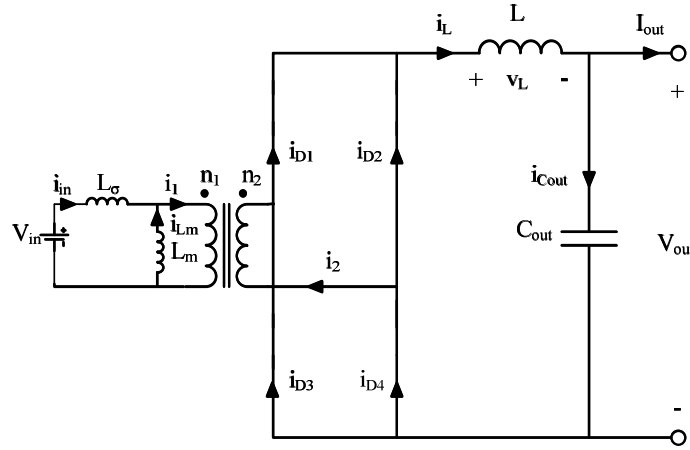


Figure 7.3: Equivalent circuit of the FB converter during step 0.

By studying the differential equation that governs the low voltage circuit, the current on the primary side of the transformer can be expressed as

$$i_1(t) = \frac{1}{L_\sigma} V_{in} t + i_{Lm}. \quad (7.5)$$

Obviously, the current on the high voltage side will be

$$i_2(t) = \frac{n1}{n2} \left(\frac{1}{L_\sigma} V_{in} t + i_{Lm} \right). \quad (7.6)$$

The input current will performs as

$$i_{in}(t) = \frac{1}{L_\sigma} V_{in} t. \quad (7.7)$$

This step will last until the current in the diodes $D2$ and $D3$ decrease to zero. This will happen when the current on the high voltage side of the transformer reaches the value of the inductor current (i_L). In order to obtain an approximation of this time it can be assumed that the inductor current is similar to the output current. If the load is considered to be a resistance, the time that this step will take can be calculated as

$$t_1 = \left(\frac{V_{out}}{R_{load}} - \frac{n1}{n2} i_{Lm} \right) \frac{n2}{n1} \frac{L_\sigma}{V_{in}}. \quad (7.8)$$

Where

R_{load} Resistance of the converter's load (Ω)
 t_1 time of step 0.

On the high voltage side, the voltage over the inductor will be negative ($-V_{out}$), decreasing its current.

7.1.2 Step 1

This step will start when $D3$ and $D4$ are switched off by the current in the secondary side of the transformer. In that moment, the short-circuit will disappear and the behaviour of the circuit will change. The scheme of the circuit during this step is presented in Figure 7.4.

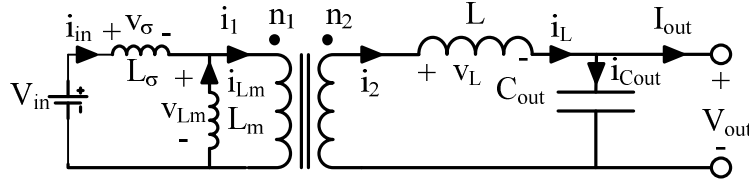


Figure 7.4: Equivalent circuit of the FB converter during step 1.

The new boundary conditions are

$$i_{in}(0) = \frac{1}{L_{\sigma}} V_{in} t_1 \quad (7.9)$$

$$i_1(0) = \frac{1}{L_{\sigma}} V_{in} t_1 + i_{Lm} . \quad (7.10)$$

The positive voltage that now drops on the transformer will force i_{Lm} to change, leading to a differential equation for the low voltage side as

$$V_{in} = L_{\sigma} \left(\frac{di_1}{dt} - \frac{di_{Lm}}{dt} \right) + V_{Lm} . \quad (7.11)$$

Where

$$V_{Lm} = -L_m \frac{di_{Lm}}{dt} . \quad (7.12)$$

The equations on the high voltage side can be expressed as

$$V_L = \frac{n2}{n1} V_{Lm} - V_{out} \quad (7.13)$$

$$i_2 \equiv i_L = \frac{n1}{n2} i_1 . \quad (7.14)$$

With the knowledge of (7.12), (7.13) and (7.14), (7.11) can be operated in order to obtain the voltage drop over the magnetizing inductance as

$$V_{L_m} = \frac{LL_m V_{in} + L_\sigma L_m \left(\frac{n2}{n1}\right) V_{out}}{LL_m + L_\sigma L_m \left(\frac{n2}{n1}\right)^2 + L_\sigma L} \quad (7.15)$$

As mentioned in Chapter 4, the maximum output voltage of the converter is limited by the winding ratio of the transformer.

$$V_{out} \leq \frac{n2}{n1} V_{in} \quad (7.16)$$

If we further evaluate (7.16), the maximum voltage over the magnetizing inductance can be found as

$$V_{L_m} = \frac{LL_m + L_\sigma L_m \left(\frac{n2}{n1}\right)^2}{LL_m + L_\sigma L_m \left(\frac{n2}{n1}\right)^2 + L_\sigma L} V_{in} \quad (7.17)$$

From (7.17), it can be understood that the magnetizing voltage will always be lower than the input voltage. This result is logical, because the leakage inductance reduce the energy transferred to the high voltage side of the converter. Even, if the leakage inductance was reduced to zero, equation (7.17) could be expressed as

$$V_{L_m} = V_{in} \quad (7.18)$$

That is exactly the result obtained when the ideal converter was studied in chapter 4.

From (7.17) the magnetizing current on the transformer can be derived as

$$i_{L_m}(t) = -\frac{V_{L_m}}{L} t + i_{L_m}(0) \quad (7.19)$$

To avoid that the transformer saturates, the value of this current at the end of the step (t_2) must be equal to $-i_{L_m}(0)$. For that, t_2 must satisfy

$$t_2 = \frac{2i_{L_m}(0)L}{V_{L_m}} \quad (7.20)$$

The voltage over the leakage inductance can be obtained by deducting the magnetizing voltage to the input voltage, as can be seen in Figure 7.4. From this voltage, the leakage current can be derived. Note that this current will coincide with the input current.

$$V_{\sigma} = \frac{L_{\sigma}L}{LL_m + L_{\sigma}L_m\left(\frac{n2}{n1}\right)^2 + L_{\sigma}L} V_{in} \quad (7.21)$$

$$i_{\sigma}(t) \equiv i_{in}(t) = \frac{V_{\sigma}}{L_{\sigma}}t + i_{in}(0). \quad (7.22)$$

With this, the currents on the transformer can be expressed as

$$i_1(t) = i_{Lm}(t) + i_{in}(t) \quad (7.23)$$

$$i_2(t) = \frac{n1}{n2}i_1(t) + i_2(0). \quad (7.24)$$

Finally, as can be seen in (7.13) the voltage over the inductor on the high voltage side is now positive, increasing the current according to

$$i_L(t) = \frac{1}{L} \left(\frac{n2}{n1}V_{Lm} - V_{out} \right)t + i_L(t_1). \quad (7.25)$$

7.1.3 Step 2

This step commences when SW1 and SW4 are disconnected. Then, D_{SW2} and D_{SW3} will conduct the input current i_{in} since this current cannot sharply decrease to zero because of the leakage inductance. As a result, a negative voltage will appear over the transformer.

On the high voltage side, the four diodes will immediately conduct again. This is due to the negative voltage that appears on the secondary of the transformer that forward bias $D2$ and $D3$, and the inductance current that forces $D1$ and $D4$ to continue conducting. This commutation effect is further studied in [6]. Consequently, the transformer will be short-circuited again. In Figure 7.5 the equivalent circuit for this step is presented.

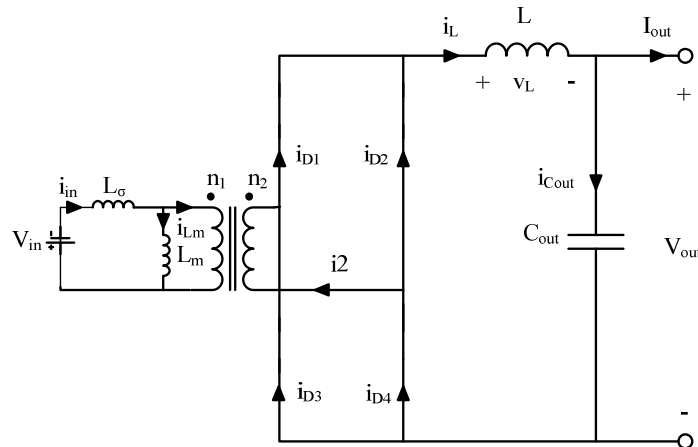


Figure 7.5: Equivalent circuit of the FB converter during step 2.

As the secondary of the transformer is short-circuited, the voltage over the magnetizing inductance will be zero, and its current will be kept constant.

As shown in Figure 7.5, over the leakage inductance a negative voltage drop equal to the input voltage will appear. This negative voltage will force the input current to decrease, as can be seen in (7.26) which represent the differential equation on the low voltage side.

$$i_{in}(t) = i_{in}(t_2) - \frac{V_{in}t}{L_{\sigma}} \quad (7.26)$$

The input current will decrease until it reaches zero. In that moment D_{SW2} and D_{SW3} will stop conducting and the transformer will be isolated from the voltage source, changing the performance of the circuit again.

On the high voltage side a negative voltage equal to the output voltage will appear over the inductance again. Consequently, the current in the inductance will start to decrease as shows (7.27).

$$i_L(t) = i_L(t_2) - \frac{V_{out}t}{L} \quad (7.27)$$

7.1.4 Step 3

This step will start when the transformer is isolated from the source on the primary side, keeping the short-circuit in the secondary. This leads to that the magnetizing current will remain constant. The short-circuit is due to that the four diodes on the high voltage side are conducting because the inductance current is much greater than the magnetizing current on the secondary. During this step, the circuit can be described as in Figure 7.6.

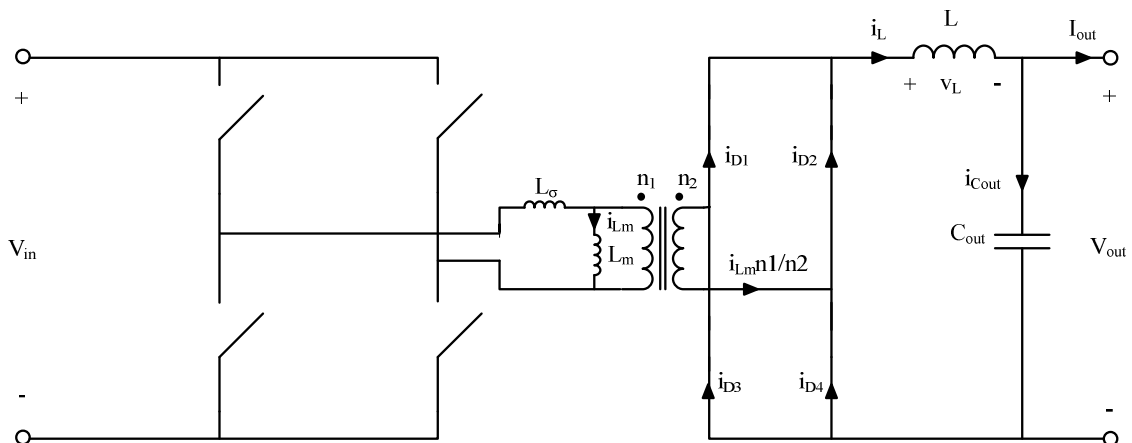


Figure 7.6: Equivalent circuit of the FB converter during step 3.

Studying the high voltage side it can be noticed that the voltage over the inductance is the negative output voltage, so the current will continue to decrease with the same slope as in the previous step. It must be noticed that this current will never reach zero, because the converter is supposed to work in CCM.

7.1.5 Step 4

In this step, *SW2* and *SW3* are connected. From here, the performance of the converter will be the same as described since step 0. Nevertheless, as the opposite part of the bridge will be acting now, the signs of the currents on the low voltage side will change.

7.2 Voltage and current waveforms of the full bridge

Once the equations of the converter have been obtained, the plots of the voltages and currents can be completed. It must be noticed that the purpose of these plots is to present, as clear as possible, the quantitative characteristics of the different signals, so the scale on the drawings could not be completely trustworthy.

Figure 7.7 presents the transformer voltages. If the magnetizing voltage is observed and compared with the ideal waveform in Chapter 4, it can be seen that its area is smaller, and accordingly the energy transferred to the high voltage side is also reduced. This is due to that there exists a period of time between the switches are connected and the occurrence of the magnetizing voltage. This time is used to charge the leakage inductance as can be seen in its voltage plot. Moreover while the magnetizing inductance is charged, the voltage over it will be lower than in the theoretical model, because parts of the input voltage will be occurring over the leakage inductance.

When studying the currents in the low voltage side, it can be seen in Figure 7.8 that the input current is the sum of the magnetizing current and the current on the primary of the transformer. Studying its plot it can be seen that the current experiences a quite big increase in the first moments (step 0) due to the leakage inductance. In addition, it can be noticed that this current will not immediately go to zero when the switches are disconnected, producing a negative voltage drop over the transformer. This effect is caused by the leakage inductance too.

It must be noted that the input current will change its drift in the step 2, due to that it will be conducted by the antiparallel diodes of the opposite switches, as was explained earlier. Then, this current will return to the source and thus some energy, will not be transferred to the high voltage side. That means that will power appear reactive.

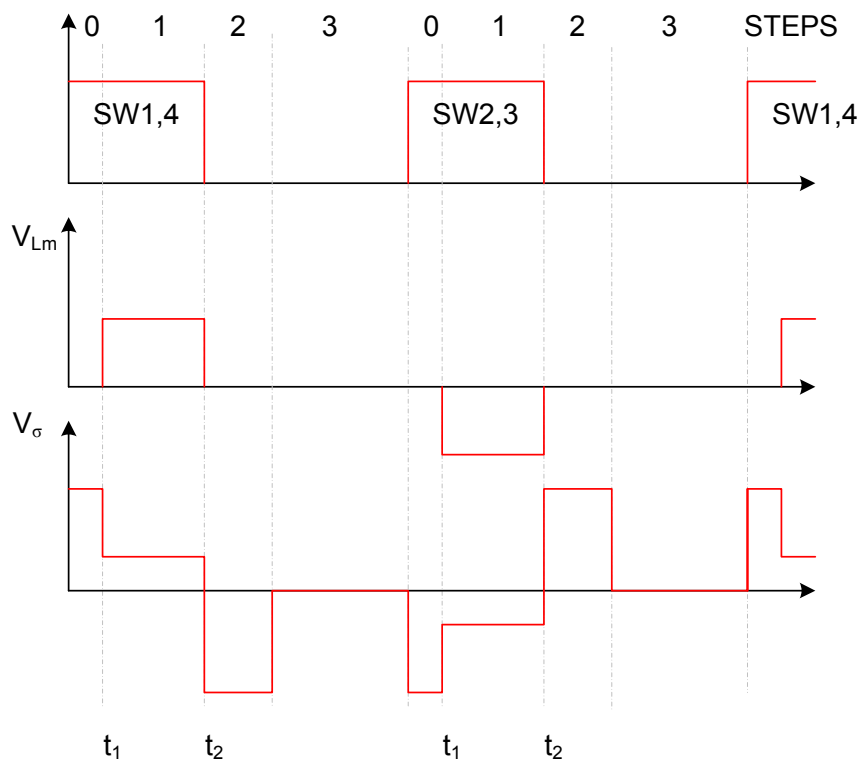


Figure 7.7: Voltage waveforms on the transformer of the full bridge converter

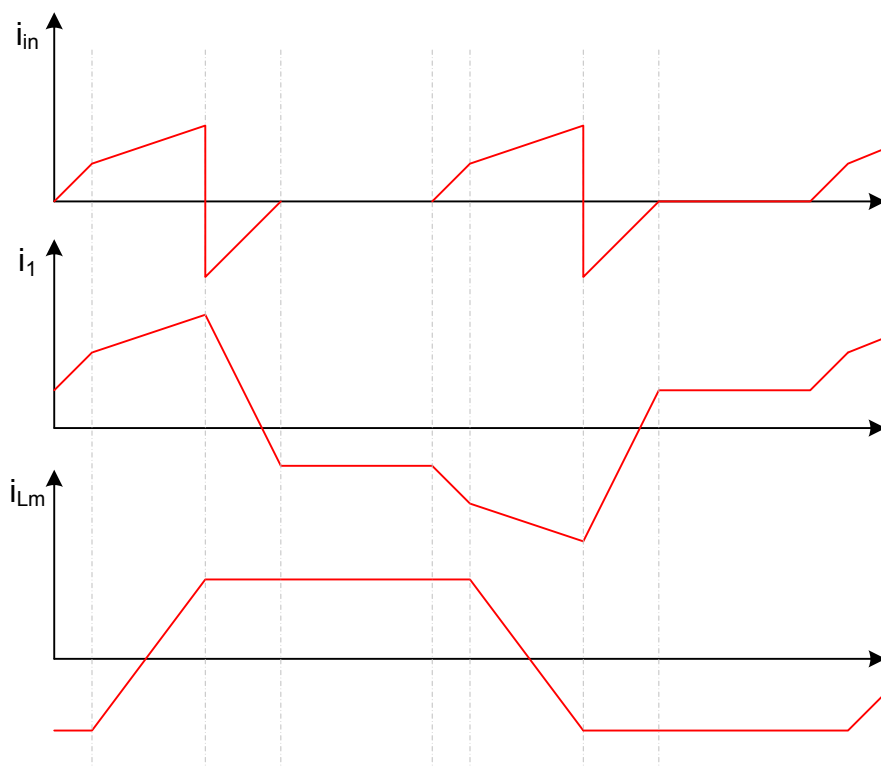


Figure 7.8: Currents waveforms on the low voltage side of the full bridge converter.

The performance on the high voltage side will also be affected by the leakage inductance as shows Figure 7.9. It can be observed that the positive voltage area on the inductance is smaller in comparison with the case for the theoretical converter. This is due to the reduction on the voltage over the magnetizing inductance as explained before. As a result, the current will be increased less, and thus, the energy available at the output of the converter lower.

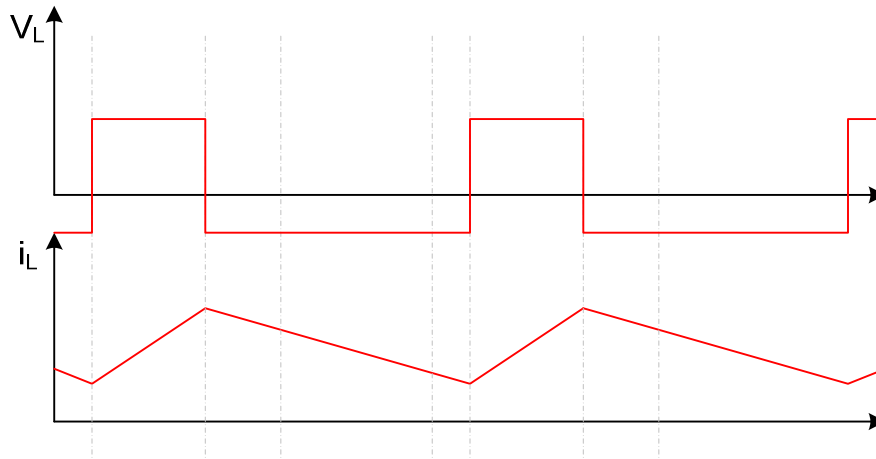


Figure 7.9: Voltage and current waveforms on the inductor of the full bridge converter.

Let's continue by studying the waveforms on the semiconductor devices.

In Figure 7.10 the performance of the switches is shown. As can be observed, here the antiparallel diodes of the switches are also represented. This is because the input current will require a path in which it can flow while it is decreasing. In the theoretical model, this current was decreased instantly, but now, due to the leakage inductance it will require a finite time to decrease.

Studying the figure, it can be noticed that while two of the antiparallel diodes (D_{SW2} and D_{SW3} , for example) are conducting, there will be a voltage equals to the input value over the other two switches ($SW1$ and $SW2$).

At last, the waveforms of the diodes are presented in Figure 7.11. It is noticeable that when the four diodes are conducting (steps 2 and 3) the currents over them will not be completely balanced due to the magnetizing current, which flows trough the transformer during these periods. Besides, the time the diodes will be experiencing a voltage drop that is lower than in the theoretical study due to the fact that less energy is being transferred, as was commented before.

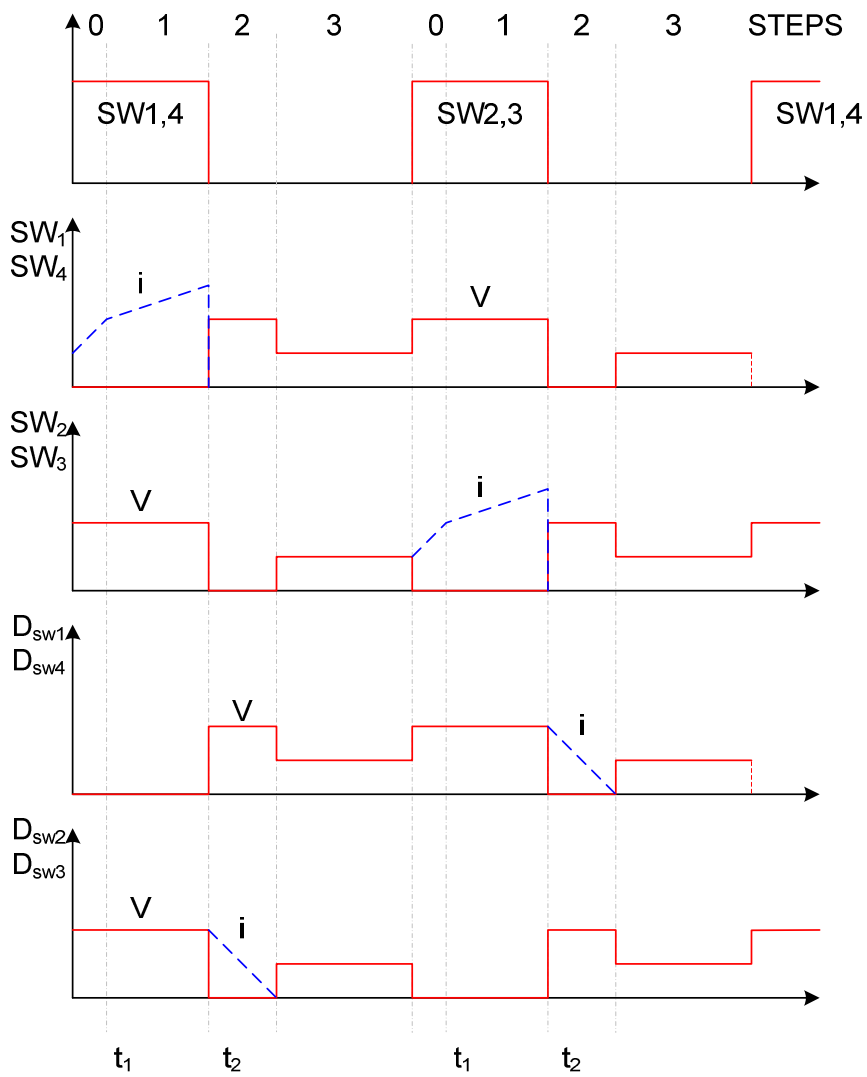


Figure 7.10: Voltage and current waveforms on the switches of the full bridge converter.

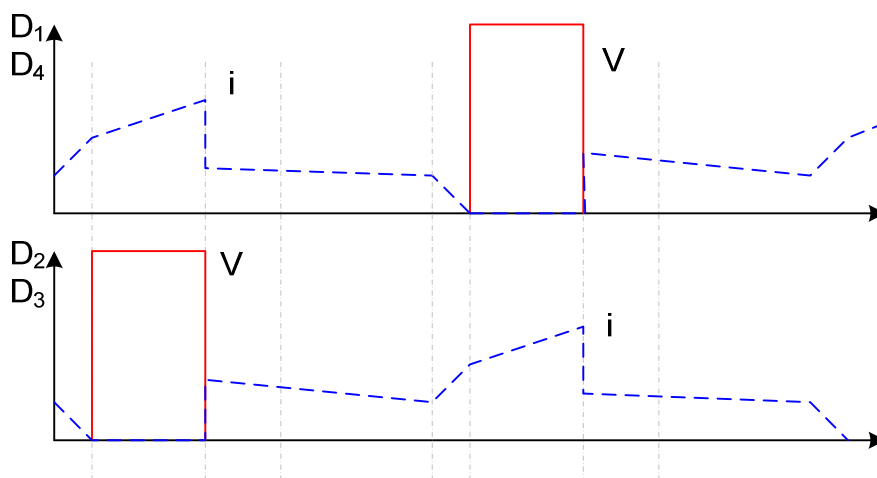


Figure 7.11: Voltage and current waveforms on the diodes of the full bridge converter.

7.3 Analysis of the full bridge depending on the transformer parameters

As has been studied, the performance of the converter will be deeply influenced by the transformer. Therefore, the output voltage of the full bridge must be studied depending on the transformer parameters, as winding ratio, leakage inductance and magnetizing inductance. This voltage will also be analyzed in this section depending on the switching frequency; due to this variable will appear in the equations that describes the transformer behavior. Finally, it will be studied how the main inductance must be dimensioned depending on the frequency and the winding ratio to fit the specifications.

7.3.1 Definition of the transformer parameters and equations

As can be seen in Figure 7.1, the transformer was modelled as an ideal transformer with the magnetizing and the leakage inductance. The windings resistances were omitted from the model in order to simplify the analysis.

To analyze how the output voltage of the full bridge converter is affected, the ideal converter studied in Chapter 4 must be reviewed. There, the equation than expresses the output voltage was derived by using a volt-second balance on the inductor, obtaining

$$V_{out} = 2 \frac{n_2}{n_1} D V_{in} . \quad (7.28)$$

The equation shows that if the duty cycle and the input voltage are kept constant, the output voltage is directly influenced by the winding ratio of the transformer. If the volt-second technique is applied in the real full bridge converter, using the inductor waveforms presented in Figure 7.9, can be understood that the equation that defines the output voltage in the real converter can be expressed as

$$V_{out,real} = 2 \frac{n_2}{n_1} \frac{t_{on} - t_1}{T} V_{Lm} . \quad (7.29)$$

From (7.29) it can be realized that the output voltage will now depend not only on the winding ratio of the converter but on the voltage over the magnetizing inductance and t_1 that, as was commented in the chapter before, will depend on different parameters of the transformer and the circuit. It must also be noticed that the frequency cannot be skipped from the equation as was done in (7.28) using the definition of the duty cycle, due to that t_1 is also divided by the switching period.

Equation (7.29) can be developed with the knowledge of (7.15), which expresses V_{Lm} depending on the circuit parameters, to

$$V_{out,real} = \frac{2 \frac{n_2}{n_1} LL_m (t_{on} - t_1) V_{in}}{T \left(LL_m + L_m L_\sigma \left(\frac{n_2}{n_1} \right)^2 + L_\sigma L \right) - 2 \left(\frac{n_2}{n_1} \right)^2 L_m L_\sigma (t_{on} - t_1)}. \quad (7.30)$$

As can be seen, this equation expresses the output voltage depending on the circuit parameters (transformer parameters and the main inductance), the frequency (with a fixed duty cycle, t_{on} will depend directly on the switching period) and t_1 .

t_1 can be obtained by using the definition of average current as shows (7.31) and knowing that the value of the average input current is about 1.5 kA for the rated conditions, as was determined in Chapter 5.

$$I = \frac{1}{T} \int_0^T i(t) dt. \quad (7.31)$$

This integral can be expressed in terms of areas by using the input current waveform on Figure 7.8 and the current equations obtained before as

$$I = \frac{2}{TL_\sigma} \left(\frac{V_{in} t_1^2}{2} + V_{in} t_1 (t_{on} - t_1) + \frac{V_{in} - V_{Lm}}{2} (t_{on} - t_1)^2 - \frac{V_{in} t_1 + (V_{in} - V_{Lm})(t_{on} - t_1)}{2} t_3 \right). \quad (7.32)$$

Where t_3 is the time needed by the input current to reach zero in step 2 (see Figure 7.7) and can be obtained using (7.26), replacing the input current by zero. With that, t_3 can be expressed as

$$t_3 = \frac{t_1 V_{in} + (V_{in} - V_{Lm})(t_{on} - t_1)}{V_{in}}. \quad (7.33)$$

By using (7.33), t_1 can be isolated from (7.32) as

$$t_1 = \frac{-B + \sqrt{B^2 - 4AC}}{2A}. \quad (7.34)$$

Where:

$$A = \frac{1}{2} (V_{in} - V_{Lm}). \quad (7.35)$$

$$B = V_{in} t_{on}. \quad (7.36)$$

$$C = \left(\frac{V_{in} - V_{Lm}}{2} + \frac{(V_{in} - V_{Lm})^2}{2V_{in}} \right) t_{on}^2 - \frac{ITL_\sigma}{2}. \quad (7.37)$$

From the equations, it can be noticed that t_l will depend on the input voltage, the frequency (T and t_{on}), the leakage inductance and the voltage of the magnetizing inductance V_{Lm} . This voltage, as was mentioned before can be expressed as function of the circuit parameters and the output voltage by using (7.15).

As a result, if the frequency and the circuit magnitudes are kept constant, the output voltage will depend on t_l , and t_l will depend on the output voltage. That means that an iterative method will be needed in order to solve (7.30) and (7.34). The structure of a possible scheme to solve the system is shown in Figure 7.12.

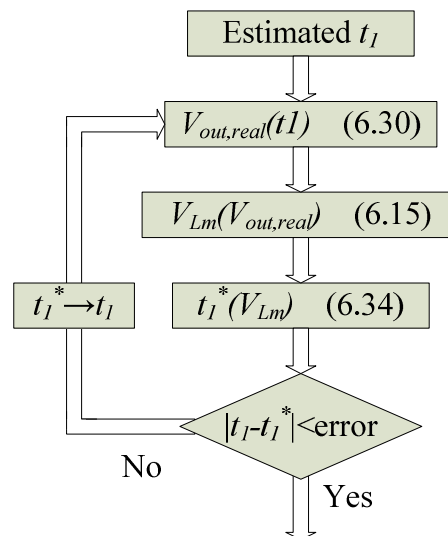


Figure 7.12: Output voltage iterative flowchart.

As can be seen in the figure, an initial value for t_l must be estimated. Depending on how correct this estimation is; the number of iterations will be lower. This t_l is used to calculate the output voltage and then, the value of the magnetizing voltage. As was explained before, this variable can provide a new estimation for t_l . Finally, the program compares the previous t_l with the obtained value repeating the loop (using the new quantity) until the differences between the t_l calculated in the iteration n and the value from the iteration $n+1$ are small enough.

The implementation of this program was done in Matlab® and can be reviewed in Appendix B.

Once the equations that describes the output voltage has been derived and the calculation process presented, it can be analyzed how the transformer parameters affects the performance of the output voltage, which will be called $V_{out,real}$. First, it will be studied how the converter is influenced by the winding ratio of the transformer, following with the analysis of the transformer inductances. Finally, the output voltage will be studied as function of the switching frequency, as was described before.

7.3.2 Influence of the winding ratio on the output voltage

Reviewing (7.30), it can be seen that the winding ratio (n_2/n_1) appears on both sides of the division that means that the behaviour of the output voltage will depend on the values of the parameters that follows it. It must be notice that in the denominator, the winding ratio appears squared but it is multiplied by the leakage inductance that usually will present a very low value compared with the magnetizing inductance. While, in the numerator, the winding ratio appears multiplied by the magnetizing inductance, as well as the input voltage that will be a large value. This can lead us to guess that this will be the most important effect to the output voltage. It means that if the winding ratio increases, the output voltage will increase too, which is the case in the ideal converter.

In Figure 7.13, the real output voltage divided by the ideal one as a function of the winding ratio has been plotted. There, it can be observed, as the ratio increases, the differences between the real and the ideal voltage are a slightly higher.

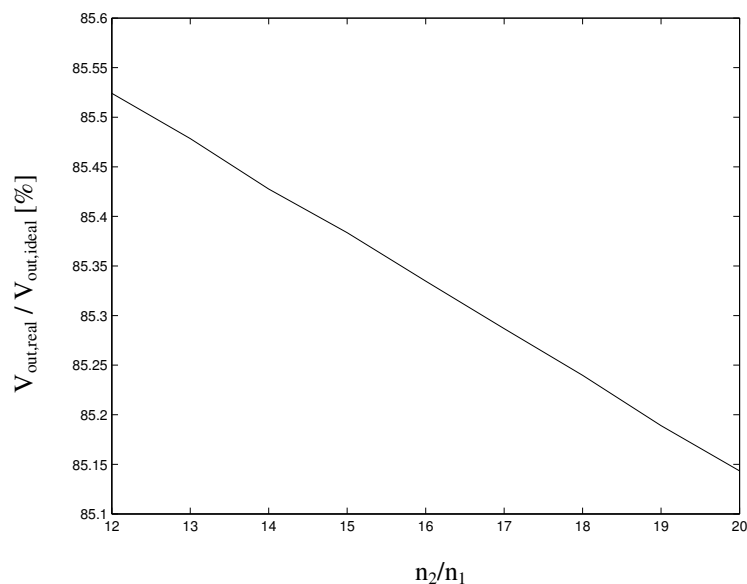


Figure 7.13: Real output voltage divided by the ideal voltage depending on the transformer winding ratio for frequency=3100Hz, $L_\sigma=3.8\mu H$, $L_M=810\mu H$.

7.3.3 Influence of the transformer inductances on the output voltage

Studying (7.30) as a function of the leakage inductance (L_σ) it can be seen that the output voltage will depend inversely on it, due to that this variable only appear in the denominator of the equation. Thus, if the leakage inductance increases, the output voltage will decrease.

Analyzing the output voltage dependence on the magnetizing inductance in equation (7.30) it can be seen that, as happened with the winding ratio, that this variable will appear on both sides of the equation. Nevertheless, in this case it does not appear squared on any side. This allows to express (7.30) as

$$V_{out,real} = \frac{K_1 L_m}{K_2 L_m + K_3} . \quad (7.38)$$

Where K_3 will include the switching period (T) and the leakage inductance (L_σ), which as mentioned before has a low magnitude compared to the other parameters in the equation. With this assumption, (7.38) could be developed to

$$V_{out,real} = \frac{K_1 L_m}{K_2 L_m} = K . \quad (7.39)$$

Then, as soon as the magnetizing inductance will present a minimum value, it will not influence the performance of the output voltage.

7.3.4 Influence of the switching frequency on the output voltage

If the ideal full bridge converter were analyzed, the frequency would not affect its performance because, as the transformer was considered ideal, the circuit would not need a finite time to change between its different states (that in this report were called steps). Due to that, the equation that rules the output voltage for the ideal converter, (7.28), presents only the duty cycle, assuming that the circuit will work in the same way at 50 Hz or at 100 kHz.

Nevertheless, when the real converter is studied, leakage inductance will be present. This produces some inertia in the transformer that will need a finite time to change its state. Due to that, the frequency, or a variable that depends directly on it as t_{on} , will appear in the output voltage equation, (7.30), and in the t_I equation, (7.34).

Due to the complexity of both equations it is difficult to guess how the frequency will affect the output voltage, but if it is studied qualitatively, it can be understood that, if the frequency is increased, in the same period of time that the leakage inductance will be loaded and discharged more times and, although it will take less time if the frequency is high, the energy transferred will be lower and thus also the output voltage.

In Figure 7.5 two analyses were completed. First, a converter with a quite non-ideal transformer was studied, that means that the leakage inductance was relatively high and the magnetizing inductance low. It can be seen (solid line) that the output voltage will sharply decrease with the frequency. The second analysis was accomplished for a nearly ideal transformer (dashed line). It is interesting to notice that the output voltage will be much less affected by the frequency, even more, for low values it will not be influenced, and the performance will be like the ideal converter.

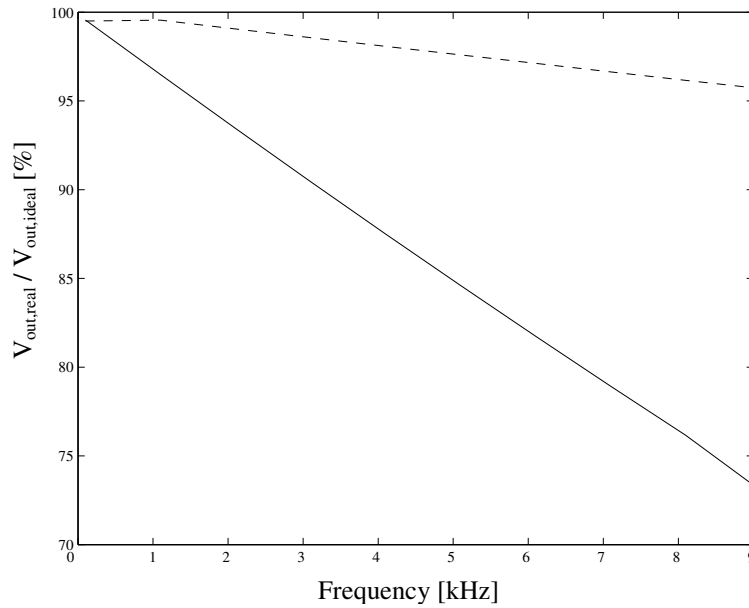


Figure 7.14: Real output voltage divided by the ideal one depending on the switching frequency. Solid for a quite non-ideal transformer, dashed for a nearly ideal transformer.

7.3.5 Analysis of the main inductance as function of the frequency and the winding ratio

In order to complete this section, the main inductance must be studied due to that it is the last circuit parameter that appears in the output voltage equation (7.30).

This inductance, as was explained in Chapter 4, is used to store the energy and delivers it to the output capacitor, which has a large influence on the performance of the output current by determining the ripple of the current that flows through the capacitor, i_L . This current can be reviewed in Figure 4.6.

To derive the expression that describes this effect, the theoretical model of the converter will be used in order to simplify it. The process to obtain it is described in [1] and uses a linear approximation for the current ripple and the capacitor voltage. This gives

$$\Delta i_L = \frac{n_2}{n_1} \frac{V_{in}}{2L} (1 - 2D) DT . \quad (7.40)$$

$$\Delta V_{out} = \frac{\Delta i_L}{16C_{out}} T . \quad (7.41)$$

From (7.40) the inductance can be directly isolated, giving

$$L = \frac{n_2}{n_1} \frac{V_{in}}{2\Delta i_L} (1 - 2D) DT . \quad (7.42)$$

The equation shows that the value of the inductance will depend on the winding ratio, the input voltage, the duty cycle, the frequency and the current ripple. This parameter is fixed by the specifications. A good value for it is the 10% of the output current for rated conditions. This current can be easily obtained by using the rated output power (5MW) and the rated output voltage (15kV). So the output current will be 333A and the current ripple about 33.3A. The duty cycle used to dimension the inductance will obviously be the rated value that can be checked in Chapter 5. The input voltage used will be the rated one (3.3kV).

Therefore, the inductance value will depend on the frequency (via t_{on}) and the winding ratio. Figure 7.15 shows how these parameters shape the dimension of the inductance. There, it can be seen that the winding ratio influences directly the value of the coil while the frequency will depend inversely. This means that if the frequency increases, a smaller inductance will be required because the time between the energy transfers will be lower and thus the amount of energy that needs to be stored.

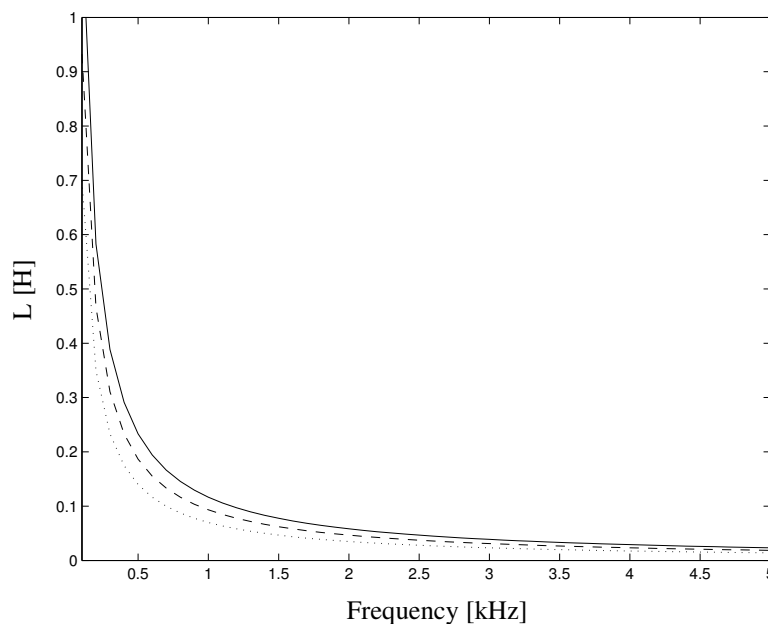


Figure 7.15: Magnitude of the full bridge inductance depending on the switching frequency and the winding ratio. Solid for a winding ratio of 20, dashed for a winding ratio of 16, dotted for 12.

Chapter 8

Design of the converter

Once the performance of the converter has been thoroughly analyzed, the design of the specific application can be accomplished.

For that, the design process will first be presented, then followed by the dimensioning of all the converter components. That is: The transformer and its core material, the windings and the switches. Next, the design performance will be analyzed, in order to find the most suitable device. The chapter will finish with a small study about how the final design will be affected by the development of the semiconductor devices.

8.1 Definition of the design process

The process to obtain the most suitable converter for the wind turbine application will follow two basic steps. The first one will be to design a converter that could satisfy the specifications for all the possible values of the construction and operating variables over an appropriate range of each of them. This will lead to a vast database of possible designs. The next step will use this database to obtain the optimum design for a specific criterion. This criterion will be based on economical facts of the converter as will be explained later.

Consequently, this section will be divided in two parts; the first one will describe the process to obtain the designing database, while the second part will define the criterion used to obtain the definitive design.

8.1.1 Converter database

As has been introduced before, a complete database of converters will be created in order to be able to choose the most suitable one.

This database will consist of a converter design for each possible combination of the six variables (in an appropriate range). Moreover, every design will fulfill the application requirements. These requirements can be summarized in the fact that, for the rated conditions, the converter must perform as the ideal model that was presented in Chapter 6, where the full bridge topology was elected.

This means that, for the rated input power and voltage, and for the rated duty cycle, the converter will provide the rated output voltage.

The method used to find an implementation will be based on a flowchart composed by nested loops. This structure will guarantee that all the possible combinations of the six variables are analyzed.

Then, for every parameter, and using the transformer equations derived in Chapter 5, the converter design parameters will be estimated for the theoretical winding ratio calculated in Chapter 6. With that, by means of the iterative scheme used in the converter analysis of Section 6.3, the real output voltage will be obtained.

Next, if the output voltage is lower than the theoretical one, the winding ratio will be increased and all the converter parameters will be recalculated, until the output voltage fulfills the desired condition.

In order to clarify the scheme, Figure 8.1 can be reviewed.

The selection of the winding ratio as degree of freedom to satisfy the application specifications is based on the results obtained in the converter analysis in Section 6.3. There, it can be seen that the output voltage will depend on four variables: frequency, winding ratio and the transformer inductances. However, the two inductances cannot be modified directly, due to the fact that they depend on the transformer parameters. So, the two options left will be to increase the winding ratio or decrease the frequency.

A frequency decrease will increase the number of turns on the primary, at least, in one unit; due to that it is a discrete variable. This will lead to an increase in the number of turns on the secondary, n_2/n_1 times. That means that, any frequency variation will add one foil and n_2/n_1 cables to the transformer. While, a unitary increment of the winding ratio will add to the transformer N_1 cables.

As a result, if it is assumed that the transformer will present a low number of turns, the variation of the winding ratio will cause smaller modifications on the transformer than changing the frequency, providing a finer control for the iterative program.

It can be cleared by the example in Table 8.1, where it is assumed that the initial number of turns on the primary is 5 and the initial winding ratio is 13.

Table 8.1: Example of the effect of the winding ratio and frequency variation

	Winding ratio variation		Frequency variation	
	$N1$	$N2$	$N1$	$N2$
Iteration n	5	65	5	65
Iteration n+1	5	70	6	78

The implementation of the database was done in Matlab®. The program file is included in Appendix B.

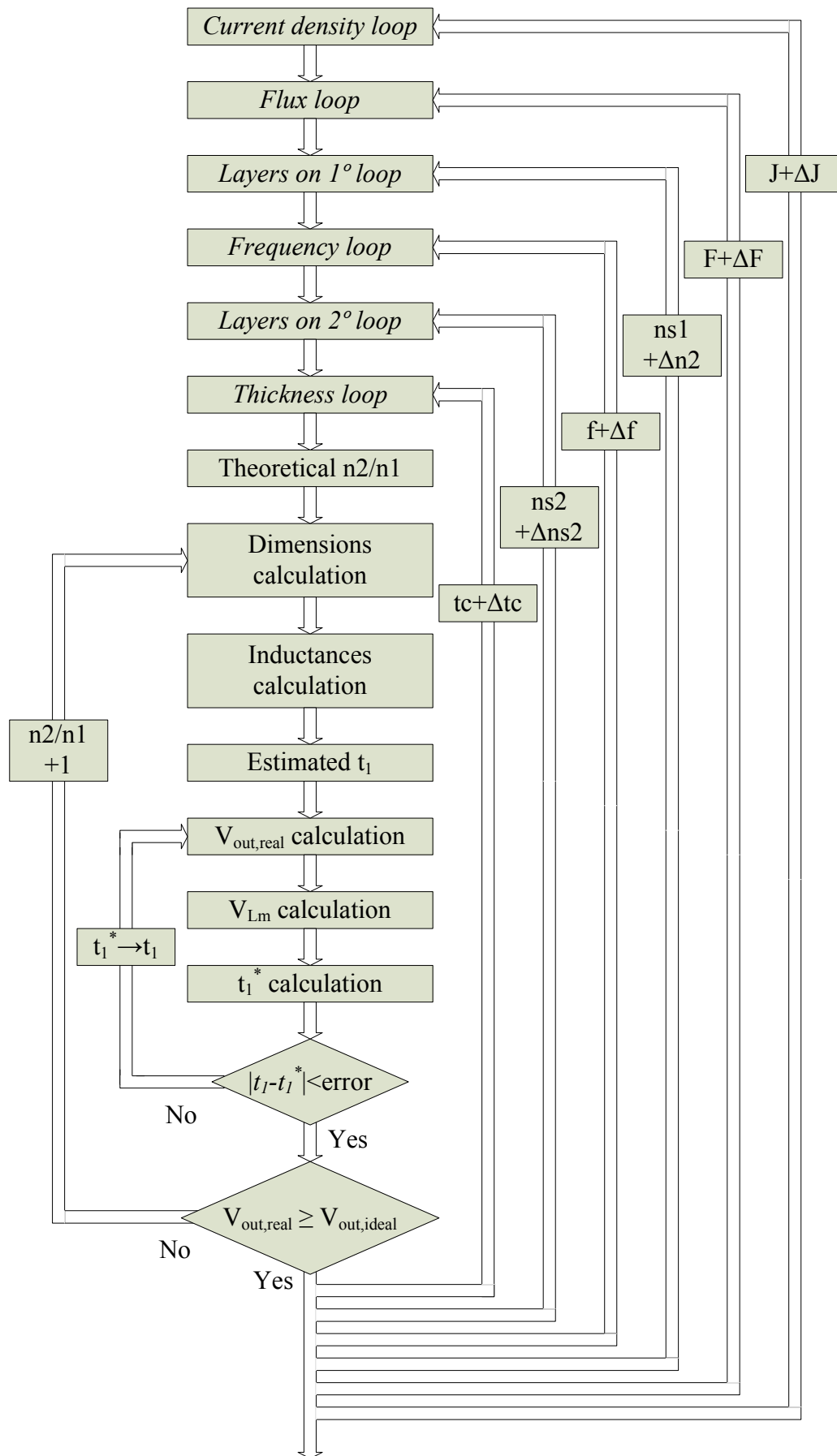


Figure 8.1: Converter database flowchart.

8.1.2 Converter optimization

Once all the possible converters for the application have been calculated, it is required to define a specific criterion in order to be able to choose the most suitable design.

This criterion will be based on the economical aspects of the converter, due to the fact that the device must present the lowest cost possible. Therefore, a first step to find the most suitable optimization criteria must be to define the converter costs.

The converter costs will be divided in two:

- Building costs.
- Losses costs.

The building costs will be those that appear when the device is made, the investment. In this study, these costs will be reduced to the materials costs, being the most significant, the core and the windings ones.

The core cost will be calculated by the volumetric cost in [SEK/m³], provided by the manufacturer, times the core volume.

The windings cost will differ depending on which kind of conductor that is used. Thus, for the foil winding it will be approximated as the copper volumetric cost times the volume of copper used in the primary turns. The cable cost will be estimated using a volumetric cost, as will be explained later.

The loss cost will be the cost of the electric energy dissipated due to the converter losses along its life cycle; that is considered to be 20 years for this study.

The converter losses will depend on the power production of the wind turbine connected to the converter. Due to that the wind speed can be treated as a random variable; the power production (that will depend on it as was explained) can be described with a density function.

Although the most correct way to obtain the average power production would be to calculate the density function and use statistic tools, in this work, the average power production will be estimated using three points:

- The 15 % of the lifetime the turbine will be working at full-load.
- The 60 % of the lifetime the turbine will be working at $\frac{1}{3}$ of the rated.
- The 25 % of the lifetime the turbine will be stopped.

This performance will force to correct the equation for the average converter losses to

$$losses_{AVG} = \frac{15}{100} losses_{full-load} + \frac{60}{100} losses_{\frac{1}{3}rated} \cdot \quad (8.1)$$

For further information about a more elaborated technique of obtaining the average power production, [1] can be consulted.

With that information, the lifetime losses of the converter can be found. These losses will come from the semiconductors and the transformer.

The semiconductor losses will also be divided in two: The conducting and the switching losses, as will be detailed after.

The transformer losses have already been described in Chapter 5, consisting of the winding and the core losses.

As a result, the total converter cost would be expressed as

$$Cost = \text{Building cost} + \text{losses} \cdot \text{lifetime} \cdot \text{energy cost}. \quad (8.2)$$

Nevertheless, this is not the most suitable parameter to optimize due to the fact that, as can be understood, it cannot be weighted the losses cost; which, in fact is the amount of money that the energy producer would have earned with an ideal converter during its lifetime, as the building cost. Moreover, the variation of the money cost during the lifetime of the converter must also be considered. Therefore, a new variable that takes into account all this features must be defined. This variable will be the energy production cost, which is described in detail in [1].

The energy production cost is defined as how much it cost to produce and deliver a unit of energy to the PCC. The total investment cost is calculated assuming that the whole investment is made in the first year and paid off during the lifetime of the wind farm. In addition, it is also assumed that some profit will be made. With that, the energy production cost can be defined as

$$E_{cost,windfarm} = K \frac{Invest}{P_{out,AVG}}. \quad (8.3)$$

The magnitude of K for this study will be $K = 7.53 \cdot 10^{-6}$, that where calculated in [2] for:

- Wind farm lifetime: 25 years.
- Interest rate: 4 %.
- Profit: 3%.

It must be noticed that, although the wind farm losses do not appear explicitly in the equations, their effect are included in the average output power.

In addition, in the literature, the energy production cost for each component in the wind park is also defined; founding that it can be expressed as

$$E_{cost,component} = K \frac{cost_{component}}{P_{in,AVG}} + \frac{E_{cost,windfarm}}{P_{in,AVG}} losses_{component} . \quad (8.4)$$

In order to use (8.4) to calculate the energy production cost of our converter, it would be needed to know the magnitudes of the energy production cost of the wind farm and the average input power.

The energy production cost of the wind farm can be estimated from [1]. The wind farm characteristics assumed will be:

- Series connected DC system.
- Output power: 300MW.
- Output voltage: 150kV.
- Average wind speed: 10m/s.
- Transmission lengths: 70Km.

With that, the value obtained was: $E_{cost,windfarm} = 0.2296$ [SEK/kWh].

Unfortunately, it was impossible to obtain a fine estimation of the average input power. Nevertheless, it will not be a problem due to we are interested to minimize the energy production cost for the converter, so its performance will be more important than its exact value. Consequently, $P_{in,AVG}$ will be skipped from Equation (8.5), defining a new variable that, despite that the energy production cost for the converter will present different values, it will perform exactly in the same way.

This variable, that will be the optimization criterion for the converter design, will be described as

$$E_{cost} = 7.53 \cdot 10^{-6} cost + 0.2296 losses . \quad (8.5)$$

Where, the *cost* will be the transformer building cost and the *losses* will refer to the total converter ones.

Due to the building cost has been reduced to the cost only the transformer, just designs that use the same model of IGBTs can be compared. This is due to in that case the semiconductors cost will be equal and, as we are only interested in the relative change, they can be neglected

In addition, the total converter losses due to both, the transformer and the semiconductors ones will depend on the parameters of the design has been used.

8.2 Definition of the core materials

Once the converter design process has been characterized, it is necessary to define the converter components. For that reason, in this section the possible core materials will be presented and analyzed.

There exist two broad classes of materials for magnetic cores. One class is integrated by iron alloys. These alloys have a large electrical conductivity and large values of saturation flux densities, but high eddy current losses. For that purpose, they can be used in a limited frequency range. In order to minimize this harmful feature, iron cores are always laminated, or made from powdered iron.

The other class of materials used for cores is formed by the ferrites. These are oxide mixtures of iron and other magnetic elements. They present quite large electrical resistivities but low saturation flux densities. Moreover, no significant eddy currents occur due to their high electrical resistivity. This feature makes ferrites to be the most suitable choice to systems that operate at high frequencies.

In order to extend the converters database as much as possible to find the best possible converter, the design process described in the previous section will be applied for three different materials, trying to cover all the possible classes described above. Thus, the materials chosen will be:

- Electrical steel non oriented (M290-50A).
- Electrical thin steel non oriented (NO12).
- Ferrite (N27).

The two first materials will be grouped in the iron alloys group. Their main difference will be the thickness of their sheets. While the M290 will present a sheet thickness of 0.5mm, the thin steel material will have 0.12mm. Obviously, the third material will represent the ferrites class.

It must be mentioned that the manufacturers of the different components used in this work will not be referenced. In some cases the information will be manipulated to hide its origin; nevertheless, in these cases it will be described how the manipulation is done. This argument can be applied to the next sections of this chapter.

Next, the three materials will be described and their main characteristics will be presented.

ELECTRICAL STEEL NON ORIENTED (M290-50A)

The M290-50A is a non-oriented fully processed electrical steel, graded according to European Standard EN 10106. The material is presented in sheets of 0.5mm of thickness.

The density losses function will be derived from the manufacturer data sheets, assuming that it will perform as was described in Equation (5.47). With that, the function found is

$$p_{core} = 874 f^{1.5} B^2 . \quad (8.6)$$

Where the core density losses are provided in [kW/m³], and the frequency and core flux must be introduced in [kHz] and [T] respectively.

From the data sheets it can be obtained the other necessary material properties. These are summarized in Table 8.2.

Table 8.2: Steel material properties.

Material property	Symbol	Units	M290-50A
Relative permeability	μ_r		800
Saturation flux density	B_{sat}	T	≈ 1.2
Conventional density	ρ	Kg/dm ³	7.6

The material price was supplied by the manufacturer as a volumetric cost of 98800 SEK/m³.

ELECTRICAL THIN STEEL NON ORIENTED NO12

The NO12 is a thin fully processed non-oriented electrical steel, supplied at a nominal thickness of 0.12mm, especially suited for use at medium to high frequencies (200 - 2000 Hz).

As was done before, the core density losses can be extracted from the manufacturer data sheets, leading to

$$p_{core} = 306 f^{1.2} B^{1.6} . \quad (8.7)$$

Using the same units than before.

The other material properties are presented in Table 8.3. It must be noticed that the relative permeability was obtained from the slope of the magnetic field strength as a function of the magnetic polarization.

Table 8.3: Thin steel material properties.

Material property	Symbol	Units	NO12
Relative permeability	μ_r		6885
Saturation flux density	B_{sat}	T	≈ 1.4
Conventional density	ρ	Kg/dm ³	7.65

In that case, the material price, provided as a volumetric cost 1790100 SEK/m³.

FERRITE N27

The N27 is a typical ferrite material, presented in a multitude of core shapes and dimensions.

The core density losses for the material can be found as

$$p_{core} = 78.6 f^{1.29} B^2 . \quad (8.8)$$

The other material properties are compiled in Table 8.4.

Table 8.4: Ferrite material properties.

Material property	Symbol	Units	N27
Relative permeability	μ_r		2000
Saturation flux density	B_{sat}	T	0.5

To obtain a volumetric cost for this material the price of a standard core was used and then it was divided by its core volume, obtaining a cost of 471559 SEK/m³.

As a conclusion, features of the materials can be compared. Thus, the two steel materials will present a saturation flux more than the double of the ferrite material. Nevertheless, the density losses for the same conditions will be quite large in the iron alloys. It is especially noticeable if the ferrite and the normal steel are compared, being its losses more that ten times the N27 ones.

If the material costs are compared, the normal steel will be the cheapest compared with the others. However, the most perceptible fact is that the thin steel will be the most expensive, with a cost of almost 4 times that of the ferrite and more than 18 times the normal steel prize. This exceptionally high cost will penalize this material in the optimization, although it combines the advantages of the two classes: Moderate low density losses and high saturation flux.

8.3 Definition of the transformer conductors

In this section, the transformer conductors will be defined. It should be stressed that almost all of their features were defined in Section 5.3 when the transformer was described.

In fact, the primary winding will be developed by copper foils, and the secondary by cables, composed by a Litz structure of conductors and a strong isolation. The equations necessities to dimension the windings can be found in Section 5.3.

It must be noticed that, from those equations the conductors dimensions will depend on the transformer currents. For that reason, a more detailed analysis of these currents must be completed.

Until here, the only current parameters that have been used are the average currents, which were derived from the power and voltage specifications. Nevertheless, in order to dimension the conductors, the RMS values of the currents will be needed.

To obtain the primary RMS current, the only information available is the magnitude of the average value and the input current waveform of Figure 7.8. Due to the fact that this waveform will depend on too many variables, it will be approximated to a simpler plot. The result of this simplification can be seen in Figure 8.2, where the waveform has been modeled as two rectangular steps for each period. The dimensions of these steps will be, for the temporal axis equal to t_{on} , and for the current equal to the I_{max} .

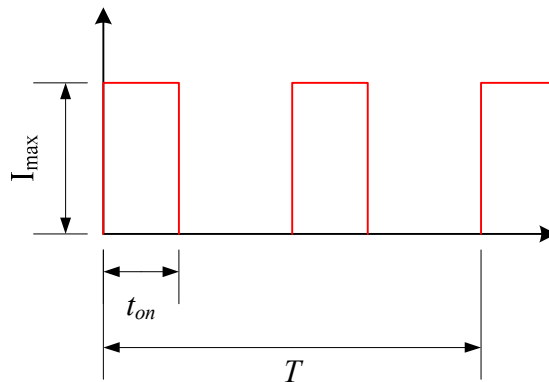


Figure 8.2: Simplified input current waveform.

With that, and using the definition of average current from (7.31), it can be found that

$$\bar{I} = 2 \frac{t_{on}}{T} I_{max} . \quad (8.9)$$

Where, by means of the duty cycle, the peak current can be isolated as

$$I_{max} = \frac{\bar{I}}{2D} . \quad (8.10)$$

The RMS value can be obtained using its definition, leading to

$$I_{RMS} = \sqrt{\frac{1}{T} \int_0^T i(t)^2 dt} = \sqrt{\frac{2(I_{max})^2 t_{on}}{T}} . \quad (8.11)$$

That can be expressed in terms of the average value as

$$I_{RMS} = \frac{\bar{I}}{\sqrt{2D}} . \quad (8.12)$$

In order to calculate the secondary RMS current, the ideal transformer relation, $i_1 N_1 = i_2 N_2$ can be used, leading to the fact that the secondary current will perform as the primary. Thus, the previous equations can also be used here.

Once the transformer currents have been defined, the last conductors parameter can be studied: the cost.

The foil winding cost will be estimated using the volumetric cost of the copper and multiplying it for the copper volume needed to elaborate the winding. That, neglects the cost of the isolation due to its volumetric cost is much cheaper and its area much smaller than the copper ones.

The copper volumetric cost found was 1460120 SEK/m³.

As a result, the foil cost can be expressed as

$$Cost_{foil} = cost_{copper} A_{Cu} l_w N_1. \quad (8.13)$$

To obtain the cable cost, the isolation must be considered, which complicates the cost derivation. The available information to calculate the isolation cost was a list of cable prices with the same conducting area and different isolation thicknesses (to different voltage isolation levels) from a determined manufacturer.

Due to the fact that the conducting area was fixed for all the cables, and the isolation material was always the same, the cable cost (for one meter) could be expressed as a function of the isolation volume. In Figure 8.3, the cable cost for the different isolation volumes is presented. It is also plotted the function that fits better these data.

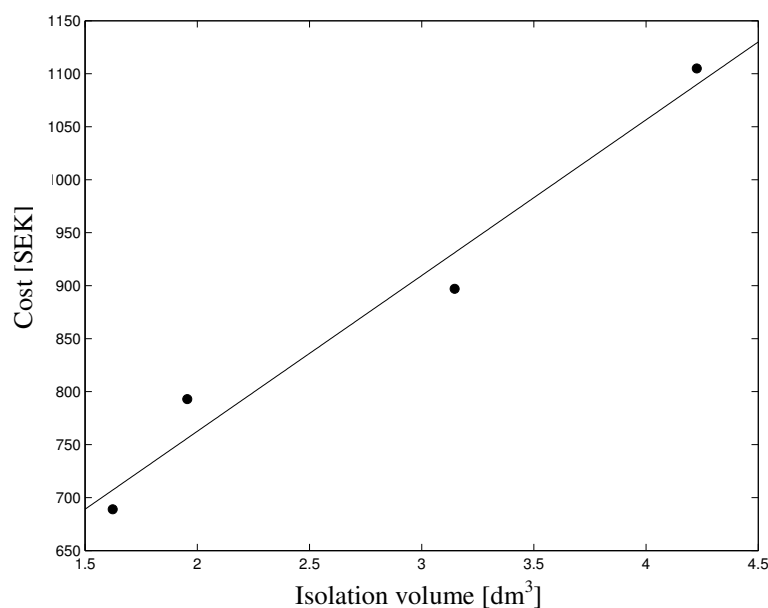


Figure 8.3: Plot of the cable cost as a function of the isolation volume.

From the figure it can be realized that the most suitable function to fit the results will a shape as

$$cost = B + AV_{isolation} \cdot \quad (8.14).$$

Where:

$$B = 468 \text{ SEK.}$$

$$A = 147144 \text{ SEK/m}^3.$$

If the physical sense of this parameters if analyzed, it can be noticed that the constant (B) will represent the cost of the conductor while A will represent the volumetric cost for the isolation.

With that, the cable volumetric cost can be estimated as a weighted average between the isolation and the copper volumetric cost. Moreover, as the conductor will be made of Litz wires, the conductor area must be corrected as was explained in Chapter 5.

It must be noticed that the wires isolation will be neglected, as was done for the foils, so the equation that describes the cable volumetric cost can be found as

$$cost_{cable} = \frac{A_{Cu} / Litz}{A} cost_{copper} + \frac{A_{isolation}}{A} cost_{isolation} \cdot \quad (8.15)$$

Where A will be the total cable area and $Litz$ the correction the factor for the conducting area. To obtain the isolation area, it will be used the isolation thickness defined in Chapter 5. The copper area can be calculated from Equation (5.5), using the secondary RMS current and the current density allowed.

The cost will be calculated for:

- Secondary current: 540A.
- Current density: 2A/mm².

Leading to a cable volumetric cost of 250399 SEK/m³.

The election of these values is explained in next section.

At last, the cable cost can be estimated as

$$Cost_{cable} = cost_{cable} A_{Cu2} I_w N_2 \cdot \quad (8.16)$$

8.4 Dimensioning of the transformer. The worst operation point

While the core materials and the conductors have been described, in this section the transformer converter will be dimensioned, attending to its most stressing point of operation.

The first transformer parameter that is affected by the circuit specifications is the number of turns because it will directly depend on the converter output voltage.

Accordingly, the number of turns must be able to hold up the maximum output voltage that, as was defined in Chapter 6, will be $V_{out,max} = 20.25kV$.

The system specifications will also affect the copper areas of the windings. The windings must be designed so that they are dimensioned to be able to transmit the maximum currents that will appear in the converter.

For the primary winding, the maximum current will appear when the turbine is providing its maximum value, as was described in Chapter 5 is 5MW. As this power will always be supplied at 3.3kV, the average current will be around 1500A. Nevertheless, for dimensioning the conductors, the RMS current must be used. This parameter can be obtained using Equation (8.12), giving a current magnitude about 2500A.

For the secondary winding, it must be considered that the converter will be connected in series with the others wind turbine systems. That means that, the maximum secondary current will be determined for the whole leg.

Studying the leg performance, it can be realized that the maximum current will appear when all the turbines were providing their maximum power. Therefore, in this situation, the whole system will be working at their rated output voltage (15kV), leading that the maximum current will be the same as the one that was studied for one single converter. That means that the maximum average current on the secondary will be 333A, and the RMS value around 540A.

As a result, Table 8.5 summarizes the circuit conditions and its effects on the transformer parameters.

Table 8.5: Transformer worst operation point.

Circuit parameter	Situation	Trans. parameter affected
Output voltage	Maximum value (20.25kV)	Number of turns
Primary current	Maximum RMS value (2500A)	Primary copper area
Secondary current	Maximum RMS value (540A)	Secondary copper area

At last, it must be mentioned that it should not be necessary to make a thermal analysis of the transformer due to the fact that, as was mentioned before, the current density will be directly controlled in the design, setting it to reasonable value.

8.5 Definition of the semiconductors

The last converter components that will be dimensioned are the semiconductors. By reviewing Figure 4.6 with could note that four switches will be needed on the low voltage side and four diodes on the secondary. To develop the switches, IBGTs were the selected devices.

8.5.1 IGBTs dimensioning

The IGBTs are controlled semiconductor devices, especially suitable for switching; due to they can be controlled by the gate voltage as MOSFETs, and present a power scheme as BJT transistors, reducing the conducting losses.

The commercial IGBTs devices usually include a diode connected in antiparallel. This will be very useful for our application, as was explained in the theoretical analysis of the real converter in Chapter 7.

As has been mentioned, the real IBGTs will present two kinds of losses:

- Switching losses.
- Conducting losses.

The switching losses derive from the fact the device requires a finite time to change its state, losing some energy on it. Thus, the IGBT will present a turn-on and a turn-off energy. The antiparallel diode will also require a reverse recovery energy.

These energy losses per pulse are provided in the manufacturer data sheets for the nominal collector current and the nominal collector-emitter voltage. The typical technique to adapt the values to the working point of the specific application is to assume that the energy losses will be both linearly dependent on these variables. With the aim of considering the worst possible case, the maximum collector current must be the parameter used.

In order to estimate the power losses of the converter; it is necessary to calculate the number of events that occurs in each switch for a period. From the Figure 7.10, where the waveforms of the switches of the real converter were plotted, it can be realized that, for one period, each switch will experience a turn-on and a turn-off cycle, as well as the antiparallel diode will conduct one time. Using that information, the power losses in each IGBT can be obtained by multiplying the energy losses in one period, times the switching frequency.

The expression for the switching losses for one IGBT will be defined as

$$losses_{switching} = \frac{E_{on} + E_{off} + E_{rec}}{I_{C,nom} V_{CE,nom}} I_{C,max} V_{CE} f . \quad (8.17)$$

Where:

- E_{on} Turn-on energy loss per pulse.
- E_{off} Turn-off energy loss per pulse.
- E_{rec} reverse recovery energy loss per pulse.
- $I_{C,nom}$ Nominal collector current.
- $V_{CE,nom}$ Nominal collector-emitter voltage.
- $I_{C,max}$ Application maximum collector current (see figure 8.2).
- V_{CE} Application collector-emitter voltage.
- f switching frequency.

From (8.17) it can be deduced that the switching losses will depend on the converter working point and that they will increase linearly with the frequency.

The conducting losses will come from the power dissipation produced in the power line of the IGBT.

From the output characteristic obtained in the data sheets, this power line can be modelled as a voltage source connected in series with a resistance, as Figure 8.4 shows.

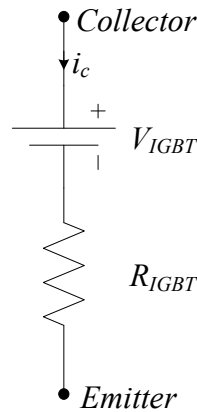


Figure 8.4: IGBT power line model.

Thus, the power losses for an IGBT can be calculated from

$$losses_{conducting} = V_{IGBT} \overline{I_C} + R_{IGBT} I_{C,RMS}^2 . \quad (8.18)$$

The conducting losses in the antiparallel diodes will be neglected in this study, due to the fact that the average and RMS current through them will be much lower than in the IGBTs, as can be understood from the converter analyses in the chapters before.

Equation (8.18) shows that the conducting losses will also depend on the working point of the system.

Thus, the IGBT losses can be found as

$$losses_{IGBT} = \frac{E_{on} + E_{off} + E_{rec}}{I_{C,nom} V_{CE,nom}} I_{C,max} V_{CE} f + V_{IGBT} \overline{I_C} + R_{IGBT} I_{C,RMS}^2 \quad (8.19)$$

In addition, it must be emphasized that (8.19) describes the losses for one IGBT, while each switch will be formed by several of them, in order to manage the voltage and current levels of the converter. In fact, a switch will be disposed by a number of series connected IGBT packs to hold up the voltage requirements. While, each pack will have a group of parallel-connected IGBTs to handle the current levels.

This feature will affect to the current and voltage levels over each IGBT on the switch. Thus, as the converter will have four switches, the switches losses can be expressed as

$$losses_{switches} = 4 \left[\frac{E_{on} + E_{off} + E_{rec}}{I_{C,nom} V_{CE,nom}} \frac{I_{in,max}}{n_1} \frac{V_{in}}{n_2} f + V_{IGBT} \frac{\overline{I_{in}}}{n_1} + R_{IGBT} \left(\frac{I_{in,RMS}}{n_1} \right)^2 \right] n_1 n_2 \quad (8.20)$$

Where:

- n_1 number of parallel IGBTs in each pack.
- n_2 number of series connected packs.
- V_{in} Input voltage.
- $I_{in,...}$ Input current.

At last, as it was commented, the losses will depend on the converter working point so, they will be affected by the average power production defined in Section 8.1. Therefore, the average losses for the switches will be found as

$$losses_{switches,AVG} = \frac{15}{100} losses_{switches,full-load} + \frac{60}{100} losses_{switches,1/3rated} \quad (8.21)$$

In order to cover the widest range of solutions, the optimization process will be applied for two different IGBT models. The first model will present a maximum collector-emitter voltage greater than the maximum input voltage of the converter; thus it will not be necessary to connect the IGBTs in serial. The second model will have a lower maximum voltage, so it will be necessary to series connect several packs of IGBTs. Both models will require modules to be connected in parallel to handle the input current.

If the most powerful model is selected, the commutation drivers of the converter will be much simpler due to the fact that, as was commented before, the connection of controlled semiconductor devices in series always generates problems.

Moreover, as the number of units needed will be lower, it might be logical to guess that the total losses would be smaller too. Nevertheless, it must be considered that, as the voltages and currents over each IGBT will be greater, the losses on each of them will increase. In addition, the values of the energy losses per turn (E_{on} , E_{off} , and E_{rec}), as well as the magnitudes of V_{IGBT} and R_{IGBT} , will be greater than in the less powerful IGBT model.

As a conclusion, the optimization results will determine which is the most suitable choice.

Next, the two IGBT models will be defined and their main properties presented.

BSM 400 GA 170 DLC

The IGBT properties that are of interest for this study are presented in Table 8.6.

Table 8.6: BSM 400 GA 170 DLC properties.

Property	Symbol	BSM 400 GA	Units
Collector-emitter maximum voltage	V_{CES}	1700	V
DC-collector maximum current	$I_{C,nom}$	400	A
Turn-on energy losses per pulse $I_C = 400A$ $V_{CE} = 900V$	E_{on}	170	mJ
Turn-off energy losses per pulse $I_C = 400A$ $V_{CE} = 900V$	E_{off}	135	mJ
Peak reverse recovery energy $I_C = 400A$ $V_{CE} = 900V$	E_{rec}	110	mJ
Collector-emitter saturation voltage	V_{IGBT}	1.181	V
Collector-emitter resistance	R_{IGBT}	4.528	m Ω

From the collector-emitter maximum voltage, and knowing that the maximum input voltage is 3300V, it can be deduced that, at least 2 IGBT packs will be needed. In addition, as the maximum input current is about 1500A, 4 IGBTs must shape each pack. Moreover, in order to satisfy each specification one unit will be added to each magnitude. This will improve the working conditions of the devices, extending their lifetime. As a result, the number of IGBTs needed for the converter will be:

- $n_1 = 5$.
- $n_2 = 3$.

That leads to a total number of devices of 60.

FZ 400 R 65 KF1

The IGBT properties that are of interest for this study are presented in Table 8.7.

Table 8.7: FZ 400 R 65 KF1 properties.

Property	Symbol	BSM 400 GA	Units
Collector-emitter maximum voltage	V_{CES}	6500	V
DC-collector maximum current	$I_{C,nom}$	400	A
Turn-on energy losses per pulse $I_C = 400A \quad V_{CE} = 3600V$	E_{on}	4000	mJ
Turn-off energy losses per pulse $I_C = 400A \quad V_{CE} = 3600V$	E_{off}	2300	mJ
Peak reverse recovery energy $I_C = 400A \quad V_{CE} = 3600V$	E_{rec}	1050	mJ
Collector-emitter saturation voltage	V_{IGBT}	2.25	V
Collector-emitter resistance	R_{IGBT}	7.5	m Ω

From the collector-emitter maximum voltage, it will not be needed to connect IGBTs in serial. As the maximum collector current is the same as before, 4 units will be needed in parallel.

In that case, the voltage specification is already loosely satisfied so, only the number of IGBTs in parallel will be increased. As a result, the number of IGBTs needed for the converter will be:

- $n_1 = 5$.
- $n_2 = 1$.

That leads to a total number of devices of 20.

8.5.2 Diodes dimensioning

The diodes on the high voltage side will present a similar performance as the IGBTs described above. Thus, their losses will also be divided in switching and conducting losses.

The switching losses are due to fact that, to open the diode some energy will be required.

The energy losses per pulse are provided by the manufacturer as a linear function of the forward current. Thus, this property will performance as

$$E_{rec} = KI_{for} \cdot \quad (8.22)$$

As before, the number of events for one period in each diode must be calculated. From Figure 7.11, where the diodes waveforms were plotted, it can be seen that each diode will be turned on one time during a period. Therefore, the power losses can be expressed as

$$losses_{switching} = E_{rec} (I_{for}) f . \quad (8.23)$$

The conducting losses can be estimated as was done for the IGBTs. That means that it can be modelled as a voltage source and a resistance connected in serial. The parameters that will represent these features will be V_{DIODE} and R_{DIODE} . The equation that describes these losses can be found as

$$losses_{conducting} = V_{DIODE} \overline{I_{for}} + R_{DIODE} I_{for,RMS}^2 . \quad (8.24)$$

As these diodes will be installed in the high voltage side, more than one unit in serial to hold up the voltage levels will be needed. Therefore, as the circuit demands 4 diodes, the diodes losses can be expressed as

$$losses_{diodes} = 4 \left[K \frac{I_L}{2} f + V_{DIODE} \frac{I_L}{2} + R_{DIODE} \left(\frac{I_L}{2} \right)^2 \right] n_3 . \quad (8.25)$$

Where:

n_3 number of units in serial.

It must be noticed that in Equation (8.25) the current through the main inductance I_L appears. This current, as can be seen in Figure 7.9, will present an offset and a small ripple and can be approximated to a constant. It is also remarkable that this current appears divided by two. This is due to the fact that it can be assumed that the current will flow through the two legs of the diodes bridge. In fact, if Figure 7.11 is studied, it can be seen that the diode cycle will consist in three parts: the first part, where it will conduct all the current, the second one where it will transmit one half of the current, and the third part where it will not conduct. This part will last almost as long as the time of the first part.

At last, as the losses depend on the circuit parameters, the average losses must be calculated, leading to

$$losses_{diodes,AVG} = \frac{15}{100} losses_{diodes,full-load} + \frac{60}{100} losses_{diodes,\frac{1}{3}rated} . \quad (8.26)$$

The diodes used in the converter will be similar that the antiparallel ones of the FZ 400 R 65 KF1. Table 8.8 summarizes its important properties.

Table 8.8: Diodes properties.

Property	Symbol	BSM 400 GA	Units
Maximum reverse voltage	V_{rev}	6500	V
Maximum forward current	I_{for}	400	A
Reverse recovery energy constant	K	2.2	J/A
Diode saturation voltage	V_{DIODE}	1.5	V
Diode resistance	R_{DIODE}	4.9	m Ω

From the theoretical model, it must be remembered that over each diode will experience a voltage that is two times the output voltage so, its worst working point will occur at its maximum value. In that case the voltage over the diodes will be 40.5kV, leading to that the number of units needed for each diode will be equal to six. Nevertheless, as before, one unit more will be added. Therefore, the final number of units for each diode will be

- $n_3 = 7$.

That means that the total number of units will be of 28.

8.6 Analysis of the converter designs

Once the components have been defined and dimensioned, the converters database can be executed.

In this section, will be studied the converter properties are affected by the construction and operating variables. Thus, the losses, costs and the energy cost will be analyzed.

The way that the analysis will be performed consists in studying each of the mentioned properties as a function of a specific variable, fixing the others to a constant value. The analysis will be accomplished for: frequency, flux, core thickness and current density. The number of layers on the windings will be neglected due to these variables will not affect the number of turns, and it can be considered that for each situation described by the other four variables, it can be found the optimum number of layers to build the transformer.

It must be mentioned that the analysis will be performed using a ferrite N27 core and the BSM 400 model of the IGBT.

It is also important to emphasize that the plots presented in this section has been selected in order to show, as clear as possible, the different features of the parameter studied. Therefore, it could happen that some of them would match with a not very realistic design.

8.6.1 Frequency analysis

The first converter property that will be analyzed is the losses. Figure 8.5 plots the transformer and the semiconductor losses. It also shows the sum of both, that is the total value.

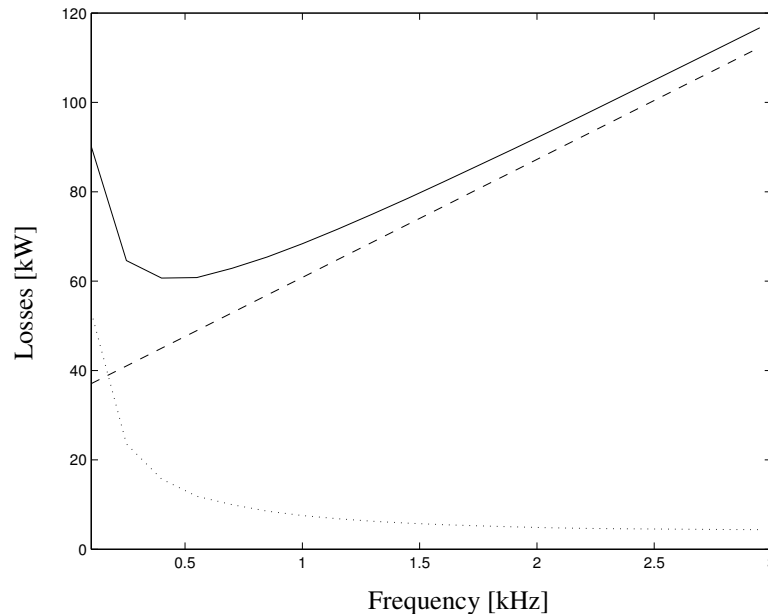


Figure 8.5: Converter losses depending on the switching frequency. Solid the total losses, dashed the semiconductor losses, dotted the transformer losses.

In the figure it can be seen that the transformer losses will decrease sharply in the low frequency range. This is due to the fact that, in this range, the number of turns decrease very fast if the frequency is increased, decreasing the amount of windings and the core volume. Obviously, these facts will lead to a reduction in the transformer losses. For the medium frequency range, it can be seen that the slope of the losses is smaller, due to the reduction of the number of turns begins to be balance with the increment on the core density losses. Moreover, for larger frequencies, the transformer losses would begin to increase due to this effect. Unfortunately, this feature cannot be noticed in Figure 8.5 due to that the frequency range was reduced in order to show more in detail the performance of the other losses.

Here, it must be mentioned that more detailed information about the transformer performance can be found in Appendix A, where a further analysis of its behaviour is presented.

The semiconductor losses will perform as equations (8.20) and (8.25) predicts. That means that it will be composed by a constant value, from the conducting losses (that depends on the circuit working point) and a linear increase due to the switching losses. Nevertheless, the most remarkable feature is the fact that, even for low frequency values, the semiconductor losses will be much greater than the transformer ones. This will lead to, as can be seen in the plot, which the optimum for the total losses will be found for a low value of the frequency.

This fact shows that the switches will have a critical influence in the final converter design, which was unexpected at the beginning of the design process.

The cost of the converter, as was explained, will consist in the building and the losses cost. For this study, the building cost will be the transformer cost, as was defined in Section 8.1. The performance of these variables can be seen in Figure 8.6.

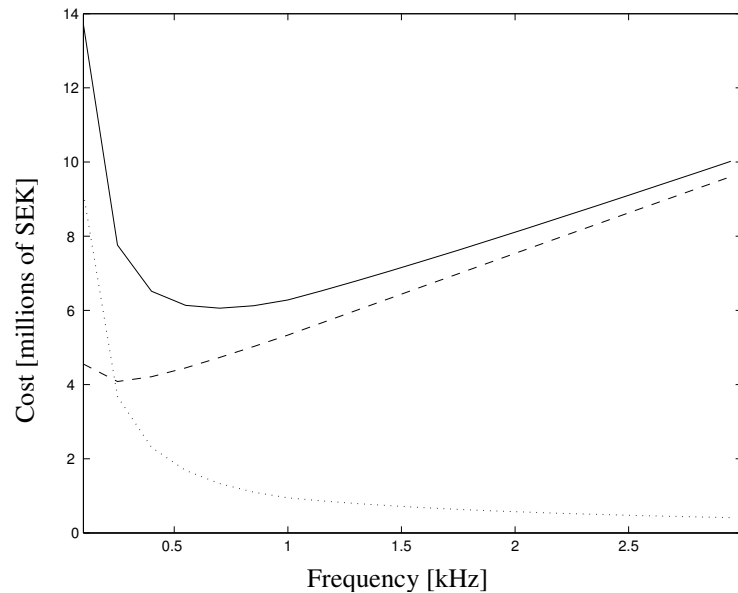


Figure 8.6: Converter cost depending on the switching frequency. Solid the total cost, dashed the losses cost, dotted the transformer (building) cost.

From the figure, it can be noticed that the transformer cost will decrease when the frequency is increased. This is due to the reduction in the number of turns mentioned. In fact, this effect will lead to a decrease of the amount of copper necessary to make the windings. Moreover, as the windings are reduced, the size of the core needed to settle them will be smaller, decreasing its cost.

The cost of the losses, estimated as the losses times the cost of the energy, will follow exactly the performance of the total losses, decreasing for the lower frequency values, reaching a minimum and beginning to increase later, as a consequence of the switching losses.

As a result, the total cost will find a minimum for a determined frequency, influenced by the losses cost as shows the figure.

At last, the energy cost performance is presented in Figure 8.7. It must be remembered that the absolute value of this energy cost is not the real one, due to the fact that, as was explained before, the thing that is really interesting of this property is its performance.

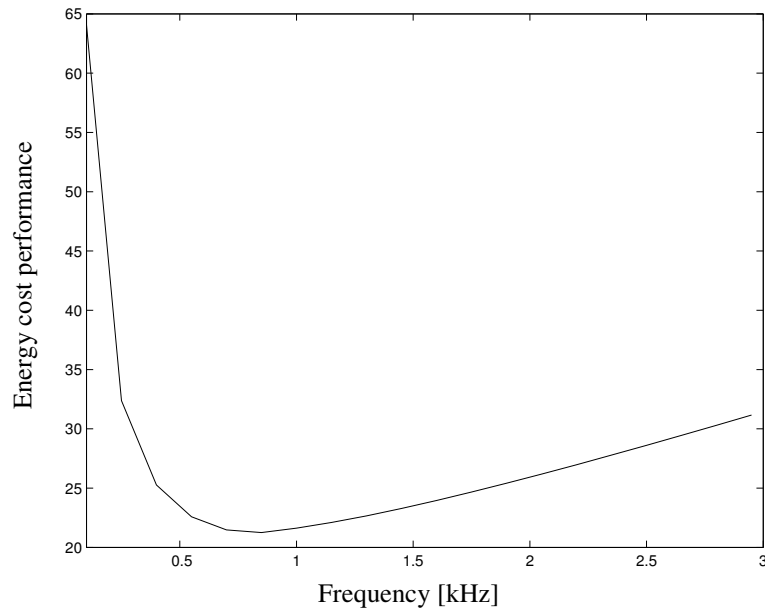


Figure 8.7: Converter energy cost depending on the switching frequency.

From the figure it can be observed that the performance of the energy cost will be similar to the total cost one. Nevertheless, if it is compared with the Figure 8.6, it can be seen that the energy cost reaches its minimum for a higher frequency compared with the total cost. This is due to the fact that the energy cost will give more importance to the building cost and they will decrease if the frequency is risen.

8.6.2 Flux analysis

To study how the transformer losses depends on the core flux, the arguments used in the frequency analysis can be used again, due to that the flux and the frequency will produce the same effects on the transformer performance. Thus, for lower flux values, the transformer losses will decrease if the flux is increased, reaching a minimum and increasing slowly in the high value range.

The core flux will not significantly affect the semiconductor losses, and accordingly they will be constant. To conclude, the total losses will perform as the transformer ones with the only difference of the offset added by the semiconductors.

By studying Figure 8.8, it can be realized that for the transformer cost, the arguments used in the frequency analysis are suitable here. This means that, for low fluxes, the transformer cost will decrease fast if the flux is raised, while for medium and large values, its reduction will be quite smooth. The cost of the losses will follow the total losses performance.

As a result, from the figure it can be inferred that for the lowest flux values, the total cost will decrease sharply if the flux increase, while in the medium and large range, it will be almost constant. This is due to the fact that, the small decrease of the transformer cost will be balanced with the increase of the total losses.

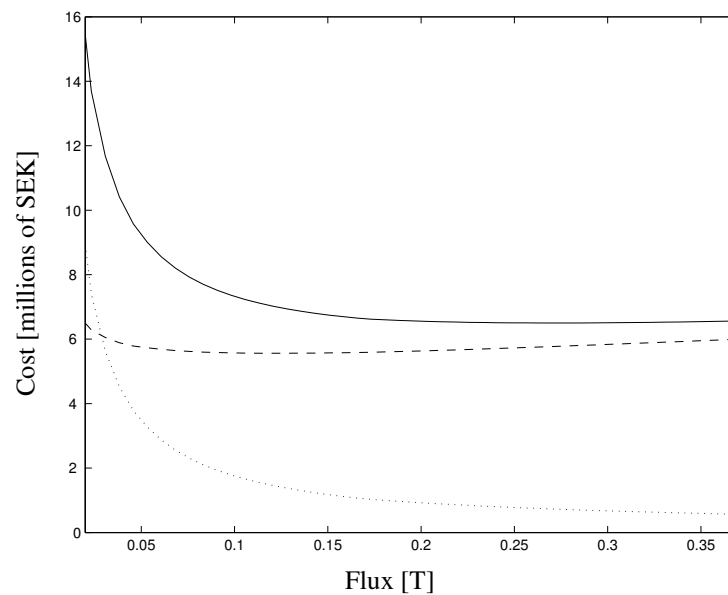


Figure 8.8: Converter cost depending on the core flux. Solid the total cost, dashed the losses cost, dotted the transformer (building) cost.

Finally, the energy cost will behave similar as the total cost for the low flux range. For higher values, as it gives more weight to the transformer costs, it will decrease very slowly if the flux is increased.

8.6.3 Thickness analysis

As in the flux analysis, the semiconductor losses will not be affected by the variation of the core thickness. Therefore, the total losses will perform as in the transformer but with an offset added.

The transformer losses will sharply decrease for the lower values of thickness, being almost constant for the medium and large values. This is due to the fact that, in the range of the low thicknesses, a small increment of it motivates a large reduction in the number of turns. This will decrease the winding and the core losses, due to as the windings will need less room, they can be smaller. Despite, in the medium-large range, the turns reduction is less significant, and the reduction in the windings losses will be balanced with the increase of the core losses, that is due to the increment of the core volume, produced by thickness growth. It must be remembered that more detailed information about that can be found in Appendix A.

The converter costs are presented in Figure 8.9. If the building costs are observed in the figure, it can be realized that, for the first thickness values (the smallest), the transformer cost will decrease. This is due to the large reduction on the number of turns, which will force the windings and the core volume to decrease and thus, the cost. Nevertheless, for medium-large thicknesses, the transformer cost will begin to increase due to the prevalent effect that there will be the increase of the core volume as a consequence of the core area increment.

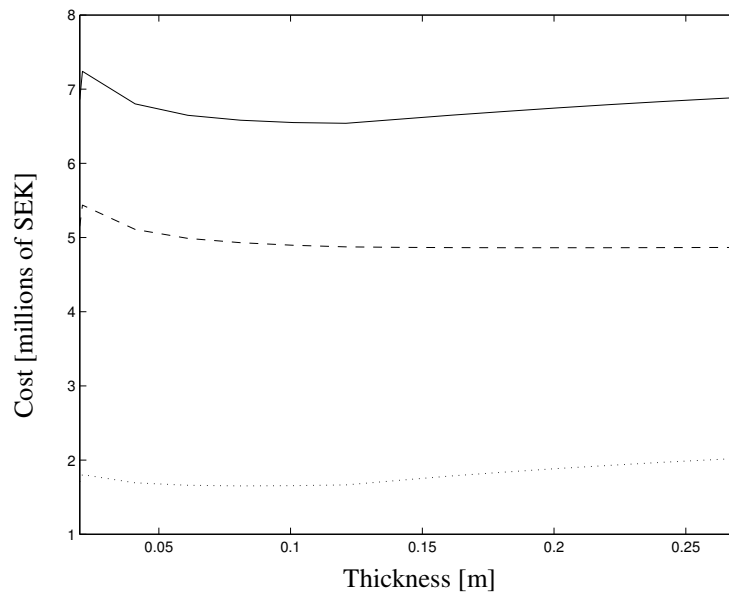


Figure 8.9: Converter cost depending on the core thickness. Solid the total cost, dashed the losses cost, dotted the transformer (building) cost.

About the cost of the losses, they will follow the performance of the total losses, as can be seen in the figure. Thus, the total cost will find an optimum value for a specific thickness.

The energy cost is presented in Figure 8.10.

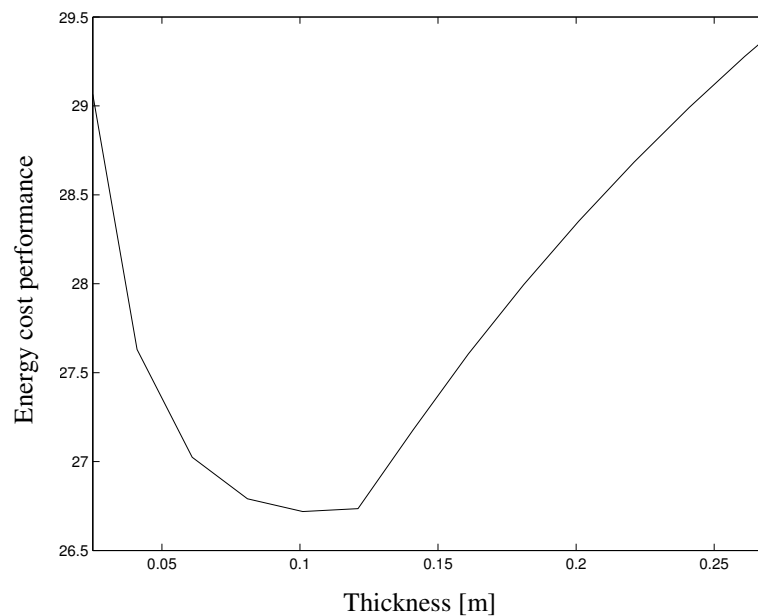


Figure 8.10: Converter energy cost depending on the core thickness.

In the figure it can be realized that the energy cost will behave like the total cost. The main differences will be that, as it enlarges the effect of the building cost, its variations will be more noticeable, as well as it will find its optimum value for a smaller thickness.

8.6.4 Current density analysis

In Figure 8.11, the converter losses have been plotted.

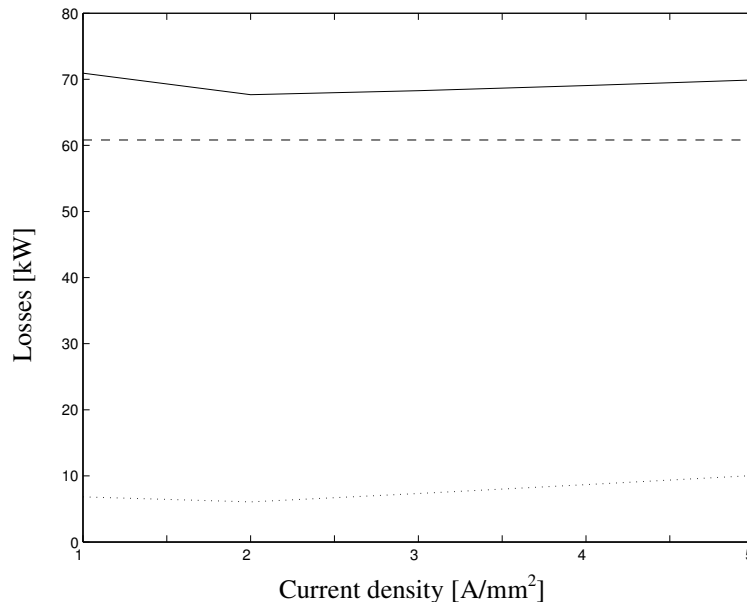


Figure 8.11: Converter losses depending on the density losses. Solid the total losses, dashed the semiconductor losses, dotted the transformer losses.

From the figure it can be realized that the total losses will perform as the transformer losses, due to the fact that the density current will not affect the semiconductor losses, only a constant offset will be added.

It can be seen in the figure that the transformer losses will smoothly decrease if the current density is increased in the low value range. Furthermore, the losses will begin to increase with the current density for the medium-large range of it. This is due to the fact that this plot was selected in order to show the two opposed effects that the current density will produce in the transformer. In fact, if the current density increases, the winding losses will increase too. On the other hand, the size of the windings will be reduced, and thus the size of the core needed. This will lead to a reduction in the core losses. Once again, a detailed description of these effects can be found in Appendix A.

The converter cost is presented in Figure 8.12.

From the figure, the transformer cost will decrease if the current density is increased. This is due to the fact that, as was mentioned before, the conductors will be reduced and thus the cost of the windings. In addition, as the windings are smaller, the core size will be reduced too, decreasing its cost. The cost of the losses will follow the shape of the total losses.

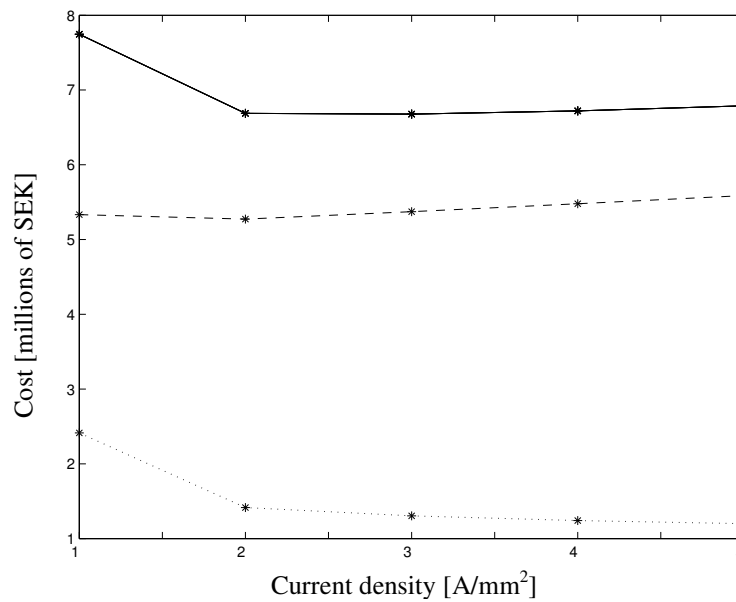


Figure 8.12: Converter cost depending on the current density. Solid the total cost, dashed the losses cost, dotted the transformer (building) cost.

As a result, the total cost will perform as presented in the figure, finding a minimum for a reasonable current density value.

At last, the energy cost will show a similar shape as the total cost but as it gives more importance to the building cost, it will find the minimum for a larger value of the current density.

8.7 Optimization results

Once the converter design has been analyzed, the optimization can be accomplished. The optimization process was executed for three different core materials, and for two models of IGBTs.

First, it will be studied the optimization results for the FZ 400 R 65 KF1. It must be remembered that this is the IGBT model that will not need to connect devices in serial, due to it is able to hold up the converter voltages. Table 8.6 presents the optimum converters for the three core materials, as well as its most important features.

Table 8.9: Optimization results for IGBT model FZ400 R65 KF1.

	FERRITE N27	STEEL M290-50A	THIN STEEL NO12
Energy cost	16.2	12.5	21.6
Construction cost [SEK]	542,396	277,035	880,766
Losses cost [SEK]	4,160,300	3,570,600	5,161,100
Losses [kW]	52.7	45.2	65.4
Transformer losses [kW]	5.4	13.6	18.1
Semiconductors losses [kW]	47.3	31.6	47.3
Current density [A/mm^2]	3	3	4
Frequency [Hz]	250	100	250
Core flux [T]	0.35	0.45	0.71
Core thickness [m]	0.1	0.24	0.04
Layers on the primary	1	1	1
Layers on the secondary	5	5	5
Winding ratio	14	13	14
Turns on the primary	11	12	13
Transformer height [m]	1.62	1.73	1.77
Transformer radius (R_{out}) [m]	0.82	0.9	0.77
Leakage inductance [H]	$3.03 \cdot 10^{-5}$	$3.6 \cdot 10^{-5}$	$3.7 \cdot 10^{-5}$
Magnetizing inductance [H]	0.0108	0.0175	0.0365
Main inductance [H]	0.315	0.732	0.315

From the table it can be seen that the minimum energy cost will occur for normal steel. In addition, this will be the one that will require a smaller investment and present the minimum losses. Thus, for this kind of IGBT the most suitable design will be the M290-50A steel.

From the results, it can be noticed that the converter design will be strongly influenced by the losses, due to that their cost will be much higher than the investment, and will determine the performance of the energy cost. Furthermore, the most important losses will come from the semiconductors, which will make the converter to operate at low frequencies in order to reduce the switching losses. This low frequency will lead the transformer to grow in size, because of the considerable number of turns required. Nevertheless, this increment in the transformer size and thus in the cost, will not affect the energy cost a lot, as has been explained earlier.

If the three materials are compared, it can be seen that the ferrite one will present lower losses than the steels. It is also interesting to note that the optimum frequency for the normal steel will be lower than for the others, due to that this material will be more appropriate for low frequencies. About the optimum fluxes, it can be seen that the thin steel will present a much higher value than the ferrite, as could be presumed when the material properties were studied. Due to its worse properties, the normal steel will present a moderate value of optimum flux.

At last, studying their core thicknesses it can be seen that the cost of the material will have a strongly influence on this variable. Thus, the thickness of the thin steel converter will be much lower than the normal steel, which was much cheaper. The ferrite will present a medium thickness, which coincides with fact that it has the medium cost.

About the electrical parameters, it must be remembered that all the converters were designed to fulfil the defined specifications. Nevertheless, it is interesting to analyze how each converter use different techniques to satisfy it. Thus, the normal steel will not need to increase the theoretical winding ratio (that was rounded to the higher value) due to that it will work at a lower frequency. That will make the transformer to work closer to the ideal model, as was studied in Chapter 7. Nevertheless, the thin steel and the ferrite will increase the winding ratio in one unit to fulfil the specifications.

At last, it must be noticed that the main inductance required to have an acceptable current ripple, will be larger for low frequencies, as it can be seen if the coil of the steel converter is compared with the others.

The converter optimization using the IGBT model BSM40 GA 170DLC is presented in Table 8.10. This IGBT model will require connecting various units in serial to hold up the converter voltage, as was commented in Section 8.5.

Table 8.10: Optimization results for IGBT model BSM400 GA 170 DLC.

	FERRITE N27	STEEL M290-50A	THIN STEEL NO12
Energy cost	14.1	13.6	18.8
Construction cost [SEK]	358,676	229,512	418,140
Losses cost [SEK]	3,915,300	4,095,500	5,374,200
Losses [kW]	49,6	51.9	68,1
Transformer losses [kW]	4,6	10.9	19,22
Semiconductors losses [kW]	45	41	48,9
Current density [A/mm^2]	3	3	4
Frequency [Hz]	400	250	550
Core flux [T]	0.356	0.218	0.712
Core thickness [m]	0.08	0.2	0.02
Layers on the primary	1	1	1
Layers on the secondary	5	5	5
Winding ratio	14	14	14
Turns on the primary	9	11	12
Transformer height [m]	1.24	1.62	1.51
Transformer radius (R_{out}) [m]	0.79	0.85	0.73
Leakage inductance [H]	$2.1 \cdot 10^{-5}$	$2.8 \cdot 10^{-5}$	$2.9 \cdot 10^{-5}$
Magnetizing inductance [H]	0.0065	0.0128	0.0167
Main inductance [H]	0.197	0.315	0.1435

For this kind of IGBTs, it can be seen that the working frequencies of the three materials are higher than in Table 8.9. This is due to the fact that, with this type of semiconductors, the switching losses will be lower and they will influence the energy cost performance less. Nevertheless, the optimum converter for these IGBTs will be the steel model again. This is due to, although the switching losses will have less influence, the optimum frequency will still be quite low, and thus the properties of the steel (specially the cost) will be the most appropriate.

It can also be observed that the other variables will present similar values as in the previous optimization. Thus, if both tables are compared, the optimum fluxes for the three converters will be almost the same, as well as the core thicknesses. In addition, it can be noted that as the frequency for the steel has been increased, it will need a larger winding ratio.

If the transformer quality were studied, from the tables it can be seen that the ferrite transformers will be those which present the lower losses. Nevertheless, as the differences with the steel are much smaller than the semiconductor losses, this effect will not be relevant. In addition, as the volumetric cost of the ferrites is higher than the one made of steel, they will be penalized in the final choice. This emphasizes the fact that the semiconductor devices will have a large influence in the converter design.

When analyzing the results, it can be noticed that the transformer sizes are quite large in almost all the cases, due to the low value of the frequency. Therefore, as one of the desires of the Department of Power Electronics was to design a compact device, a condition to reduce the transformer size will be added. The new condition for the optimization will be to limit the transformer height to one meter.

Moreover, as was commented, in order to prevent thermal problems, the current density allowed in the conductors must be limited. This maximum level will be fixed at 2 A/mm^2 , which will be a reasonable value for non-forced cooling conductors.

The results of the optimizations with these new conditions for the two IGBTs models are presented in Table 8.11 and 8.12. It must be noticed that only the most important features of the designs are presented in order to make easier the comparison between them.

Table 8.11: Optimization results for IGBT model FZ400 R65 KF1. Total height limited to 1 meter. Density current limited to 2 A/mm².

	FERRITE N27	STEEL M290-50A	THIN STEEL NO12
Energy cost	19	16.8	25.3
Construction cost [SEK]	500,350	177,380	1,325,200
Losses cost [SEK]	5,252,000	5,312,400	5,272,700
Losses [kW]	66,6	67,3	66.8
Transformer losses [kW]	3.5	20	19.5
Semiconductors losses [kW]	63.1	47.3	47.3
Current density [A/mm ²]	2	2	2
Frequency [Hz]	400	250	250
Core flux [T]	0.356	0.407	0.712
Core thickness [m]	0.14	0.2	0.1
Transformer height [m]	0,94	0.99	0.9
Transformer radius (R_{out}) [m]	0.89	0.93	0.89

Table 8.12: Optimization results for IGBT model BSM400 GA 170 DLC. Total height limited to 1 meter. Density current limited to 2 A/mm².

	FERRITE N27	STEEL M290-50A	THIN STEEL NO12
Energy cost	14.8	15.3	20.6
Construction cost [SEK]	369,060	177,380	632,500
Losses cost [SEK]	4,151,100	4,812,700	5,449,200
Losses [kW]	52.6	61	69,1
Transformer losses [kW]	3.7	20	20.1
Semiconductors losses [kW]	48.9	41	49
Current density [A/mm ²]	2	2	2
Frequency [Hz]	550	250	550
Core flux [T]	0.356	0.407	0.654
Core thickness [m]	0.1	0.2	0.04
Transformer height [m]	0.9	0.99	0.99
Transformer radius (R_{out}) [m]	0.86	0.93	0.84

From the Table 8.11, it can be concluded that the most suitable converter for the IGBT model FZ400 is the normal steel one. This converter will present a higher working frequency than the model obtained from the optimization without any restriction and the same model of IGBT. Moreover it will present smaller dimensions and thus, the building cost will be substantially lower. Nevertheless, the transformer will have more losses. The semiconductor losses will also increase as a consequence of the higher value of the frequency.

If the same study is performed for the results of the other IGBT model (Table 8.12), it can be seen that now, the optimum converter will be the ferrite one. This is due to, as the switching losses of the semiconductor model are less important, the frequency will be increased more, being the ferrite properties the most appropriated for it. In addition, this converter can be compared with the optimum model obtained in the optimization without restrictions (for the same IGBT model), which was the steel one. Thus, the energy cost will be a bit higher in the ferrite model. This is due to the construction cost, because the total losses will be almost equal. Nevertheless, if the transformer sizes are compared, it can be seen that the ferrite one will be much more compact than the steel transformer obtained in the previous optimization.

Therefore, in order to choose the most suitable converter, the models that must be compared are:

- Steel M290 with FZ400 IGBTs
- Ferrite N27 with BSM400 IGBTs

Finally, the converter chosen will be the ferrite one, due to that it will present a lower total loss and the most compact design, which was one of the requirements of the converter. It must be mentioned that this decision is based on the fact that, it is assumed that differences between using the most powerful IGBTs (that not require series connection) and the smaller model (that require series connection) are not too high. Thus, if these differences were important, the most suitable design would be the converter with the FZ400 IGBT model.

About the thin steel, it can be seen in the optimizations that always the worst energy cost comes out. This is due to its high core cost forces to design a mediocre and expensive transformer, obtaining high losses and a large investment. This was even though its properties were quite suitable

As a conclusion, the values of the construction and operating variables for the final design will be

Table 8.13: Construction and operating values for the final design.

Design variable	Value
Core material	Ferrite N27
Current density	2 A/mm ²
Switching frequency	550 Hz
Core Flux	0.356 T
Core thickness	0.1 m
Layers on the primary	3
Layers on the secondary	5
IGBT model	BSM 400 GA 170 DLC
Number of IGBTs	60
Number of diodes	28

The converter dimensions are presented in Table 8.14.

Table 8.14: Dimensions of the final design.

Dimension	Value
Winding ratio	13
Turns on the primary	5
Turns on the secondary	65
Transformer height	0.9 m
Transformer radius	0.86 m

The converter losses can be found in Table 8.15

Table 8.15: Losses of the final design

Losses	kW
Transformer losses	3.7
Semiconductor losses	48.9
Total losses	52.6

The converter costs are in Table 8.16

Table 8.16 Costs of the final design

Cost	SEK
Construction cost	369,126
Losses cost	4,151,100

At last, the electrical parameters must be presented, but first the output capacitor C_{out} must be calculated. The expression to obtain it can be found in (7.41), which was defined in the previous chapter when the process to calculate the main inductance was described. It must be remembered that this equation assumes the ideal model of the converter and uses a linear approximation for the current ripple and the capacitor voltage. Therefore, from there, the output capacitor can be isolated as

$$C_{out} = \frac{\Delta i_L}{16\Delta V_{out}} T. \quad (8.27)$$

The output voltage ripple will be limited to 5% of the rated output voltage. This means that $\Delta V_{out} = 750V$. The current ripple was defined in Chapter 7, and will be equal to 33.3A. Thus, the output capacitor will be $C_{out} = 5 \cdot 10^{-6} F$.

Then, the electrical parameters can be found in Table 8.17.

Table 8.17 Electrical parameters of the final design

Parameter	Symbol	Value
Main inductance	L	0.133 H
Leakage inductance	L_σ	$1.35 \cdot 10^{-5} H$
Magnetizing inductance	L_M	0.0038 H
Output capacitor	C_{out}	$5 \cdot 10^{-6} F$

8.8 Analysis of the converter design performance with the evolution of the semiconductors

One of the most important conclusions that can be obtained from the converter design is the fact that the semiconductors affect in a very important way the performance of the converter. Thus, if Table 8.15 is studied, it can be seen that the transformer losses are less than the 10% of the total, being the other 90% caused by the IGBTs and diodes. That means that we have managed to design a very good transformer but its effect in the power transmission system is less significant due to the semiconductor losses.

Nevertheless, the semiconductors technology advances very fast; creating new models that improve the properties of them regularly. For that reason in this section, the converter design will be optimized for a non-real IGBT model that will present fewer losses.

This “future” IGBT will present similar properties as the FZ400 R65 KF1, which means that not serial IGBTs will be needed, but the switching losses will be reduced 20 times. For the optimization it also was considered that the switching losses of the high voltage diodes were reduced in the same way. It must be noticed that this tremendous reduction in the switching losses is quite unrealistic, but it will help to present the effects of the IGBTs evolution on the converter clearer.

With these assumptions, the results obtained can be checked in Table 8.18. It must be noticed that the optimization was run without any restriction (on the current density or in the transformer length) in order to show the effect of the semiconductors clearer.

Table 8.18: Optimization results for the future IGBT based on the model FZ400 R65 KF1.

	FERRITE N27	STEEL M290-50A	THIN STEEL NO12
Energy cost	8.2	9.1	12.4
Construction cost [SEK]	191,783	181,854	268,962
Losses cost [SEK]	2,342,400	2,663,900	3,584,600
Losses [kW]	29.7	33.7	45.4
Transformer losses [kW]	5	9.7	18.2
Semiconductors losses [kW]	25.7	24	27.2
Current density [A/mm^2]	3	3	5
Frequency [Hz]	850	550	1150
Core flux [T]	0.356	0.134	0.538
Core thickness [m]	0.061	0.18	0.02
Transformer height [m]	0.78	1.35	0.97
Transformer radius (R_{out}) [m]	0.76	0.83	0.69

If the results are compared with those in Table 8.9 (that belongs to the FZ400 optimization without restrictions), it can be noticed that the energy cost has been reduced drastically. Thus, the worst value (the thin steel one) will be better than the best one in the previous optimization.

With that, the best choice now will be the ferrite, instead of the steel. This is due to the fact that, as the switching losses will be much less important, the converter can be operated at higher frequency, and in that range the ferrite properties will be more suitable. In fact, if the results are compared, the frequencies have been increased more than three times.

This growth in the frequency has led to a reduction of the transformer sizes, reducing the investment for the ferrite to less than one half. It is interesting to stress the fact that, instead of improving the transformer losses, the frequency increase has been used to reduce the transformer cost. This is due to that the variation of the transformer losses will still be less important than the semiconductor losses and that the energy cost gives more importance to the investment than the cost of the losses.

In addition, if the final design chosen in the chapter before it is compared with this future design, it can be seen that the new one presents better values in almost all the properties. In fact, the future design presents almost a 50% of investment reduction. Besides, it is interesting to mention that the transformer losses in the actual design will be a 26% lower than in the future one. That proves the fact that, if more money is invested in the transformer building, better properties will present. Nevertheless, an intermediate solution must always be reached to obtain the optimum.

As a conclusion, the improvement of the semiconductor properties will lead to a reduction of the size of the transformer and thus, the building cost. In addition, as the switching losses will decrease, although the converter will be operated at higher frequency, the total losses will decrease, leading to a more efficient transmission of the electric power.

Chapter 9

Simulation of the converter

At last, once the converter as been designed and its electrical parameters defined, it is simulated in Pspice® in order to check that it satisfies the voltage specifications.

In addition, in a second section, the converter waveforms obtained in the simulation will be compared with those that were plotted from the differential equations in Chapter 7.

9.1 *Check-up of the converter performance*

In this section the converter will be simulated for the rated conditions and for the maximum output voltage situation to test that the circuit fulfils the specifications. It must be noticed that it will not be necessary to test the lower voltage limit due to the fact that, as was described in Chapter 4, this topology is able to provide zero volts.

In order to obtain more precise results, the real full bridge model will be simulated, adding the effects of the resistances of the transformer windings, and the real switches and the real diodes.

To calculate the magnitude of the windings resistances, Equation (5.39) can be used, where the length can be obtained from (5.41) and the conductor area from (5.42). With that, the primary winding resistance will be equal to $R_{w1} = 0.28m\Omega$.

If the same process is followed for the secondary conductor, and using the winding ratio, the resistance of the secondary winding will be $R_{w2} = 2.7m\Omega$.

To obtain the electrical parameters of the real switches, the loss model on Figure 8.4 can be reviewed. There, it can be seen that it can be approximated to a DC-voltage source and a resistance. Moreover, to obtain the model for the switch, the fact that several IGBTs will be connected must be considered. Thus, there will be 3 packs of IGBTs connected in serial, and each pack will present 5 IGBTs disposed in parallel. With that, using basic principles of circuit theory, the switches can be modelled as:

- $V_{SW} = 3.543V$.
- $R_{SW} = 2.7m\Omega$.

Finally, the real diodes can be modelled knowing that each one presents seven units connected in serial. Then, the circuit parameters for the diodes are:

- $V_D = 10.5\text{V}$.
- $R_D = 34.3\text{m}\Omega$.

With that the converter can be modelled in Pspice®. The first simulation will be accomplished for the rated conditions. This means that the circuit inputs will be

- $P = 5\text{MW}$.
- $V_{in} = 3.3\text{kV}$.
- $D = 0.185$.

It must be noted that, as the maximum input power cannot be limited in the software, the load will be simulated as a resistance dimensioned to dissipate the power required. The equation to calculate it can be found as

$$P = \frac{U^2}{R}. \quad (9.1)$$

Where the load resistance can be isolated as

$$R_L = \frac{V_{out}^2}{P}. \quad (9.2)$$

Using (9.2) with the data above, the load will be equal to $R_L = 45\Omega$.

The results of the simulation for the rated conditions are plotted in Figure 9.1.

There, it can be seen that the output voltage ripples around 15kV, as it was designed for. So, the circuit at rated conditions will behave as it was supposed. In addition, if the voltage ripple is measured, it will present a value close to 1000V, instead of the 750V that were specified. This can be due to the simplification used to dimension the output capacitor, which underestimates its value. As a conclusion, a somewhat bigger capacitor would be suitable to fulfil this specification.

If the output current is studied, it must be noticed that in the figure this signal has been plotted ten times its value in order to show it clearer. There, it can be seen that it will fluctuate close to 330A, which means that the power supplied is 5MW, as was expected. About the current ripple, its magnitude will be of 30A. Therefore, it will fulfil the current specification, which was fixed as a 10% of the output current.

In the lower graphic, the input current is plotted, as well as its average and RMS value. By studying the average input current, it can be seen than its magnitude is about 1500A, to provide the input power required. In addition, the RMS value will be 2400A, which is close to the value predicted in the previous chapter.

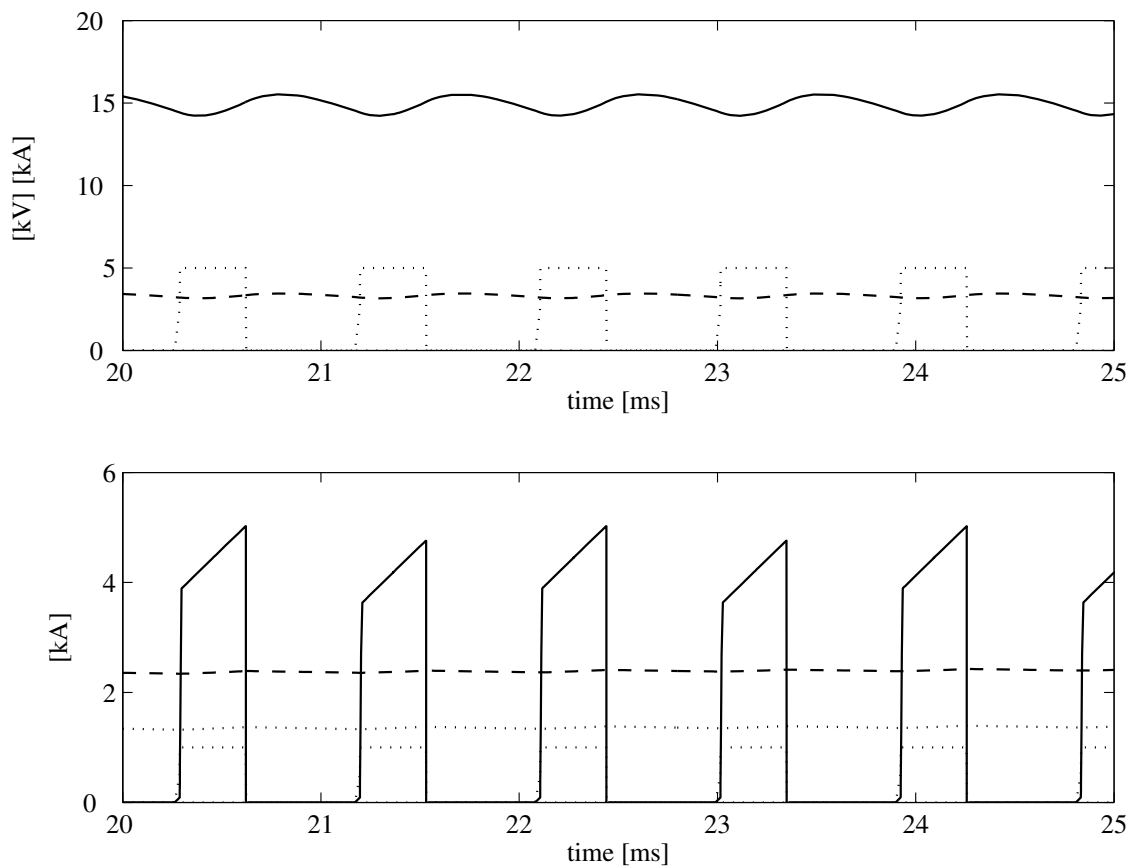


Figure 9.1: Converter simulation for the rated conditions. Upper plot, solid output voltage, dashed output current (amplified ten times), dotted grey switching pulses. Lower plot, solid input current, dashed RMS input current, dotted AVG input current, dotted grey switching pulses.

The other working point that will be checked is when the maximum voltage is required and the wind turbine is providing its minimum one. In fact this will be the most stressing point for the converter, and the duty cycle will be carried to its maximum.

It must be noticed that if the wind turbine is supplying its minimum voltage, the power provided will be lower than the rated. In order to calculate this power, first it must be obtained the wind speed for this working point from Equation (6.2). There, it can be seen that the minimum voltage (1.65kV) is provided at 4 m/s. Then, if this value is used in (6.1), the power supplied will be 145.2kW. As a conclusion, the input parameters will be

- $P = 145.2\text{kW}$
- $V_{in} = 1.65\text{kV}$
- $D = 0.4999$.

The load can be calculated using (9.2), and knowing that the maximum voltage will be 20.25kV. In that case, the load resistance will be equal to $R_L=2825\Omega$

The results of the simulation are presented in Figure 9.2.

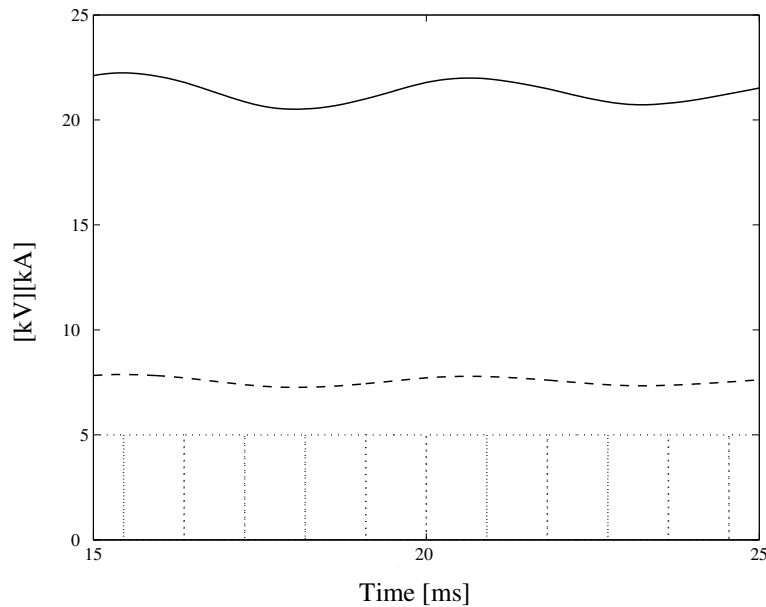


Figure 9.2: Converter simulation for the maximum output voltage. Solid output voltage, dashed output current (amplified one thousand times), dotted and dotted grey switching pulses.

From the figure, it can be seen how the switching pulses are almost overlapped due to the duty cycle is fixed at its maximum value. In addition, if the voltage signal is studied, it can be realized that it will present a somewhat larger value than the specified (20.25kV). This is due to the fact that the winding ratio is a discrete variable, and when it was calculated in theory in Chapter 6 and was corrected in the design in Chapter 8, it was always rounded to the higher value. This feature is quiet fine, due to that it will balance small losses that would appear in the physical device and that has been skipped in this study.

About the current, it must be noticed that it is plotted amplified 1000 times to show it clearer. From the figure it can be seen that its value will ripple around 7A. This confirms that the output power will be the estimated one.

9.2 Comparison of the converter waveforms

Finally, in order to check that the converter performance matches with the theory developed in Chapter 7, and that is the base of the design process, the converter waveforms obtained in the simulation are going to be compared with the plots drawn in the mentioned chapter. Here it must be considered that those plots are derived directly from the differential equations that describe the converter performance.

The first waveform that will be studied is the input current. In Figure 9.3, a detailed plot of this signal obtained in the simulator for the rated conditions can be seen. In this plot the switching pulses are also shown in order to easier recognize the different steps in the waveform. It must be noticed that these signals will be scaled properly to clarify the figure.

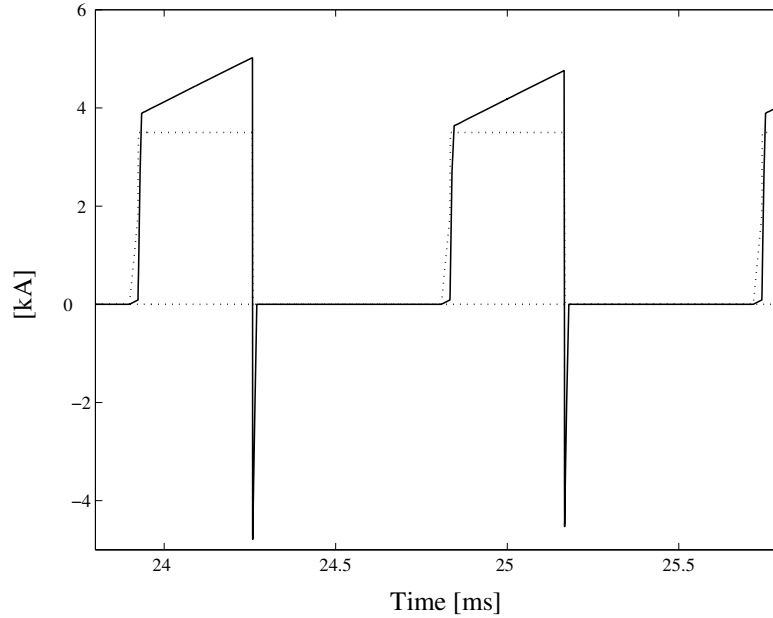


Figure 9.3: Simulated input current waveform for the rated conditions. Solid input current, dotted switching pulses.

If this plot is compared with the input current waveform in Figure 7.8, some conclusions can be deduced. The most noticeable is that the rising during the first instants is much sharper than which was plotted in the theoretical figure. This means that t_l , which was the time needed to load the leakage inductance, will be very small, making the converter to perform close to the ideal model (without leakage inductance).

If the falling time is studied, it can be verified that the current sense changes in this step due to that the antiparallel diodes of the opposite switches will return this current to the source, and thus some energy that will not be transferred. This time, that was called t_3 in Chapter 7, will be a bit longer than t_l , as (7.6) describes. In fact, the equation can be developed to

$$t_3 = \left(1 - \frac{V_{Lm}}{V_{in}}\right) t_{on} + \frac{V_{Lm}}{V_{in}} t_l. \quad (9.3)$$

Where, as $V_{Lm} < V_{in}$ and $t_{on} \gg t_l$, the falling time will always be larger than t_l .

As a conclusion, it can be seen that the performance of the simulated waveform will coincide with the theoretical one, differing only in the time scale of some of the features. However, it must be remembered that these scales on the theoretical plots were chosen in order to present as clear as possible the characteristics of the signals.

Moreover, in order to check that the theoretical equations were correct, the most important values of the simulated waveform will be compared with the theoretical values. The results are presented in Table 9.1.

Table 9.1: Comparison between the theoretical and simulated parameters of the input current.

Parameter	Theoretical value	Simulated value
t_1	$1.35 \cdot 10^{-5}$ s	$1.2 \cdot 10^{-5}$ s
t_3	$1.75 \cdot 10^{-5}$ s	$1.4 \cdot 10^{-5}$ s
i_1	3373A	3600A
i_2	4509A	4750A

From the table it can be seen that the differences in the values of t_1 are about a 10%, while for t_3 are smaller than the 20%. About the currents, for i_1 the error will be around the 6% and for i_2 around 5%. These differences can be due to effect of the real semiconductors (that was neglected in the theoretical analysis) and the accuracy of the simulations, and leads us to affirm that the equations obtained in Chapter 7, describes the converter performance quite properly.

Following the study of the low voltage side, the next waveforms that will be compared are the voltage and current of the switches. In the Figure 9.4 these waveforms are plotted for the switch 1, as well as the current on its antiparallel diode.

If the simulated switch voltage is studied, it can be seen that its performance is the same as in the theoretical waveform in Figure 7.10. Nevertheless, a feature that was not considered in the theoretical waveforms appears. Thus, it can be seen that at the end of the step 2 (see Figure 7.10), it appear an oscillation before establishing in the voltage level predicted in the theoretical waveform. This can be due to the fact that this is just the first moment when the transformer is short circuited, and it could appear a parasitic effect in the real switches.

About the currents, it is interesting to realize how the antiparallel diode conducts when the opposite switch (switches 2 and 4 in this case) are closed.

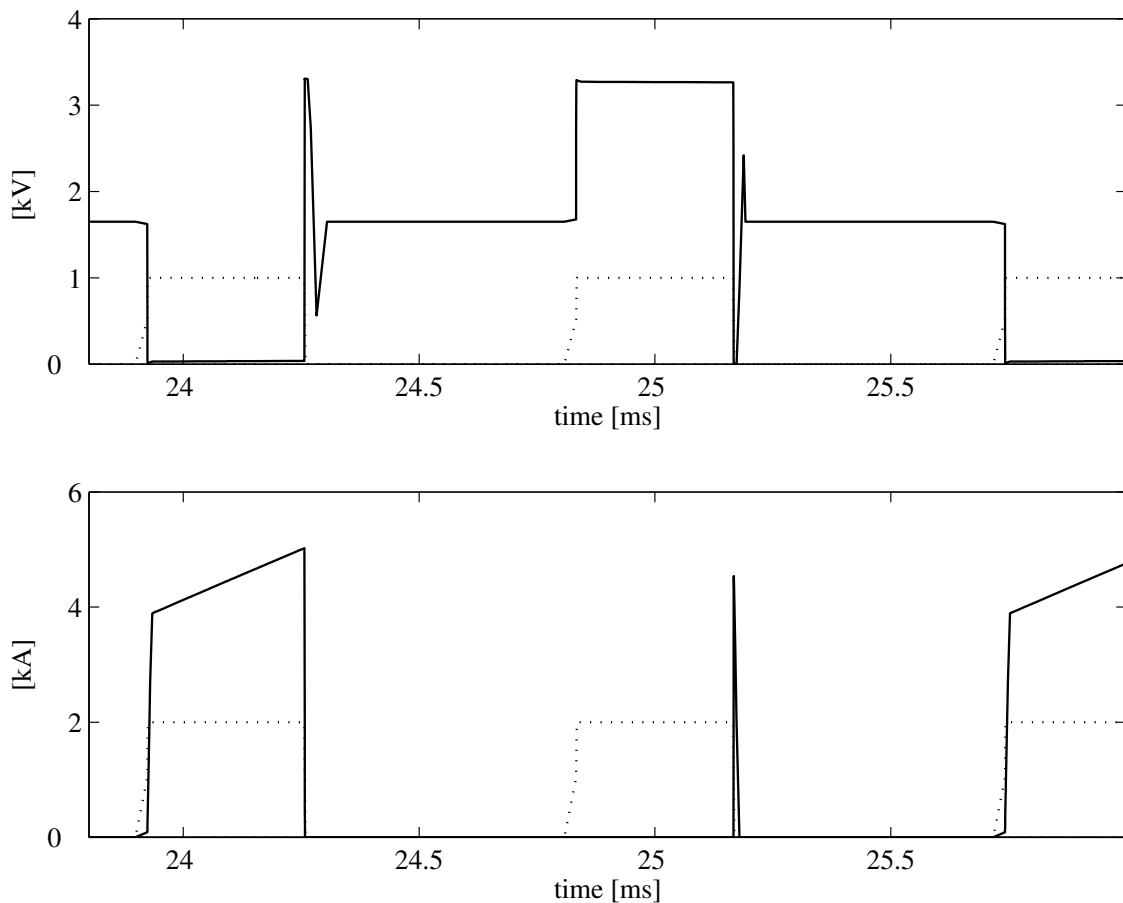


Figure 9.4: Simulated waveforms on switch 1 for the rated conditions. Upper plot, solid switch voltage, dotted switching pulses. Lower plot, solid switch current, solid grey antiparallel diode current, dotted switching pulses.

Now, the performance of the high voltage side will be analyzed so the next signals that will be studied are the voltage and the current over the main inductance. Figure 9.5 shows the simulation results for the rated conditions. Again, the switching pulses are also plotted.

If the voltage obtained from the simulation is compared with the theoretical waveform in Figure 7.9, it can be seen that it will perform mostly in the same way. Nevertheless, an oscillation appears on the voltage rise that has not been considered in the theoretical model and can be caused by the fact that in the simulation the diodes and switches are considered real, as was explained before.

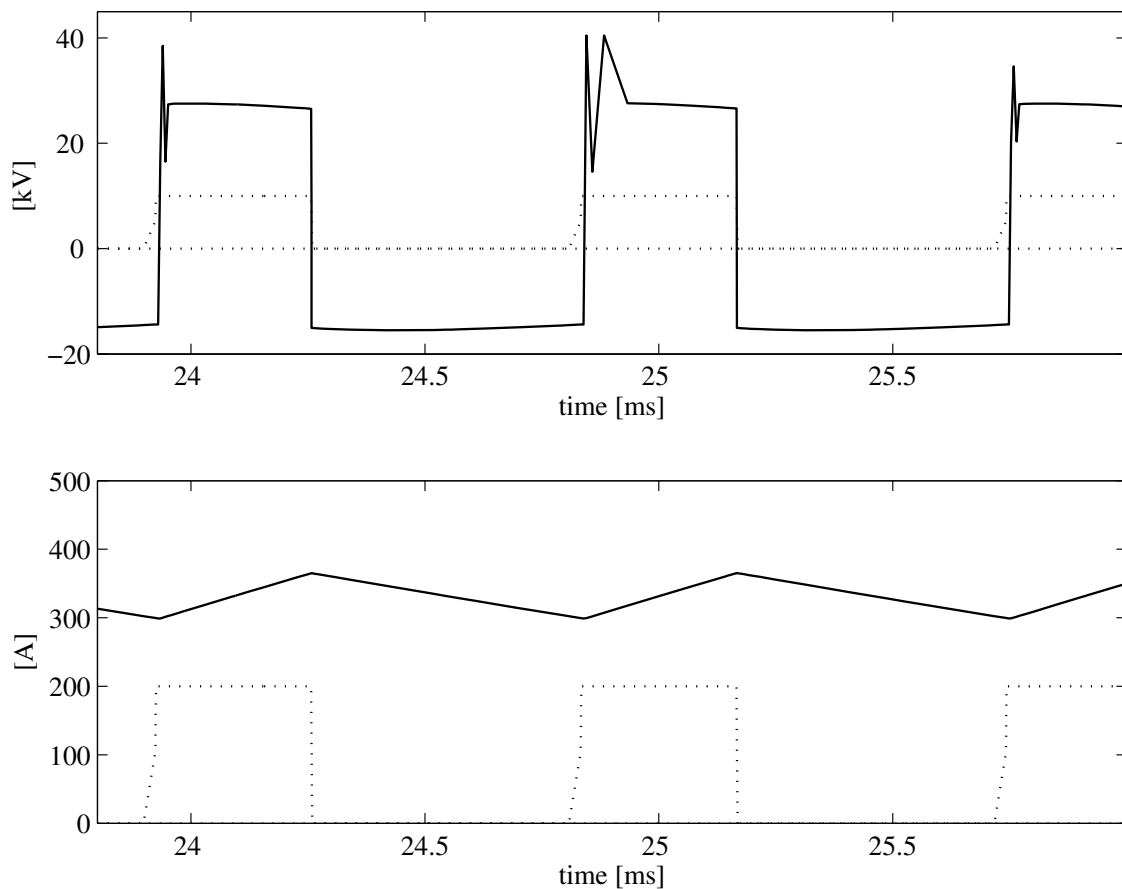


Figure 9.5: Simulated voltage and current over the main inductance for the rated conditions. Upper plot, solid inductance voltage, dotted switching pulses. Lower plot, solid inductance current, dotted switching pulses.

In addition, if the voltage levels are measured, it can be seen that the values will be very similar to the ones described in the idealized waveforms in Figure 4.7. This means that the harmful effects of the magnetizing inductance will not be very important. In fact, the positive voltage should be the input voltage times the winding ratio and minus the output voltage. This, for the rated conditions means that the maximum voltage will be around 28kV that is approximately what appears in the figure. Following the same argument, the negative voltage should be the output voltage that, for the rated conditions is 15kV, and is the value that appears in the plot.

About the current in the inductance, it can be seen that it will perform as in the theoretical model. The only difference will be the fact that in the simulated waveform, t_l will be much lower than in the theoretical one, as it was commented.

Finally, the waveforms of the high voltage diode will be analyzed. The results from the optimization for the rated conditions are presented in Figure 9.6.

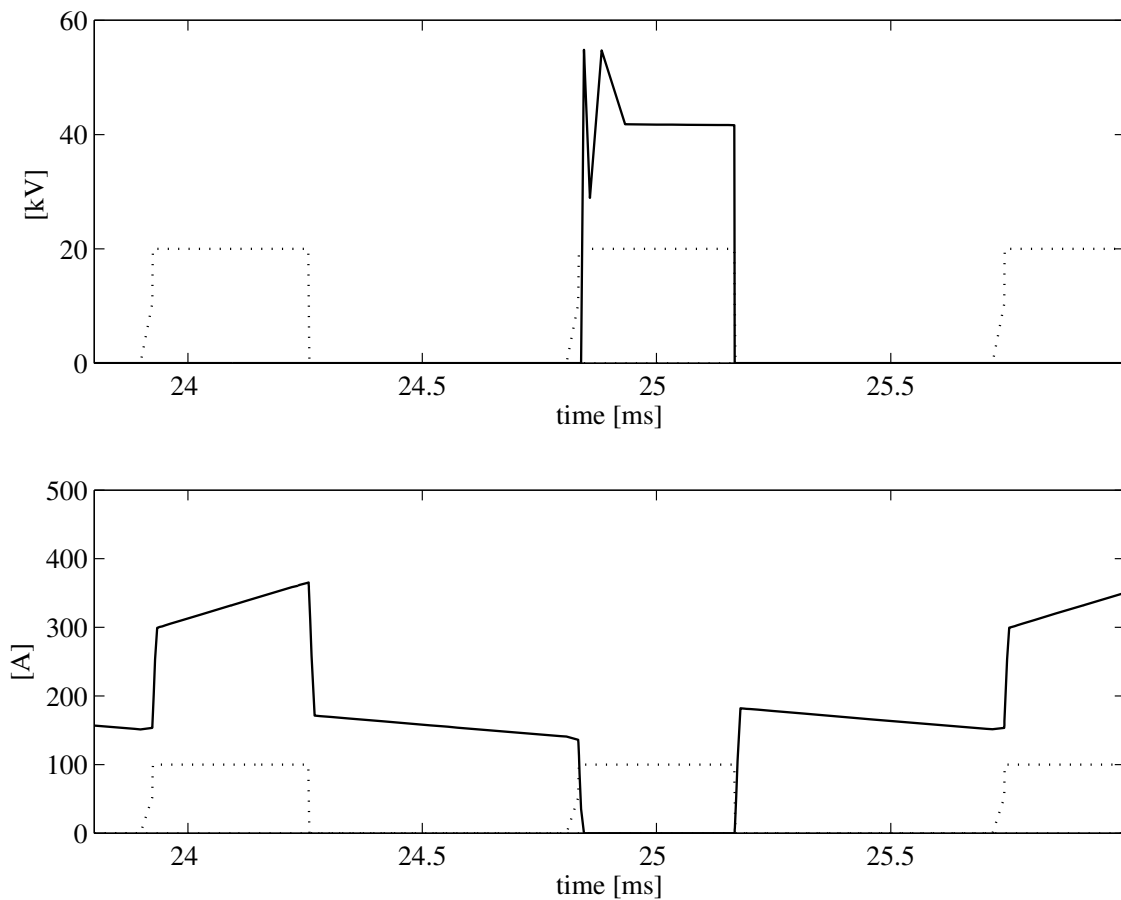


Figure 9.6: Simulated waveforms on diode 1 for the rated conditions. Upper plot, solid diode voltage, dotted switching frequency. Lower plot, solid diode current, dotted switching pulses.

As in the case with the switches, the diode voltage will perform as the theoretical waveform in Figure 7.11, with the only difference that some oscillations due to the real behaviour of the device will occur. Moreover in the figure it can be seen that the voltage level which must hold up the diode is the input voltage times the winding ratio, and for this case will be up to 40kV.

If the current over the diode is studied, its performance will be similar than the theoretical one. In addition, it is interesting to study the periods where the four diodes will be conducting (steps 2 and 3 in Figure 7.11) and how our specific diode will not conduct always the same level of current. This is due to the fact that, some current will flow through the secondary of the transformer, and thus depending on the sense of this current, the diode will conduct somewhat more than one half of the output current, or a bit less.

Chapter 10

Conclusions

The design of a DC/DC converter for DC series-connected wind farms was accomplished in this project.

The wind turbines used in this work have a rated power of 5MW. Moreover, the output voltage of the turbine (the input voltage for the converter) will depend linearly with the wind speed, being its maximum value equals to 3.3kV and its minimum just one half. In addition, the type of wind turbines used will be the variable speed DC one [1], which will be connected to the general system by the DC/DC converter that is of interest for this study.

The DC series connected wind farm is shaped by legs, which contain several wind turbines connected in serial to provide the desired voltage level. The legs are connected in parallel in order to supply a greater power level. This layout leads to some special characteristics. Thus, due to that a leg is composed by a large number of turbines, the current in it will not be seriously influenced by the performance of one single turbine. Therefore, it can be affirmed that the leg current will be fixed by the operation point of the whole leg. This leads to that the voltage provided by each turbine will directly depend on the power production of it. For that reason, it can be understood that if a leg is working at a specific point of operation and suddenly the power production of one wind turbine begins to decrease, its output voltage will decrease too; being this lack of voltage supplied by the other wind turbines, that will be forced to increase their voltage level.

The two possible topologies considered in this work were the full bridge isolated boost converter and the full bridge converter. Both are based in the same principle that basically consist in chopping the energy supplied in a DC voltage and transfer these energy packets through a transformer to increase their voltage level. The last step is to rectify this signal in order to provide a DC voltage again. In spite of, each topology will present different features. Thus the FBIB will present the boost inductor in the low voltage side, supplying a voltage range from a minimum value equal to the input voltage times the transformer winding ratio, to a maximum voltage close to infinite (theoretically). Besides, the FB will have the inductor placed on in the high voltage side, and its voltage will be in a wide range, from a minimum magnitude close to zero to a maximum equal to the input voltage times the winding ratio.

The transformer chosen was a quite innovating design composed by two windings that are disposed as a circumference and several U-cores that cover them. The primary winding is manufactured using copper foils, while the secondary is made with a cable. This is due to the fact than the secondary of the transformer will have to hold up the voltage level of the whole leg, and thus it must be strongly isolated. In addition, this type of winding is what motives the transformer shape, due to that the cable cannot be twisted as wires, requiring a large radius of curvature.

With that, the task of the converter will be to provide a suitable output voltage to the leg, independently of the voltage of the turbine. In addition, the system must be able to supply an output voltage higher than the rated value (15kV). For that, the overrating used was 1.35. About the minimum output voltage, two values were used to dimension the converter; a less restrictive level equal to the 65% of the rated value and a more demanding value of the 30%.

The two topologies were compared, and the outcome was that the most suitable one was the full bridge converter. This is due to the fact that this topology was able to provide a voltage in a wide range, from zero to 20.25kV (the overrated output voltage), while the full bridge isolated boost converter presented serious difficulties to reach a reasonable minimum level. In addition, the FBIB yielded in the switches more than 7kV of voltage drop, and the FB only 3.3kV. As drawback, stronger diodes was required in the full bridge, due to the voltage drop over them was about 40kV, while this voltage on the full bridge boost converter was only 20kV.

Due to that the full bridge was the topology chosen, the effect of the transformer leakage inductance on it was theoretically studied, and the result was that it reduced the amount of energy transferred in each packet. In fact, it was observed that the first instants of each switching pulse were used to load the leakage inductance. Thus, some energy was stored there until the pulse was finished, returning then to the turbine through the antiparallel diodes of the opposite switches. This power, which was never transferred to the high voltage side, is reactive power and forces the converter to be over dimensioned.

The process followed to design the converter was composed by two basic steps. The first step was to create a database of converters for all the possible values of the variables chosen to define the design. The second step was an optimization process to select the most suitable one. This optimization was based on the energy cost of the converter.

In order to extend as much as possible the converters database, three different core materials were used, in an attempt to cover all the possible classes of them. Thus, the materials chosen were normal steel, a thin steel and a ferrite. In addition, two different models of IGBTs were used. The first model was able to hold up the voltage levels without series connection, while the smaller one required connecting three of them in series.

With that, the optimizations were executed with the result that the large magnitude of the switching losses had a strong influence in the optimum design. Thus, this optimum was forced to work at very low frequencies, requiring a very large transformer for that. It was also found that the less powerful model of the IGBT set up (that requires series connection), produced less switching losses, allowing the converter to work at higher frequencies.

Due to the large size of the transformers, it was necessary to add a new condition to the optimization in order to guarantee a compact design, which was one of the aims of the project. This condition was to limit the transformer height to one meter. Therefore, the new optimum designs presented quite compact dimensions, at expense of a somewhat higher energy cost. This was due to the fact that, in order to obtain a smaller transformer, it was necessary to increase the frequency, and thus the switching losses.

At last, the final choice was between a steel core converter with the most powerful IGBT model and a ferrite core design with the smaller IGBT one. Due to the fact that it was impossible to obtain any cost information of the semiconductors, the energy cost values of the converter could not be used make a comparison. Finally, the ferrite model was chosen, due to that it presented the most compact design and lower losses. Nevertheless, it must be mentioned that this decision was based on the fact that it was assumed that the differences between using the most powerful IGBT (that not required series connection) and the smaller model (that required series connection), were not too large. Thus, if these differences were found to be important, the most suitable design would be the steel converter.

Due to that it was found that the switching losses were one of the most important facts for the converter design, it an optimization was completed for an ideal future IGBT model which presented very low losses. The results obtained showed that this ideal converter presented a quite smaller transformer, due to that it was able to operate at much higher frequencies. This size decrease lead to that the energy cost of the transformer was drastically reduced.

At last, the selected converter was simulated in Pspice®, and it was found that it was able to satisfy all the specifications. Moreover, it was interesting to check, by comparing the theoretical waveforms with the simulated ones, that the differential equations derived in the theoretical analysis were able to describe the converter performance quite well.

References

- [1] Stefan Lundberg. Performance comparison of wind park configuration. Department of Electric Power Engineering. Chalmers University of Technology. Göteborg, Sweden 2003.
- [2] Stefan Lundberg. Configuration study of large wind parks. Department of Electric Power Engineering. Chalmers University of Technology. Göteborg, Sweden 2003
- [3] Stefan Lundberg, Torbjörn Thiringer. Control of a wind farm utilizing series-connected wind turbines with a DC voltage output. Department of Electric Power Engineering. Chalmers University of Technology. Göteborg, Sweden.
- [4] N. Fröhleke, R. Mende, H. Grotstollen, B. Margaritis, L. Vollmer. Isolated Boost Full bridge topology suitable for high power and power factor correction. Institute for Power Electronics and Electrical Drives. University of Paderborn. Paderborn, Germany.
- [5] Andrés Barrado. Notes from Electrónica Industrial. Department of Electronic Technology. Carlos III University of Madrid. Leganés, Spain 2004.
- [6] Ned Mohan, Tore M. Undeland, William P. Robbins. Power electronics. Converters, applications and design. Third edition. John Wiley & Sons.
- [7] Robert W. Erickson, Dragan Maksimović. Fundamentals of power electronics. Second Edition. Kluwer Academic Publishers.
- [8] Ned Mohan. A step-by-step instruction set for simulating power electronics using Pspice® schematics. Minnesota Power Electronics Research & Education. Minneapolis, USA 1998.

Appendix A

Transformer analysis

In this appendix, the transformer defined in Chapter 5 will be analyzed based on the construction and operating variables. Thus, it will be especially useful to understand the performance of the transformer losses that were briefly described in analysis of the converter in Chapter 8.

The method used to obtain the database necessary to accomplish the analysis is based on create a six-dimension matrix to store each design parameter, calculated over an appropriate range of each variable. The ranges chosen are presented in Table A.1. Here, it must be mentioned that the core material used to complete it is the ferrite N27.

In order to guarantee that the design parameters are calculated for all the possible values of the variables, a sequential scheme as the presented in Figure A.1 will be followed. The implementation of this program can be revised in Appendix B.

Table A.1: Construction and operating variables ranges.

Variable:	Lower limit	Upper limit	Step
Current density [A/mm^2]	1	5	1
Flux [T]	0.001	0.5	0.01
Layers on the primary	1	3	1
Frequency [Hz]	100	10000	500
Layers on the secondary	1	5	1
Thickness [m]	0.001	0.3	0.02

The way the analysis will be performed consists in studying the different design parameters depending only on one of the variables, fixing the other five to a constant value. Since the behaviour of a parameter as function of a specific variable can change depending on the magnitudes of the other fixed variables, more than one plot and explanations will be used when required.

The analysis for each variable will be structured as follows: First the dimensional parameters will be studied, giving special importance to the number of turns, following by studying the performance of the transformer inductances and finishing with the losses analysis.

At last, it must be emphasized the fact that the plots presented here were selected in order to show as clear as possible the different features of the parameter studied. This means that they could match with unrealistic transformers.

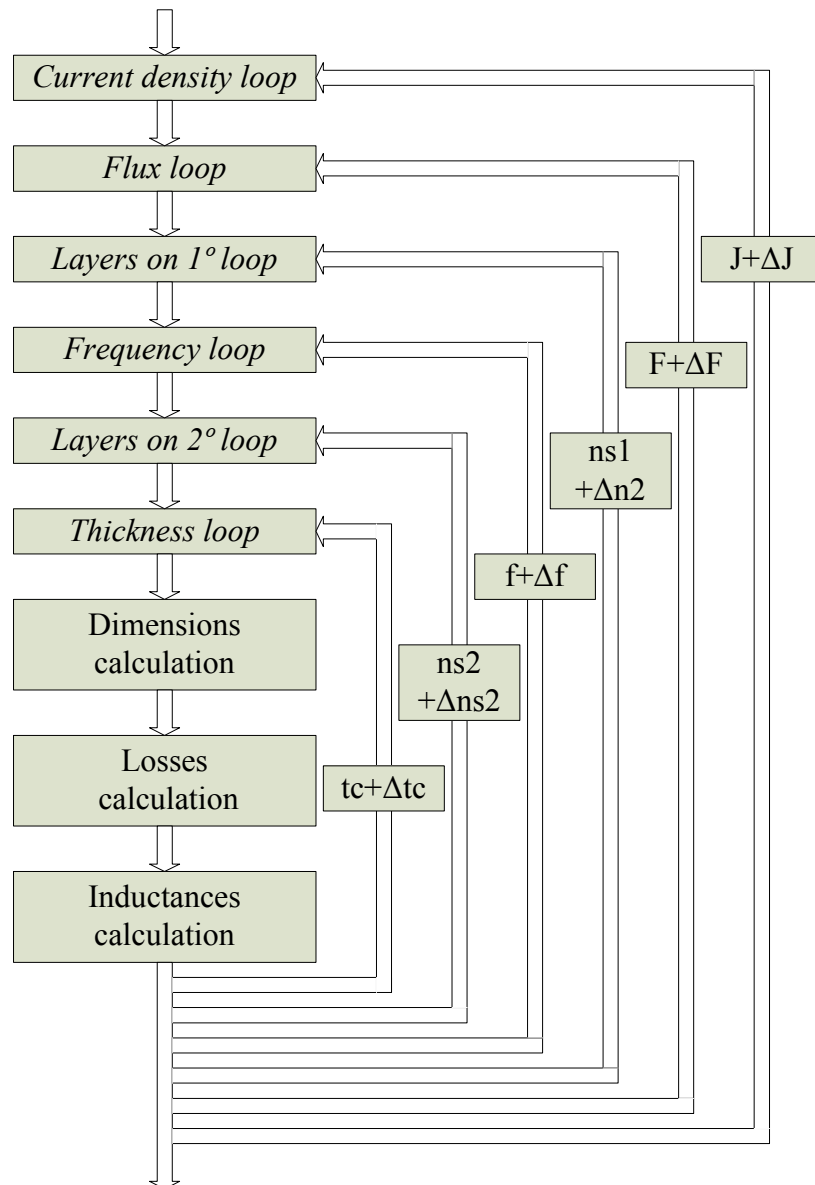


Figure A.1: Transformer calculations sequential flowchart.

A.1 Current density analysis

The first parameter that will be analyzed as function of the current density is the turns on the primary.

The current density will influence the size of the copper areas, due to the currents in the converter are fixed. Thus, if the current density allowed in the wires increases, the size of them will be reduced. The conductors reduction carries a reduction of the windings circumference and thus R_l as (5.10) describes.

Logically, if the transformer thickness is kept constant and R_l reduced, the core area will decrease, raising the number of turns on the transformer as (5.18) predicts. As a_c affects inversely the number of turns, the magnitude of the variation will depend on the value of the constant that it divides. That means that if the flux and the frequency are very low, the variation of the number of turns depending on the current density will be very sharp while, if those variables are fixed in high values, the slope of the function will be smooth.

The Figure A.2 shows the plot of the turns on the primary depending on the density current.

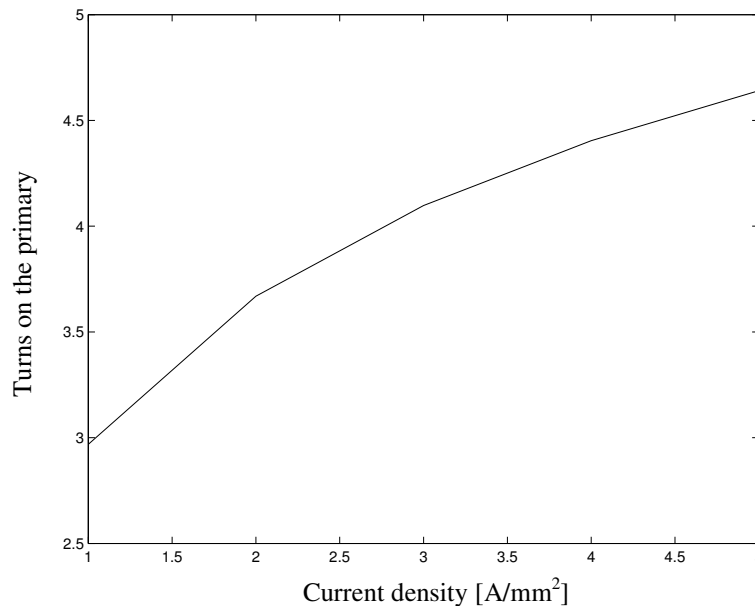


Figure A.2: Transformer turns on the primary depending on the density current.

As N_l is modified by the current density, the transformer dimensions will be affected too. It must be noticed that, when the turns on the transformer are very high, their variation will deeply influence the dimensions of the device. This forces to complete two analyses for the transformer dimensions, depending on the value of N_l .

First, it will be studied assuming that N_l presents a large value, which means that the frequency, the flux and the thickness have low magnitudes.

In that case, due to N_l increases with J , the winding window must be larger, increasing a_w and h_w . In this situation h_{w3} will be which limits the windows height. The transformer height will also be increased.

About r_{out} , there will appear two conflicting effects: on one hand, as a_w increases, $R3$ will increase leading to an increase in the outer radius but, on the other hand, a_c is reduced, decreasing it. From (5.27), can be seen that $R3$ is squared so, presumably, it will be the stronger effect.

At last, for the core volume it will appear two conflicting effects again. r_{out} will increase, as well as R_3 , and these features will force the core volume to grow. Nevertheless, R_l will be reduced, and it would make the core volume to decrease so, the final result will depend on which is the stronger effect.

In Figure A.3 the plot of all these parameters can be checked.

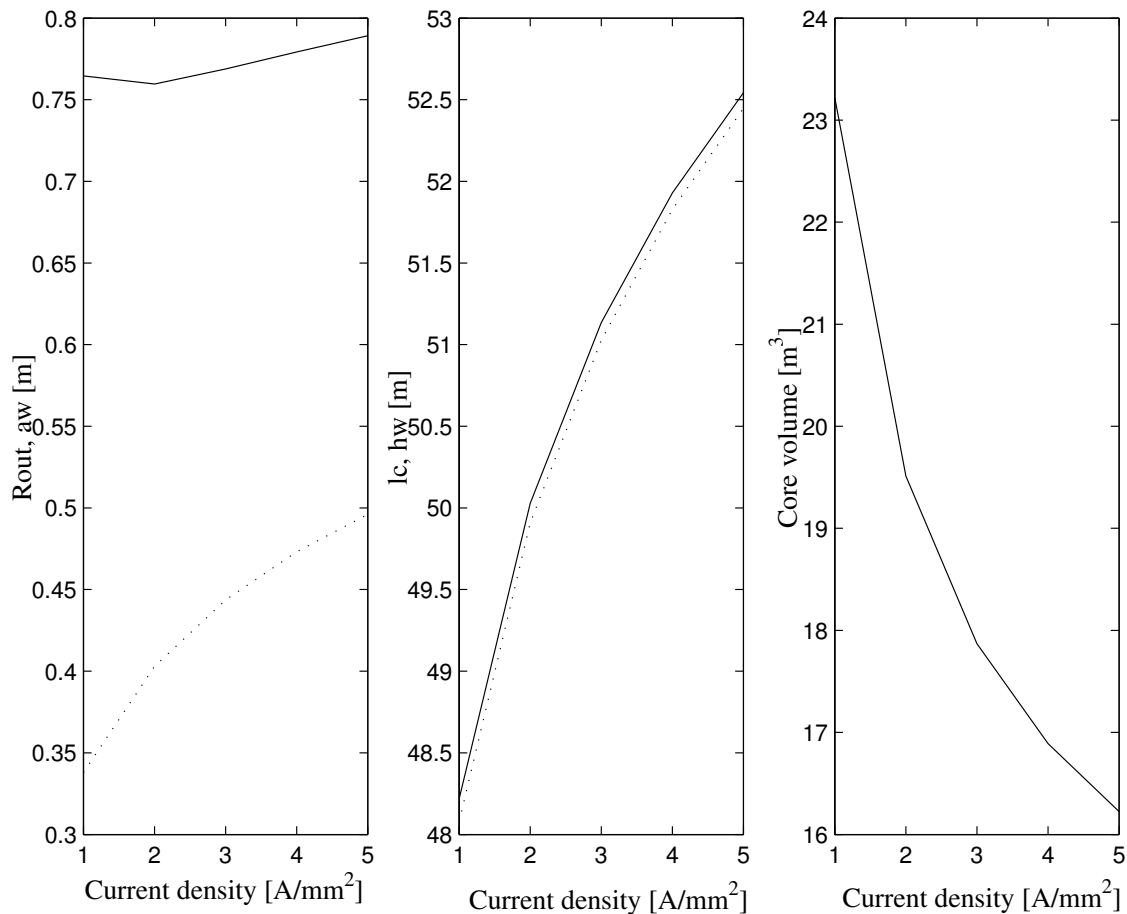


Figure A.3: Transformer dimensional parameters depending on the current density for a large value of N_l . Left solid r_{out} , dotted a_w . Centre solid l_c , dotted h_w . Right solid V_c .

The second analysis that will be done, will assume that the number of turns is medium or low. In that case there will be some changes in the performance of the parameters.

For a_w , although the number of turns still increases, their effect is less important and will be confronted with the effect of reduction that provides the fact of that, as the density current increases, the cable size is reduced. As a result, the final performance of the parameter will be difficult to predict, but can be guess that it will not be hardly affected.

As a_w is not be much influenced, r_{out} will decrease due to the only important effect will be the reduction of the core area.

The winding height, h_w , will be decreased, due to, as the number of turns is smaller, the h_{w1} or h_{w2} will govern the final parameter, and they are reduced when the copper areas decreases. The total height will follow the performance of h_w .

The behaviour of the core volume will be quite clear, due to both, r_{out} and R_l are reduced. Reviewing Equation (5.32) can be seen that, in this case it will always decrease.

Figure A.4 shows all these parameters.

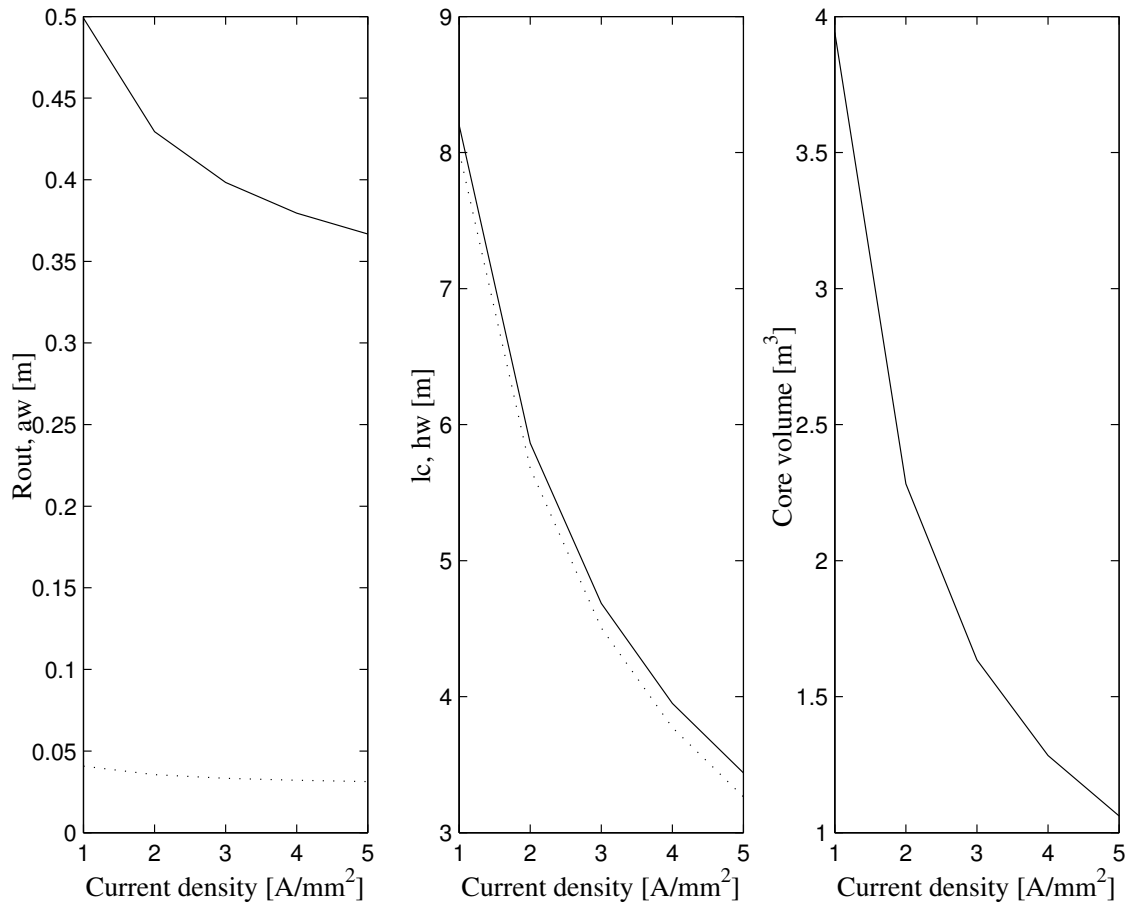


Figure A.4: Transformer dimensional parameters depending on the current density for a low value of N_l . Left solid r_{out} , dotted a_w . Centre solid l_c , dotted h_w . Right solid V_c .

The transformer analysis depending on the density current will continue by studying how the inductances are affected. In that case two studies must be accomplished again, depending on the number of turns.

The first analysis will consider that N_l has a large value. Table A.2 represents the different geometrical effects that were studied before, and how the performance of the inductances is affected, based on equations (5.37) and (5.38).

Table A.2: Effects of the current density on the transformer inductances for large value of N_1 .

Geometrical effect	L_σ	L_M
$N_1 \uparrow$	\uparrow	\uparrow
$a_w \uparrow$	\uparrow	\downarrow
$h_w \uparrow$	\downarrow	\downarrow

In the table can be seen that there will be opposed effects. Nevertheless, must be remembered that the turns on the primary appears, in both equations, squared, and that here we have assume that N_1 will present a large value. In conclusion it can be inferred that the both inductances will grow with the effect of the current density.

The second analysis assumes that N_1 presents a low value. In that case a new table can be made to clarify how the inductances are affected.

Table A.3: Effects of the current density on the transformer inductances for low value of N_1 .

Geometrical effect	L_σ	L_M
$N_1 \uparrow$	\uparrow	\uparrow
$a_w \downarrow$ (very smooth)	\downarrow	\uparrow
$h_w \downarrow$	\uparrow	\uparrow

In Table A.3 can be seen that if the density current increases, the magnetizing inductance will always grow if the number of turns is not very high. About the leakage inductance, must be notice that only one of the three effects reduces it. Furthermore, as was explained before, the reduction of a_w will be very small, so it will not influence decisively the performance of the inductance.

In conclusion; the values of both inductances will increase with the current density, being this effect more pronounced when the turns on the primary are high.

At last, the transformer losses will be analyzed. Once again the analysis will be divided in two parts, depending on the magnitude of N_1 .

For the case where the number of turns is very high, the most important losses will be the winding ones; due to the transformer will require a large amount of conductors. Moreover, a large number on turns means that the flux and the frequency present low values and that leads to have low core density losses.

If Equation (5.44) is reviewed, it can be seen that the winding losses will increase with the density current. This is due to that in the equation appear the number of turns (that will increase with J) and the current density itself. It also appears the copper area but, as the current density is squared, its effect is cancelled. As a result, the total losses will increases with the density current for large values of N_1 , as can be seen in the upper plot of Figure A.5.

If the number of turns is lower, the effect of the winding losses, despite it will have the same performance as before, will be less important. In that case, the values of frequency and flux will be higher, and the core density losses considerable. Therefore, the most important losses will be the core ones. And, as the density losses are not affected by the density current and the core volume decreases, the total losses will decrease too. This feature can be checked in the lower plot of Figure A.5.

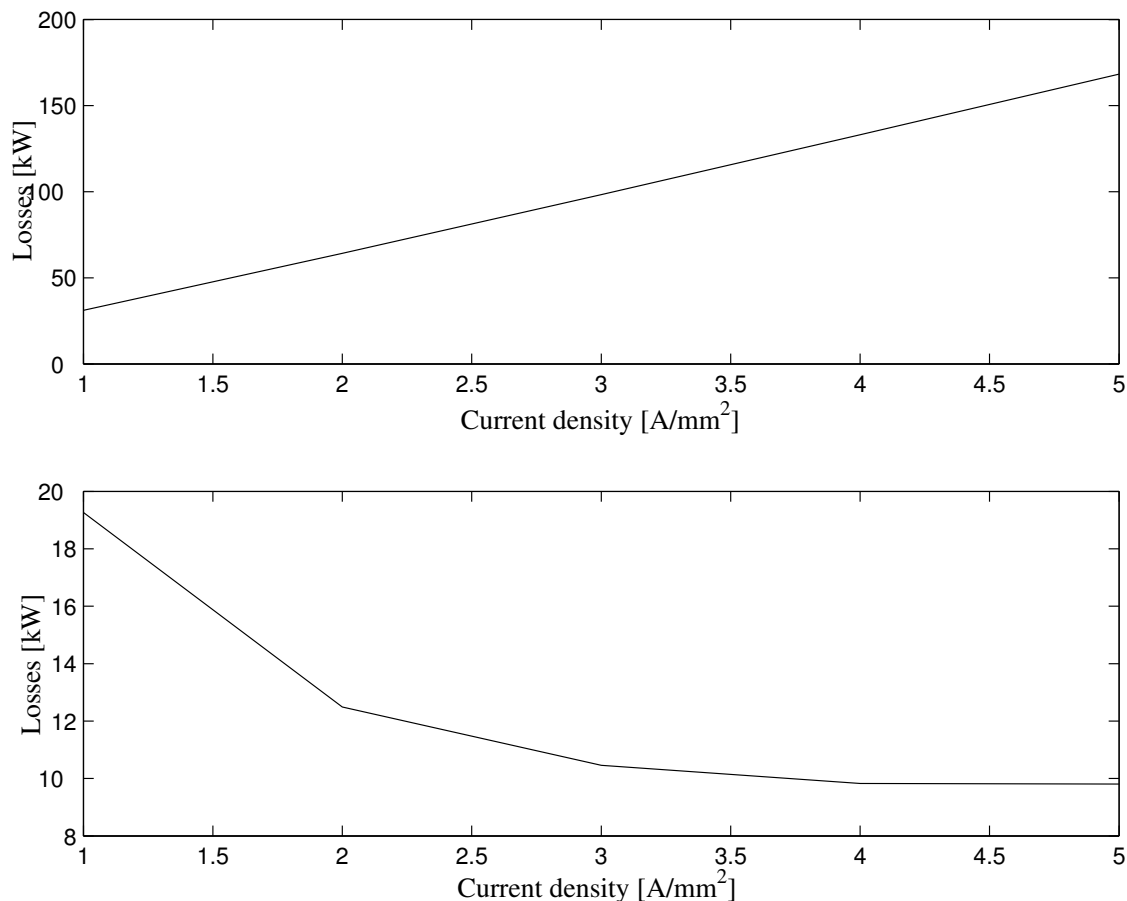


Figure A.5: Transformer losses depending on the current density. Upper plot for a large value of N_I . Lower plot for a low value of N_I .

A.2 Flux analysis

The next variable that will be studied is the core flux. This variable has a direct effect on the number of turns. Studying (5.18) can be seen that it appears in the denominator of the equation so, if the flux increases, the number of turns will be reduced. The performance of the parameter will be the typical of an inversely linear function.

The reduction of N_I leads to a decreasing in the dimensions of the winding window. In fact, if Equation (5.21) is analyzed, leaving all the other variables constant, it will present two components: a linear function of N_I and a constant. In conclusion, a_w will follow the performance of N_I adding an offset.

To analyze the performance of h_w it must be studied its three different limits. h_{w2} and h_{w3} will decrease with the number of turns, as equations (5.23) and (5.24) describes. h_{w1} will not be affected by the flux or its consequences so it will remain as a constant. As a result, the winding height will decrease of kept constant. Additionally it must be noticed that experience has prove that h_{w1} will govern this variable only at very high frequencies (where the foils are forced to be very thin), so the h_w will decrease with the core flux.

The outer radius (r_{out}) will also be reduced due $R3$ will decrease following the diminution of a_w . The transformer height will also decrease as the winding height.

Due to r_{out} and $R3$ decrease, and $R2$ and $R1$ are not affected, Equation (5.32) asseverates that the core volume will decrease. This, as well as the other dimensional parameters can be seen in Figure A.6.

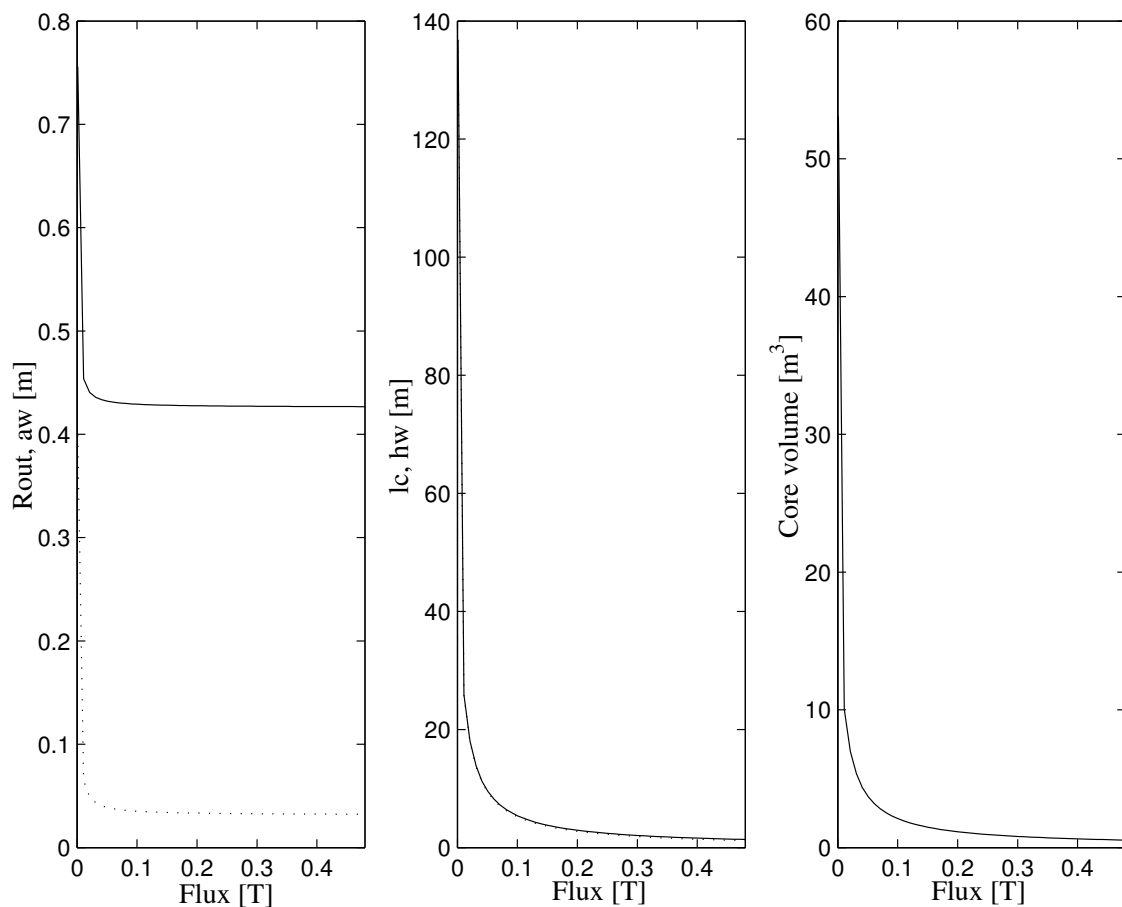


Figure A.6: Transformer dimensional parameters depending on the core flux. Left solid r_{out} , dotted a_w . Centre solid l_c , dotted h_w . Right solid V_c .

The results of the transformer inductances analysis, depending on how the dimensional parameters are affected by the flux, are presented in Table A.4.

Table A.4: Effects of the core flux on the transformer inductances.

Geometrical effect	L_σ	L_M
$N_I \downarrow$	\downarrow	\downarrow
$a_w \downarrow$	\downarrow	\uparrow
$h_w \downarrow$	\uparrow	\uparrow

Although it appears effects that would force the inductances to increase, the most important fact will be the reduction of the number of turns, leading the inductances to be reduced as N_I .

The last part of the flux analysis must be the losses study. Reviewing Equation (5.46) can be noticed that, as B increases so does the core losses density. Nevertheless, checking Figure A.7 can be realized that the core volume will sharply decrease for low values of the flux, decreasing the total losses. In addition, the N_I reduction will lead to a decrease of the winding losses as (4.44) and (4.45) express.

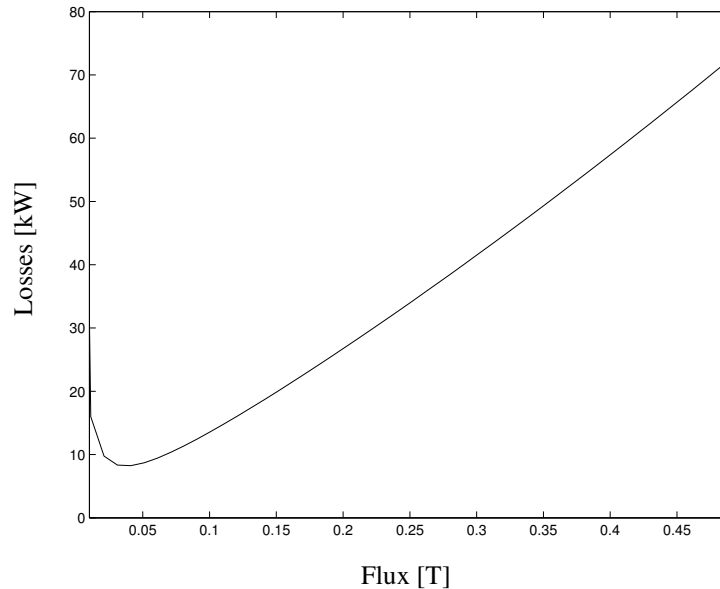


Figure A.7: Transformer losses depending on the core flux.

Checking the figure it can be seen that for the lower flux values, the transformer losses will brusquely decrease. This is due to N_I decreases sharply for this range of values as a consequence of the (5.18) shape. This leads to the prevalent effects will be the reduction of the winding losses and the core volume. Nevertheless, after the losses reach a minimum value, they begin to increase due to, now, the prevalent effect will be the increasing of the core density losses.

A.3 Frequency analysis

The variation of the frequency will produce the same effects as the core flux for the design parameters, due to it appears in the same position in the equation that describes the number of turns. Therefore, the arguments used there would be applicable in this analysis.

The only difference with the flux analysis will appear studying the performance of a_w because, to the N_l reduction effect, will be added the reduction of the foil thickness as a consequence of the rising on the frequency.

As a conclusion, the plot of the total losses is presented in Figure A.8. There can be confirmed that its shape is similar than the losses in the flux analysis.

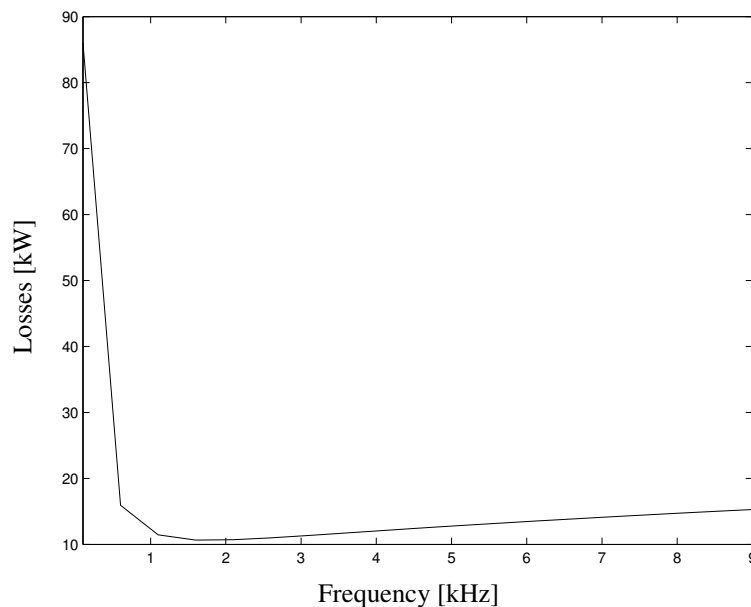


Figure A.8: Transformer losses depending on the switching frequency.

A.4 Thickness analysis

The increasing of the core thickness (t_c) will involve a diminution of $R2$ and thus a rising on the core area, as Equation (5.13) describes.

In order to analyze how the core area affects N_l , Equation (5.18) must be reviewed again, noticing that the performance of the parameter will be similar as in the flux and the frequency analysis. Consequently, the number of turns will decrease when the core thickness grows.

The magnitude of a_w , as happened in the previous analysis, will decrease with the core thickness, due to the reduction of the number of turns. Otherwise, for the outer radius (r_{out}) will appear two conflicting effects since the core area increment forces it to rise, the diminution on a_w produce just the opposite (due to R^3 will go down too). Regardless, if a_w performance is observed in Figure A.9, can be realized that it only changes noticeably for low values of thickness so, it will be the prevalent effect for this range, decreasing the outer radius. While, for medium and large values of t_c , the effect of the core area will rule the r_{out} performance, as can be seen in the figure.

The winding length will present a similar behaviour as in the flux analysis, decreasing its magnitude as a consequence of the N_l reduction. Accordingly, the total length will decrease too.

If the core volume is studied, the diminution of R_2 will lead it to increase, as well as the increasing of r_{out} for medium and large values of t_c . On the other hand, the reduction of a_w and thus R_3 would try to reduce the volume. As a result, based on the Figure A.9, it can be inferred that the increasing effects will rule the performance of the parameter.

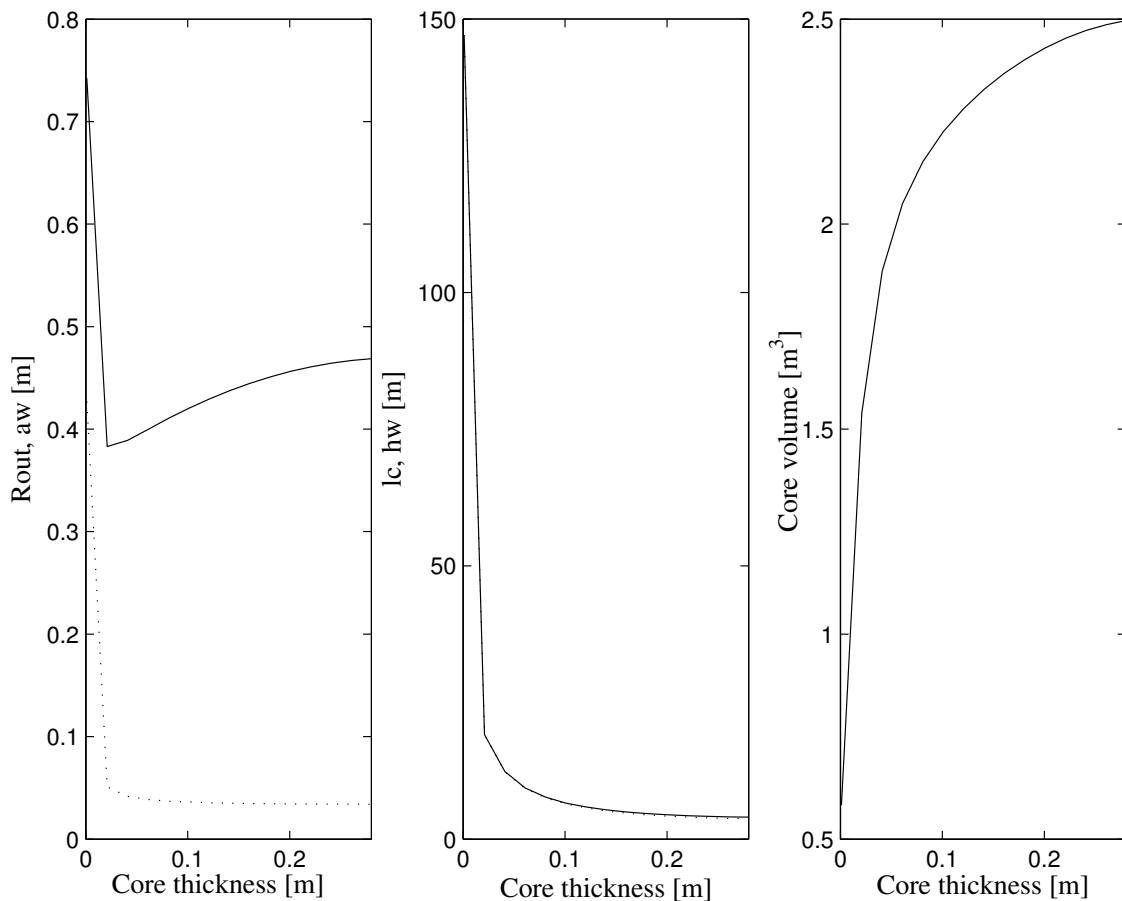


Figure A.9: Transformer dimensional parameters depending on the core thickness. Left solid r_{out} , dotted a_w . Centre solid l_c , dotted h_w . Right solid V_c .

To analyze the leakage inductance, in Table A.5 has been presented the effect of the dimensional parameters for low and medium-large ranges of the core thickness.

Table A.5: Effects of the core thickness on the leakage inductances.

Low thickness		Large thickness	
Geometrical effect	L_σ	Geometrical effect	L_σ
$N_I \downarrow$	\downarrow	$N_I \downarrow$	\downarrow
$a_w \downarrow$	\downarrow	$a_w \uparrow$	\uparrow
$h_w \downarrow$	\uparrow	$h_w \downarrow$	\uparrow

From the table can be seen that for low core thickness, N_I and a_w effects will force the leakage inductance to decrease. Though, for large thickness the N_I effect will be the only one that will reduce this parameter. Nevertheless, as can be seen in the previous plot, the variations of a_w and h_w are not very noticeable for this t_c range. Moreover, if the plot on Figure A.10 is studied, can be seen that the inductance decreases sharply in the low thickness range, remaining almost constant for the other t_c values. That means that the effects in this range will be balanced.

For the magnetizing inductance, the effects of the dimensional parameters are summarized in Table A.6. Once again, it has been divided attending to the core thickness magnitude.

Table 7.6: Effects of the core thickness on the magnetizing inductances.

Low thickness		Large thickness	
Geometrical effect	L_M	Geometrical effect	L_M
$N_I \downarrow$	\downarrow	$N_I \downarrow$	\downarrow
$a_w \downarrow$	\uparrow	$a_w \uparrow$	\downarrow
$h_w \downarrow$	\uparrow	$h_w \downarrow$	\uparrow
$a_c \uparrow$	\uparrow	$a_c \uparrow$	\uparrow

Attending to the table, it could be affirmed that, for low core thicknesses, the magnetizing inductance will increase, or at least decrease slower than in the large thickness range. Nevertheless, and according to the plot on Figure A.10, its performance will be completely the opposite. This is due to the fact that N_I will decrease very fast for the lower values of t_c , being that a very important effect for the magnetizing inductance in this range. Besides, for the medium-large range, although the decreasing effect of N_I is accompanied by the a_w increasing, its total effect will be weaker than for the lower values of the core thickness. This feature will lead the slope of the magnetizing inductance to be reduced with t_c .

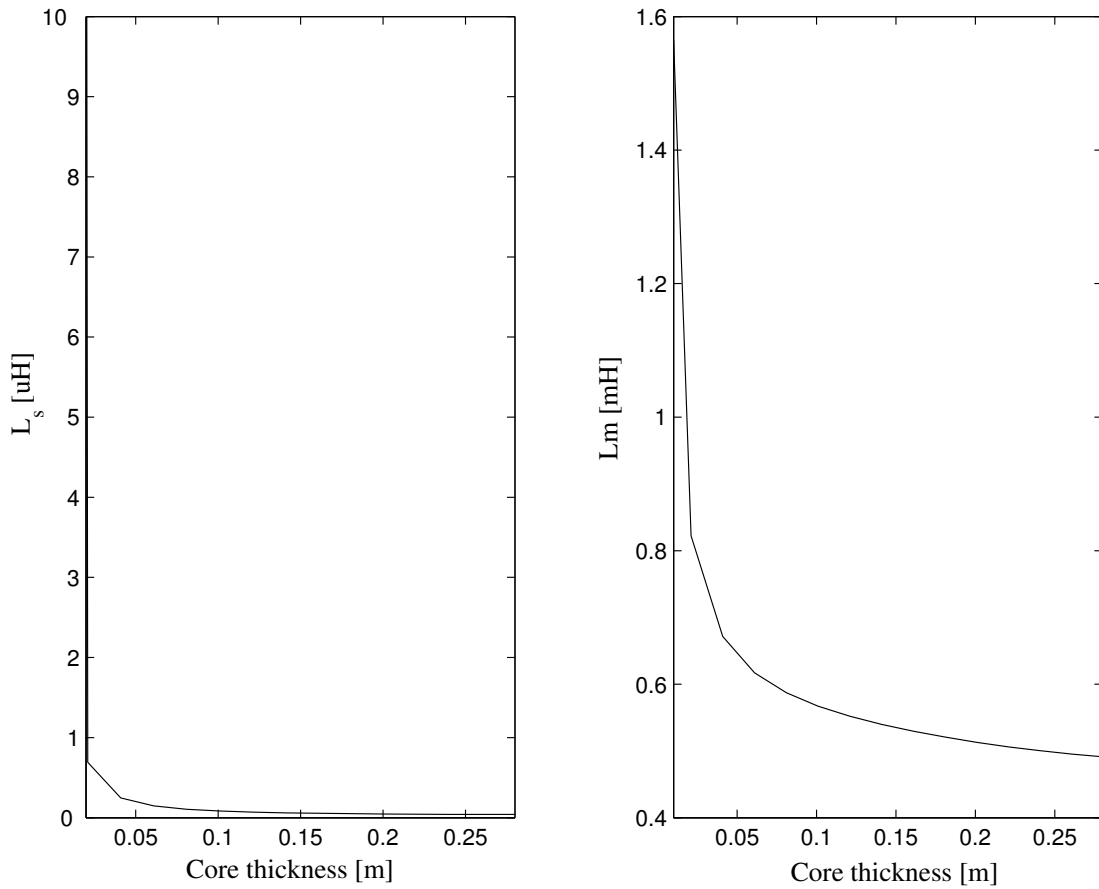


Figure A.10: Transformer inductances depending on the core thickness.

The variation of the core thickness will present two different effects for the transformer losses: As the number of turns decreases, the winding losses will be reduced. Otherwise, although the core density losses will be constant, as the core volume will increase, the total losses will increase too.

If Figure A.11 is analyzed, can be inferred that, for the lower values of t_c , the quick decrease of N_l will lead to a reduction of the total losses and, for medium and large t_c values, the slow decline in the number of turns will be balanced with the growing of the core volume.

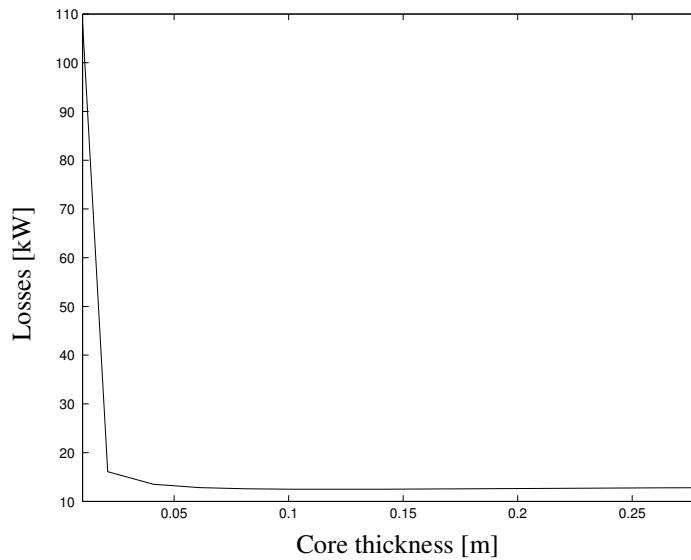


Figure A.11: Transformer losses depending on the core thickness.

A.5 Layers on the primary analysis

Attending to Equation (5.18) the number of layers on the primary will not affect the number of turns, simplifying its analysis.

If the dimensions are analyzed, it can be realized that, from (5.21), an increment on nsI (layers on the primary) will increase a_w . Moreover, as the core area will not be affected and R_3 will increase as describes (5.25), the outer radius of the transformer will rise too.

The h_w performance will depend on which is the limit that governs the parameter. If h_{w1} or h_{w2} are the most restrictive factors, the winding height will decrease. If h_{w3} is the one that rules the height, it will not be affected. Nevertheless, this case only will happen if the number of turns on the secondary is very large, as can be deduced from (5.18).

The performance of the core volume will depend on the increases of r_{out} and R_3 and so, it will decrease.

Figure A.12 shows the dimensional parameters as a function of nsI . Must be noticed that it is a discrete variable so only spots will be obtained.

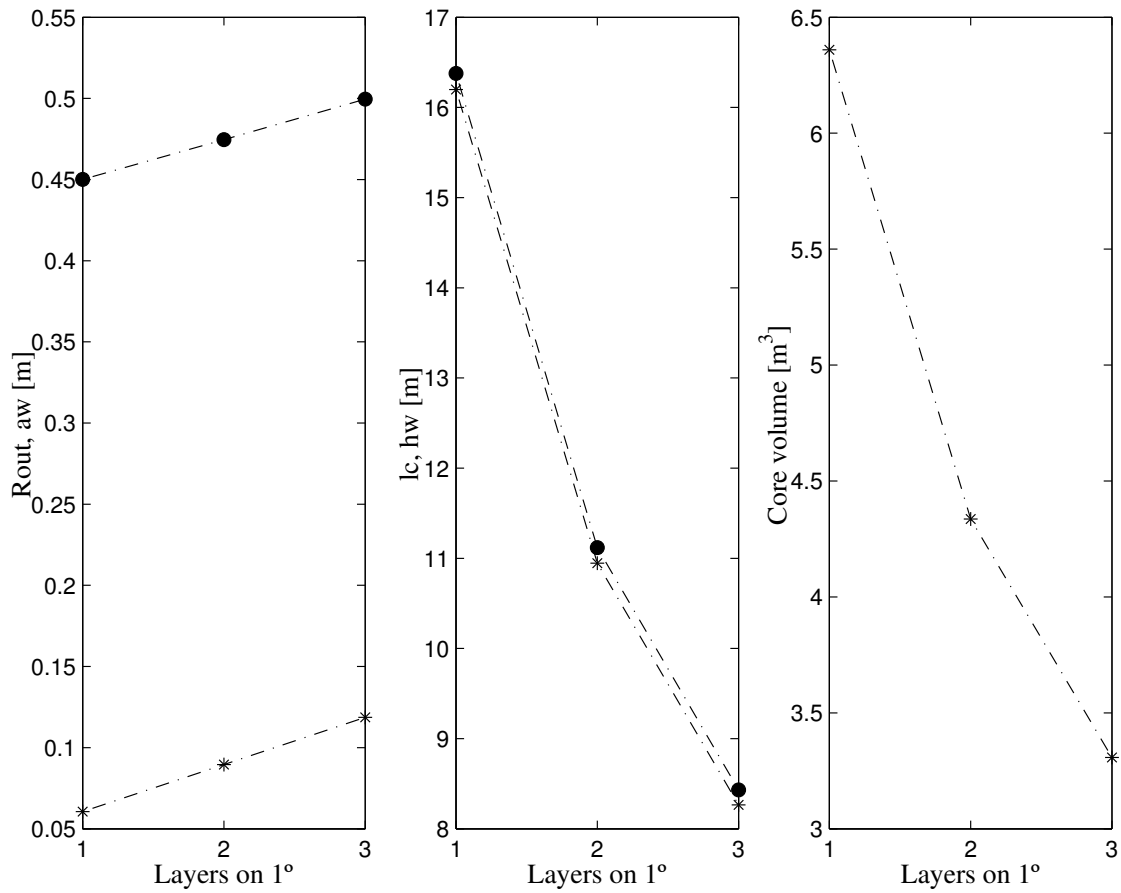


Figure A.12: Transformer dimensional parameters depending on the number of layers on the primary. Left solid r_{out} , dotted a_w . Centre solid l_c , dotted h_w . Right solid V_c .

In order to analyze the performance of the transformer inductances Table A.7 summarizes the dimensional parameters and their effect.

Table A.7: Effects of the layers on the primary on the transformer inductances.

Geometrical effect	L_σ	L_M
$N_I \sim$	\sim	\sim
$a_w \uparrow$	\uparrow	\downarrow
$h_w \downarrow$	\uparrow	\uparrow

From the table it is clear that the leakage inductance will always increase with nsI .

The magnetizing inductance will be influenced by two opposed effects but, from Figure A.12, as the slope of the winding height is more pronounced than a_w , the L_M will also decrease, as illustrates Figure A.13.

Finally, the total losses of the transformer will decrease with nsI . This is due to the fact that the winding losses and the core density losses will be constant and, as was mentioned before, the core volume will decrease, reducing the core losses.

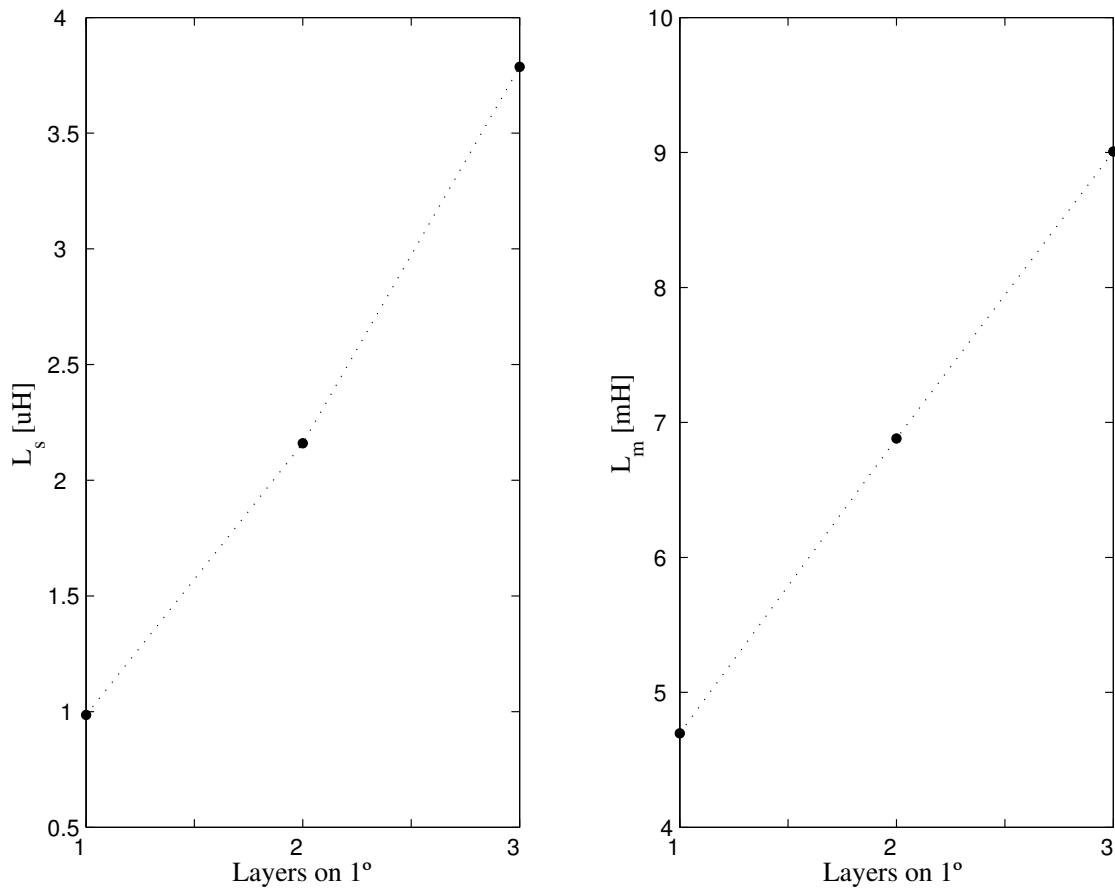


Figure A.13: Transformer inductances depending on the number of layers on the primary.

A.6 Layers on the secondary analysis

The analysis depending on the layers on the secondary will be very similar as the analysis done for the layers on the primary.

In fact, as before, the number of turns will not be affected, and a_w and r_{out} will increase, following the same arguments that were used in the previous paragraph.

If h_w is studied can be noticed that both h_{w2} and h_{w3} will decrease if the layers on the secondary raises. h_{w1} will not be affected by this variable but, as it will rule the behaviour of the parameter only for very high frequencies, the winding height will decrease. The total height, as usual, will follow the performance of h_w .

As the dimensional parameters behaves exactly as in the previous analysis, the core volume and the transformer inductances and losses will performance as was explained there. That means:

- The core volume will decrease.
- The leakage inductance will increase.
- The magnetizing inductance will increase.
- The total losses will decreases.

Appendix B

Matlab® codes

B.1 Matlab® code for the analysis of the converter depending on the transformer parameters

This code implements the iterative flowchart presented in Figure 7.12.

```
% ANALYSIS OF THE FB DEPENDING ON THE TRANSFORMER
PARAMETRES (WR,LSIG,LM)
% AND THE FREQUENCY
flag1=1;
flag2=2;
error2=1E-9;
%PARAMETRES
V1=3300;          %Input voltage (Volts)
I1=1500;          %Primary current (Amperes)
I2=330;           %Secondary current (Amperes)
INCI2=0.1*I2;     %maximum allowable output current ripple
D=0.185;          %Duty cycle
Voutideal=15000;  %Ideal output voltage (rated output voltage of the FB converter)
%DATAVECTORS
FREQUENCY=[100:1000:10000]; %switching frequency
WRVEC=[12:1:20];  %winding ratio
LSIG=[0.00000001:0.0000002:0.00001]; %leakage inductance
LM=[0.00001:0.0002:0.01]; %magnetizing inductance
VOUTREAL=zeros(10,9,50,50);
T1=zeros(10,9,50,50);
for h=1:1:10,
    f=FREQUENCY(1,h);
    T=1/f;
    t0=D*T;
    for i=1:1:9,
        WR=WRVEC(1,i);
        for j=1:1:50,
            L=((WR*V1)/(2*INCI2))*(1-2*D)*t0; %calculation of the main inductance
            Lsig=LSIG(1,j);
            for k=1:1:50,
                Lm=LM(1,k);
```



```
ro=2.2E-8;          %copper resistivity (ohm-m)
nu=(pi)*4E-7;      %foil magnetic permeability (N/A^2)
sig=1/ro;          %copper conductivity

%DATA PARAMETRES
V1=3300;           %Input voltage (Volts)
I1=1500;           %Primary average current (Amperes)
I1rms=2535;        %Primary RMS current (Amperes)
I2=333;            %Secondary current (Amperes)
Kcu1=0.55;         %fill factor on the primary (foil)
Kcu2=0.05;         %fill factor on the secondary (cable)
INCI2=0.1*I2;     %maximum allowable output current ripple
Sreq=V1*I1;        %Apparent power required for the transformer (Volt*Amperes)
D=0.185;          %Duty cycle
Voutmax=20250;     %Maximum output voltage
Voutideal=15000;   %Rated output voltage

%DEFINITION OF THE DATA VECTORS
CURRENT=[1 2 3 4 5]; %Density current
FLUX=[0.001:0.02:1]; %Core flux
LAYERS1=[1 2 3];    %Layers on the primary
LAYERS2=[1 2 3 4 5]; %Layers on the secondary
THICKNESS=[0.001: 0.02 :0.3]; %thickness for the core
FREQUENCY=[100:150:3000]; %commutation frequency
COREAREA=zeros(5,50,3,20,5,15); %vector for core areas
COREVOLUME=zeros(5,50,3,20,5,15); %vector for core volume
WRVEC=zeros(5,50,3,20,5,15); %vector for winding ratios
N1VEC=zeros(5,50,3,20,5,15); %vector for windings on the primary
AW=zeros(5,50,3,20,5,15); %vector for aw
HW=zeros(5,50,3,20,5,15); %vector for the hw
LC=zeros(5,50,3,20,5,15); %vector for the total transformer height
ROUT=zeros(5,50,3,20,5,15); %vector for the outer radium
RIN=zeros(5,50,3,20,5,15); %vector for the inner radium
LPATH=zeros(5,50,3,20,5,15); %vector for the flux path
LSIG=zeros(5,50,3,20,5,15); %vector for the leakage inductance
LM=zeros(5,50,3,20,5,15); %vector for the magnetizing inductance
LVEC=zeros(5,50,3,20,5,15); %vector for the main inductance
EVEC=zeros(5,50,3,20,5,15); %vector for the foil thick
LW=zeros(5,50,3,20,5,15); %vector for the winding length
ACU1=zeros(5,50,3,20,5,15); %vector for copper area in the primary
ACU2=zeros(5,50,3,20,5,15); %vector for copper area in the secondary

%DENSITY CURRENT LOOP
for b=1:1:5,

    fprintf('(-)\n');
    J1=CURRENT(1,b)*1000*1000; %Primary density current (A/m2)
    J2=CURRENT(1,b)*1000*1000; %Secondary density current (A/m2)
```

```

Acu1=I1rms/J1;           %Copper area in the primary (m2)
Acu2=I2/J2;             %Copper area in the secondary (m2)
Aconductor2=Acu2/0.75; %conductor area in the secondary (due to the litz
cable created)
rc=sqrt(Aconductor2/pi);
Dcable=(2*rc+0.017*2); %Copper diameter and isolation (m)
lw=2*(pi)*10*Dcable; %wire length (m)
R1=lw/(2*pi);          %R1 (m)

%FLUX LOOP
for g=1:1:50,
    F=FLUX(1,g);
    fprintf('#');

%LAYERS ON THE PRIMARY LOOP
for h=1:1:3,
    ns1=LAYERS1(1,h);

% FREQUENCY LOOP
for i=1:1:20,
    f=FREQUENCY(1,i);
    w=2*(pi)*f; %frequency (rad/s)
    T=1/f; %period
    t0=D*T; %ton for the switches
    e=sqrt(2*ro/(w*nu)); %thick of the foil to avoid skin effect (m)

%SECONDARY LAYERS LOOP
for j=1:1:5,
    ns2=LAYERS2(1,j);

%THICKNESS LOOP
for k=1:1:15,
    t1=1; %Value for t1 only to assure it to enters on the loop
    tc=THICKNESS(1,k);

loop
    WR=10; %First value for the winding ratio to enter in the
thicknes
    R2plus=R1-tc; %R2 dimensions from the thickness
    acplus=pi*((R1^2)-(R2plus^2)); %calculation of the core area for the
transformer design
    awplus=1; %Definition of the variables used in the
    hwplus=1;
    Vcplus=1;
    N1plus=1;
    N2plus=1;
    Awplus=1;
    ecplus=1;

```

```

r1plus=1;
routplus=1;
lcplus=1;
R3plus=1;
Lmplus=1;
Lsigplus=1;
Lplus=1;
Voutrealplus=1;
Vlmpus=1;

while t1>0 && N1plus>=1 && Voutrealplus<=Voutideal &&
Voutrealplus>0, %Loop to obtain the minimum winding ratio that fits the specifications

    WR=WR+1;    %increase of the winding ratio

    aw=awplus; %copy of the step n-1 variables in the step n places
    hw=hwplus;
    Vc=Vcplus;
    ac=acplus;
    N1=N1plus;
    N2=N2plus;
    Aw=Awplus;
    ec=ecplus;
    r1=r1plus;
    R2=R2plus;
    rout=routplus;
    lc=lcplus;
    R3=R3plus;
    Lm=Lmplus;
    Lsig=Lsigplus;
    L=Lplus;
    Voutreal=Voutrealplus;
    Vlm=Vlmpus;

    N1plus=Voutmax/(4*WR*F*ac*f); %Obtaining the
number of wires in the primary

    N2plus=N1plus*WR; %The Winding number in
the secondary
    Awplus=(N1plus*Acu1/Kcu1)+(N2plus*Acu2/Kcu2); %Winding
area (m2)
    awplus=(ns2*Dcable)+(N1plus*e*ns1); %New value for aw
with N1 corrected (m)
    hw1=Acu1/(e*ns1); %calculation of hw
attending to the skin effect on the foil (m)
    hw2=Awplus/awplus; %calculation of hw
attending to fit the windings in the winding area (m)
    hw3=N2plus*Dcable/ns2; %calculation of hw
attending to fit the cable on the winding area

```

```

H=[hw1,hw2,hw3];
hwplus=max(H); %Chosen of the most
restrictive limit
r1plus=R1+(awplus/2); %geometrical parameters to
obtain the new core area
R2plus=R1-tc; %and volume
acplus=pi*((R1^2)-(R2plus^2)); %core area
R3plus=R1+awplus;
routplus=sqrt(((acplus/pi)+(R3plus)^2));
ecplus=acplus/(2*pi*r1plus);
lcplus=hwplus+2*ecplus; %total transformer length
Vcplus=pi*((routplus)^2-(R2plus)^2)*lcplus-
pi*hwplus*((R3plus)^2-(R1)^2); %core volume

S=(N1plus*acplus*w*F*J1*Acu1); %calculation of the
apparent power
lpath=2*(awplus+hwplus)+2*tc+2*ecplus; %calculation of the
flux path
p=1;
Lmplus=nu*nur*(N1plus^2)*acplus/lpath; %estimation
of the magnetizing inductance
Lsigplus=(nu*(N1plus^2)*lw*awplus)/(3*hwplus*(p^2));
%estimation of the leakage inductance
Lplus=((WR*V1)/(2*INCI2))*(1-2*Drated)*t0;
%estimation of the main inductance, attending to the theoretical model
ERROR2=1;
t1plus=1E-5; %first estimation of t1

while ERROR2>error2, %loop to obtain t1 by an iterative process
t1=t1plus;
Voutrealplus=(2*WR*Lplus*Lmplus*V1*(t0-
t1))/(T*(Lplus*Lmplus+Lsigplus*Lmplus*(WR^2)+Lsigplus*Lplus)-
(2*(WR^2)*Lmplus*Lsigplus*(t0-t1))); %estimate output voltage

Vlmpplus=(Lplus*Lmplus*V1+Lsigplus*Lmplus*WR*Voutrealplus)/(Lplus*Lmplus+L
sigplus*Lmplus*(WR^2)+Lsigplus*Lplus); %Voltage on the
magnetizing inductance
A2=0.5*(V1-Vlmpplus);
%parameters to obtain t1
B2=V1*t0;
C2=(0.5*(V1-Vlmpplus)+((V1-Vlmpplus)^2)/(2*V1))*(t0^2)-
I1*T*Lsigplus/2;
t1plus=(-B2+sqrt((B2^2)-4*A2*C2))/(2*A2);
%calculation of the corrected t1
ERROR2=abs(t1plus-t1);
end
end

```

```

%STORAGE OF THE RESULTS
if Voutrealplus>0

    WRVEC(b,g,h,i,j,k)=WR-1;           %winding ratio
vector

    COREAREA(b,g,h,i,j,k)=ac;         %core areas vector
    COREVOLUME(b,g,h,i,j,k)=Vc;      %core volume
vector

    N1VEC(b,g,h,i,j,k)=N1;           %number of wires on
the primary vector

    HW(b,g,h,i,j,k)=hw;              %hw vector
    AW(b,g,h,i,j,k)=aw;              %aw vector
    LPATH(b,g,h,i,j,k)=lpath;        %vector for the flux
path

    LC(b,g,h,i,j,k)=lc;              %vector for the total
transformer height

    ROUT(b,g,h,i,j,k)=rout;          %Outer radium
inductance

    RIN(b,g,h,i,j,k)=R2;
    LSIG(b,g,h,i,j,k)=Lsig;          %leakage inductance
vector

    LM(b,g,h,i,j,k)=Lm;              %magnetizing inductance
    LVEC(b,g,h,i,j,k)=L;             %main inductance vector
    EVEC(b,g,h,i,j,k)=e;             %foil thickness
    LW(b,g,h,i,j,k)=lw;              %wire length
    ACU1(b,g,h,i,j,k)=Acu1;          %primary copper area
    ACU2(b,g,h,i,j,k)=Acu2;          %secondary copper
area

    end
    end
    end
    end
    end
    end
end

```

B.3 Matlab® code for the converter optimization

This code executes the converter optimization process.

```

%CONVERTER OPTIMIZATION
result=1E9;
K1=471559; %Core volumetric cost
K2=250399; %Cable volumetric cost
K3=1460121; %Foil volumetric cost
K4=0.000125; %Losses cost [KWs]
time=20*365*24*3600; %Converter life time (20 years)

```

```

I11=1500;    %average primary current for the full load operating point
I11peak=4285; %peak primary current for the full load operating point
I11rms=2535; %rms primary current for the full load operating point
I21=333;    %secondary current for the full load operating point
AVGI=PEAKI=RMSI
I12=500;    %average primary current for the low load operating point
I12peak=1428; %peak primary current for the low load operating point
I12rms=845; %rms primary current for the low load operating point
I22=111;    %secondary current for the low load operating point
AVGI=PEAKI=RMSI
vo=1.181;   %voltage drop on the IGBT
R=0.0045;   %Resistance on the IGBT
vd=1.55;    %voltage drop on the diode
Rd=0.0049;  %Resistance on the diode
V1=3300;
Voutideal=15000; %nominal output voltage

for br=1:1:2 %DENSITY CURRENT
    fprintf('(-)\n');
    for gr=1:1:50 %FLUX
        fprintf('#');
        for hr=1:1:3 %LAYERS ON THE PRIMARY
            for ir=1:1:20, %FREQUENCY
                for jr=1:1:5, %LAYERS ON THE SECONDARY
                    for kr=1:1:15 %THICKNESS
                        if WRVEC(br,gr,hr,ir,jr,kr)>0,
                            %transformer losses

B=Voutideal/(4*N1VEC(br,gr,hr,ir,jr,kr)*COREAREA(br,gr,hr,ir,jr,kr)*FREQUENCY
(ir)*WRVEC(br,gr,hr,ir,jr,kr)); %calculation of the transformer flux for the operation
points
                            %losses at full load

Tfullloadlosses=K*((FREQUENCY(ir)/1000)^a)*(B^d)*COREVOLUME(br,gr,hr,ir,jr,
kr)+(ro*((I11rms/ACU1(br,gr,hr,ir,jr,kr))^2)*ACU1(br,gr,hr,ir,jr,kr)*LW(br,gr,hr,ir,jr,k
r)*N1VEC(br,gr,hr,ir,jr,kr)+(ro*((I21/ACU2(br,gr,hr,ir,jr,kr))^2)*ACU2(br,gr,hr,ir,jr,k
r)*LW(br,gr,hr,ir,jr,kr)*WRVEC(br,gr,hr,ir,jr,kr)*N1VEC(br,gr,hr,ir,jr,kr));
                            %losses at 1/3 of the rated power

Tlowloadlosses=K*((FREQUENCY(ir)/1000)^a)*(B^d)*COREVOLUME(br,gr,hr,ir,jr,
kr)+(ro*((I12rms/ACU1(br,gr,hr,ir,jr,kr))^2)*ACU1(br,gr,hr,ir,jr,kr)*LW(br,gr,hr,ir,jr,k
r)*N1VEC(br,gr,hr,ir,jr,kr)+(ro*((I22/ACU2(br,gr,hr,ir,jr,kr))^2)*ACU2(br,gr,hr,ir,jr,k
r)*LW(br,gr,hr,ir,jr,kr)*WRVEC(br,gr,hr,ir,jr,kr)*N1VEC(br,gr,hr,ir,jr,kr));
                            %weighted average transformer losses

Tlosses=((15/100)*Tfullloadlosses+(60/100)*Tlowloadlosses)*(1/1000);
                            %semiconductor losses

IGBTlosses=((15/100)*((0.415/(400*900))*(I11peak/5)*(V1/3)*FREQUENCY(ir)+vo*

```

```
(I11/5)+R*((I11rms/5)^2))+60/100)*((0.415/(400*900))*(I12peak/5)*(V1/3)*FREQUENCY(ir)+vo*(I12/5)+R*((I12rms/5)^2)))*4*3*5*(1/1000);
```

```
DIODElosses=((15/100)*(0.0022*(I21/2)*FREQUENCY(ir)+vd*(I21/2)+Rd*(I21/2)^2)+(60/100)*(0.0022*(I22/2)*FREQUENCY(ir)+vd*(I22/2)+Rd*(I22/2)^2))*4*7*(1/1000);
```

```
SClosses=IGBTlosses+DIODElosses;
```

```
%total losses
```

```
TOTALlosses=Tlosses+SClosses;
```

```
FOILVOLUME=ACU1(br,gr,hr,ir,jr,kr)*LW(br,gr,hr,ir,jr,kr)*N1VEC(br,gr,hr,ir,jr,kr);
```

```
CABLEVOLUME=ACU2(br,gr,hr,ir,jr,kr)*LW(br,gr,hr,ir,jr,kr)*N1VEC(br,gr,hr,ir,jr,kr)*WRVEC(br,gr,hr,ir,jr,kr);
```

```
CORECOST=COREVOLUME(br,gr,hr,ir,jr,kr)*K1;
```

```
CABLECOST=CABLEVOLUME*K2;
```

```
FOILCOST=FOILVOLUME*K3;
```

```
LOSSESCOST=TOTALlosses*time*K4;
```

```
COST=CORECOST+CABLECOST+FOILCOST;
```

```
buffer=(COST*7.53E-6)+0.2296*TOTALlosses; %Energy cost
```

```
function
```

```
if buffer<result && LC(br,gr,hr,ir,jr,kr)<1,
```

```
result=buffer; %storage of the cost
```

```
flux=B; %storage of the flux
```

```
losses=TOTALlosses; %storage of the total losses
```

```
transformerlosses=Tlosses; %storage of the transformer losses
```

```
deviceslosses=SClosses; %storage of the devices losses
```

```
corecost=CORECOST;
```

```
cablecost=CABLECOST;
```

```
foilcost=FOILCOST;
```

```
lossescost=LOSSESCOST;
```

```
Br=br;
```

```
Gr=gr;
```

```
Hr=hr;
```

```
Ir=ir;
```

```
Jr=jr;
```

```
Kr=kr;
```

```
end
```

```
fprintf('\nTHE OPTIMIZATION RESULTS ARE:\n')
```

```
fprintf('TOTAL COST')
```

```
result
fprintf('construction cost')
corecost+cablecost+foilcost
corecost
cablecost
foilcost
lossescost
losses
transformerlosses
deviceslosses
fprintf('current density')
CURRENT(Br)
fprintf ('flux')
flux
fprintf('frequency (Hz)')
FREQUENCY(Ir)
fprintf('layers on the primary')
LAYERS1(Hr)
fprintf('layers on the secondary')
LAYERS2(Jr)
fprintf('thickness (m)')
THICKNESS(Kr)
fprintf('winding ratio')
WRVEC(Br,Gr,Hr,Ir,Jr,Kr)
fprintf('N1')
N1VEC(Br,Gr,Hr,Ir,Jr,Kr)
fprintf('main inductance (H)')
LVEC(Br,Gr,Hr,Ir,Jr,Kr)
fprintf('leakage inductance (H)')
LSIG(Br,Gr,Hr,Ir,Jr,Kr)
fprintf('magnetizing inductance (H)')
LM(Br,Gr,Hr,Ir,Jr,Kr)
fprintf('total height (m)')
LC(Br,Gr,Hr,Ir,Jr,Kr)
fprintf('Rout and Rint (m)')
ROUT(Br,Gr,Hr,Ir,Jr,Kr)
```

B.4 Matlab® code for the analysis of the transformer

This code implements the transformer analysis depending in the construction and operating variables, schematized in Figure A.1.

```
%ANALYSIS OF THE TRANSFORMER DEPENDING ON
%THE CONSTRUCTION AND OPERATING VARIABLES

%OPERATING PARAMETRES
error=0.0000001;      %iteration error
error2=1E-9;
```

```

error3=0.0000001;
flag1=1;
flag2=2;
flag3=3;
%MATERIAL PARAMETRES
%Copper
ro=2.2E-8;      %copper resistivity (ohm-m)
nu=(pi)*4E-7;  %foil magnetic permeability (N/A^2)
sig=1/ro;      %copper conductivity
%FT-3M
K=78.6*1000;   %core material constant
a=1.29;        %frequency core material constant
d=2;           %Density flux core material constant
nur=2000;      %Relative permeability
Fmax=0.5;      %saturation flux [T]

%DATA PARAMETRES
V1=3300;       %Input voltage (Volts)
I1=1500;       %Primary current (Amperes)
I2=330;        %Secondary current (Amperes)
Kcu1=0.55;     %fill factor on the primary (foil)
Kcu2=0.04;     %fill factor on the secondary (cable)
INCI2=0.1*I2;  %maximum allowable output current ripple
Sreq=V1*I1;    %Apparent power required for the transformer (Volt*Amperes)
D=0.185;       %Duty cycle
Voutideal=15000; %Ideal output voltage (rated output voltage of the FB
converter)

%DEFINITION OF THE DATA VECTORS
CURRENT=[1 2 3 4 5]; %current density
FLUX=[0.001:0.01:0.5]; %core flux
LAYERS1=[1 2 3]; %layers on the primary
LAYERS2=[1 2 3 4 5]; %layers on the secondary
THICKNESS=[0.001: 0.02 :0.3]; %thickness for the core
FREQUENCY=[100:500:10000]; %commutation frequency
TLOSSES2=zeros(5,50,3,20,5,15); %vector for transformer losses
SCLOSSES2=zeros(5,50,3,20,5,15); %vector of semiconductor losses
LOSSES2=zeros(5,50,3,20,5,15); %vector of total losses
COREAREA2=zeros(5,50,3,20,5,15); %vector for core areas
COREVOLUME2=zeros(5,50,3,20,5,15); %vector for core volume
WRVEC2=zeros(5,50,3,20,5,15); %vector for winding ratios
N1VEC2=zeros(5,50,3,20,5,15); %vector for windings on the primary
AW2=zeros(5,50,3,20,5,15); %vector for aw
HW2=zeros(5,50,3,20,5,15); %vector for the height
LC2=zeros(5,50,3,20,5,15); %vector for the total transformer height
ROUT2=zeros(5,50,3,20,5,15); %vector for the outer radium
LPATH2=zeros(5,50,3,20,5,15); %vector for the flux path
LSIG2=zeros(5,50,3,20,5,15); %vector for the leakage inductance
LM2=zeros(5,50,3,20,5,15); %vector for the magnetizing inductance

```

```

LVEC2=zeros(5,50,3,20,5,15);           %vector for the main inductance
EVEC2=zeros(5,50,3,20,5,15);           %vector for the foil thick

LW=zeros(5,50,3,20,5,15);

% PRIMARY LAYERS LOOP
for b=1:1:5,
fprintf('(-)\n');
J1=CURRENT(1,b)*1000*1000;             %Primary density current (A/m2)
J2=CURRENT(1,b)*1000*1000;             %Secondary density current (A/m2)
Acu1=I1/J1;                             %Copper area in the primary (m2)
Acu2=I2/J2;                             %Copper area in the secondary (m2)
Dcable=(2*sqrt(Acu2/pi))+0.017;        %Copper diameter and isolation (m)
lw=2*(pi)*10*Dcable;                   %wire length (m)
R1=lw/(2*pi);
for g=1:1:50,
    F=FLUX(1,g);
    fprintf('#');
    for h=1:1:3,
        ns1=LAYERS1(1,h);
        % FREQUENCY LOOP
        for i=1:1:20,
            f=FREQUENCY(1,i);
            w=2*(pi)*f;                   %frequency (rad/s)
            T=1/f;                         %period
            t0=D*T;                       %ton for the switches
            e=sqrt(2*ro/(w*nu));          %thick of the foil to avoid skin effect (m)
            %SECONDARY LAYERS LOOP
            for j=1:1:5,
                ns2=LAYERS2(1,j);
                %THICKNESS LOOP
                for k=1:1:15,
                    t1=1;                 %Value for t1 only to assure it to enters on the loop
                    Voutreal=1;           %Value for the output voltage to assure it enters on
the loop
                    tc=THICKNESS(1,k);
                    WR=13;               %theoretical value for the winding ratio

                    %TRANSFORMER CALCULATIONS
                    N1=Voutideal/(4*WR*F*ac*f); %Obtaining the number of wires in
the primary
                    N2=N1*WR;           %The Winding number in the secondary
                    Aw=(N1*Acu1/Kcu1)+(N2*Acu2/Kcu2); %Winding area (m2)
                    aw=(ns2*Dcable)+(N1*e*ns1); %New value for aw with N1
corrected (m)
                    hw1=Acu1/(e*ns1);    %calculation of hw attending to the skin
effect on the foil (m)
                    hw2=Aw/aw;          %calculation of hw attending to fit the
windings in the winding area (m)

```